Analytical Solutions for Bearing Capacity of Special Footings

Submitted in Partial Fulfillment of the Requirement for the Award of Degree of

MASTER OF ENGINEERING

In

CIVIL ENGINEERING (STRUCTURAL ENGINEERING)

Submitted by

SAURABH PRAKASH GUPTA
(Roll No - 8814)

UNDER THE GUIDANCE OF

Prof. (Mrs) P. R. Bose
Professor & HOD
Department of Civil Engineering
Delhi College of Engineering

Prof. A. Trivedi
Professor
Department of Civil Engineering
Delhi College of Engineering

DEPARTMENT OF CIVIL AND ENVIRONMENTAL ENGINEERING

DELHI COLLEGE OF ENGINEERING

DELHI UNIVERSITY, DELHI 110042

2004-2006

Science is the topography of ignorance…… The best Part of our knowledge is that which teaches us where knowledge leaves off and ignorance begins.

Oliver Wendell Holmes
1809-1894

CANDIDATE DECLARATION & CERTIFICATE

This is certify that **SAURABH PRAKASH GUPTA** a student of final year M.E. Civil (Structural Engg.), Delhi College of Engineering, carried out his Thesis work on "**Analytical Solutions for Bearing Capacity of Special Footings** " under the guidance of **Prof. (Mrs) P.R. Bose**, Professor & H.O.D and **Prof. A. Trivedi**, Professor, Department of Civil & Environmental Engineering, Delhi College of Engineering, Delhi, for the partial fulfillment of the requirement for the degree of **Master of Engineering, Civil Engineering** , specialization in Structural Engineering, from Delhi college of Engineering, Delhi.

This is certified that the matter embodied in this Thesis has not been submitted elsewhere for the award of any other degree/diploma.

Saurabh Prakash Gupta

M.E. (Structural Engineering)

Roll No. 8814

This is to certify that above statement made by candidate is true to the best of our knowledge.

Prof. (Mrs) P.R. Bose

Professor & HOD
Dept. of Civil Engineering,
Delhi College of Engineering.

Prof. A. Trivedi

Professor
Dept. of Civil Engineering,
Delhi College of Engineering.

AKNOWLEDGEMENT

I would like to take this opportunity to thanks all those who have been a constant source of inspiration and have helped in the exercise of preparing the present study.

I express my sincere gratitude to **Prof. (Mrs) P. R. Bose** and **Prof. A. Trivadi**, my **Project Guides**, for their constant inspiration, encouragement, guidance and constructive criticism and judicious evaluation that led to the compilation of this Thesis work. It was due to their constant help and assistant that this thesis work achieved its present shape.

I express my sincere thanks to all my friends and staff of Civil Engineering Department of Delhi College of Engineering, who left no stone unturned whenever I needed their assistance.

Place: D.C.E., Delhi

Date:

SAURABH PRAKASH GUPTA

M.E. (Structural Engineering)

Roll No.-8814

ABSTRACT

The analytical solutions for the bearing capacity of circular footing on sand are analyzed for two special types of footings, namely spudcan footing and skirted circular footing.

The bearing capacity solutions utilized limit-equilibrium method proposed by Terzaghi (1943) and numerical solutions found by Kumbhojkar (1993). The numerical values of the bearing capacity factor for special footings are based upon the failure surface restriction by spudcan footing and by the skirted footing.

The solutions are presented in the graphical form. The analysis of the result indicates that there is a significant improvement in the bearing capacity using spudcan and skirted footings with Kumbhojker assumptions. The experimental data of the skirted footings by other investigators also indicate an increase in ultimate bearing capacity but the magnitude differs.

Further the extent of increase in bearing capacity factors using spudcan and skirted footing provides a scope for fresh look on the application of Terzaghi and Kumbhojker approaches and its assumptions.

CONTENTS

NOMENCLATURE

ϕ = Angle of internal friction of soil.

δ = Angle of wall friction.

γ = Unit weight of soil in KN/m^3

α = Angle of inclination of sides of wedge to the horizontal surface of foundation.

θ = Angle of log-spiral.

σ' = Effective normal stress.

ζ_γ = Shape factor for circular footing.

Ω = Cone angle in Spudcan footing.

β = Angle of inclination of the soil above the ground surface.

c = Cohesion of soil.

q = Surcharge.

N_q, N_c, and N_γ = Dimensionless bearing capacity factor providing the contribution of c, q, and γ.

B = Width of footing.

D = Diameter of footing.

h = Height of cylindrical shell.

q_u = Ultimate bearing capacity of footing.

Q_u = Ultimate bearing capacity of footing with soil confinement.

q_o = Average pressure over the footing contact area.

r, r_1, and r_o = Radius of log-spiral.

D_f = Depth of foundation.

P_{pq}, P_{pc}, and $P_{p\gamma}$ = Passive force with contribution of q, c, and g respectively.

P_p = Passive force.

$K_{p\gamma}$ = Passive force coefficient.

d = diameter of cylindrical shell.

N_c', N_q' and N_γ' = Modified bearing capacity factors (for local shear faliur).

L = Length of continuous footing.

s_γ, s_c, and s_q = Shape factor of footing

d_q, d_γ, and d_c = Depth factor of footing.

i_c, i_q, and i_γ = Inclination of footing.

g_c, g_q, and g_γ = Slope factor of footing.

b_c, b_q, and b_γ = Tilting factor of footing.

dp = Differential reactive pressure on the element length ds of the failure surface.

R = Resultant reaction on failure surface.

d/D = Ratio of the diameter of cylindrical shell to the diameter of footing.

h/D = Ratio of the height of cylindrical shell to the diameter of footing.

BCR = Bearing capacity ratio, Q_u/q_u.

K_a = Rankine and Coulomb active earth pressure coefficient.

K_p = Rankine and Coulomb passive earth pressure coefficient.

$P_{p(1)}$, $P_{p(2)}$, and $P_{p(3)}$ = Rankine passive force.

F = Resultant frictional resistant force.

H_d = Height over which the Rankine Passive force acts.

W = Weight of wedge.

l_p, l_w, and l_R = lever arms.
q_c, q_q, and q_γ = The ultimate load per unit area of foundation for a soil with cohesion , friction and weight.

D_r = Relative density.

C_u = Uniformity coefficient.

C_c = Coefficient of curvature.

UPVC = Unplasticized polyvinyl chloride.

V = vertical load.

A_p = Plane area of contact of Soudcan footing.

B_p = Penitration diameter of Spudcan footing.

γ' = soil effective unit weight.

D_p = Penetration depth of Spudcan footing.

f = Circumferential tensile stress(or hoop stress).

p = Internal pressure in shell.

t = thickness of cylindrical shell.

CHAPTER-1

INTRODUCTION

The bearing capacity of shallow footing during the last fifty years has been extensively studied by several investigators [Prandtl ,1920; Reissner, 1926; Terzaghi, 1943; Meyerhof, 1951; Caquot and Kerisel, 1953; De Beer, 1963; Baki and Beik, 1970; Hansen, 1970; Vesic, 1973; Chen, 1975; Ingra and Baecher, 1983; Kumbhojkar, 1993; Zadroga, 1994; Dewaiker and Mohapatro, 1994; Frydman and Burd, 1997; Michalowki, 1997; Paolcci and Pecker, 1997; Soubra, 1999; Perkins and Madson, 2000 amongst others]. The bearing capacity solutions use the slip-line method, limit analysis method, finite element method, and limit equilibrium method. Limit equilibrium method, which is adopted by Terzaghi. Only numerical values of the bearing capacity factors differ accordingly to the specific assumption or approximation adopted in the solutions. Further more to account the original theory (e.g., footing shape; depth and tilts; rigidity and layering of solution of soil below a footing; inclination of applied loads.) a series of correction factors are applied to the $N_{c,}$ N_q and N_γ terms. This trend of enhancing the accuracy of the bearing capacity calculation without altering the basic equation is a proof of overwhelming acceptance of Terzaghi's approach regardless of the concern about its theoretical correctness. This thesis deals with the theoretical prediction of the ultimate bearing capacity of the special footings, 1. Spudcan footing and 2. Skirted footing.

In deep offshore water, the growing use of mobile Jackup units on Spudcan Footing has been raised a great deal of concern about the overall stability of jackup unit in hostile environmental forces. Mobile Jackup units consist of a floatable drilling platform supported on three or more legs, which can be raised or lowered. A detailed description of the installation procedure is given by Tan (1990). The platform legs can either be supported separately or they can be supported on a single shared mat. Most modern jackup platforms are of the former type and have approximately conical shaped footing with a protruding tip at the center. These are commonly referred as spudcan footing.

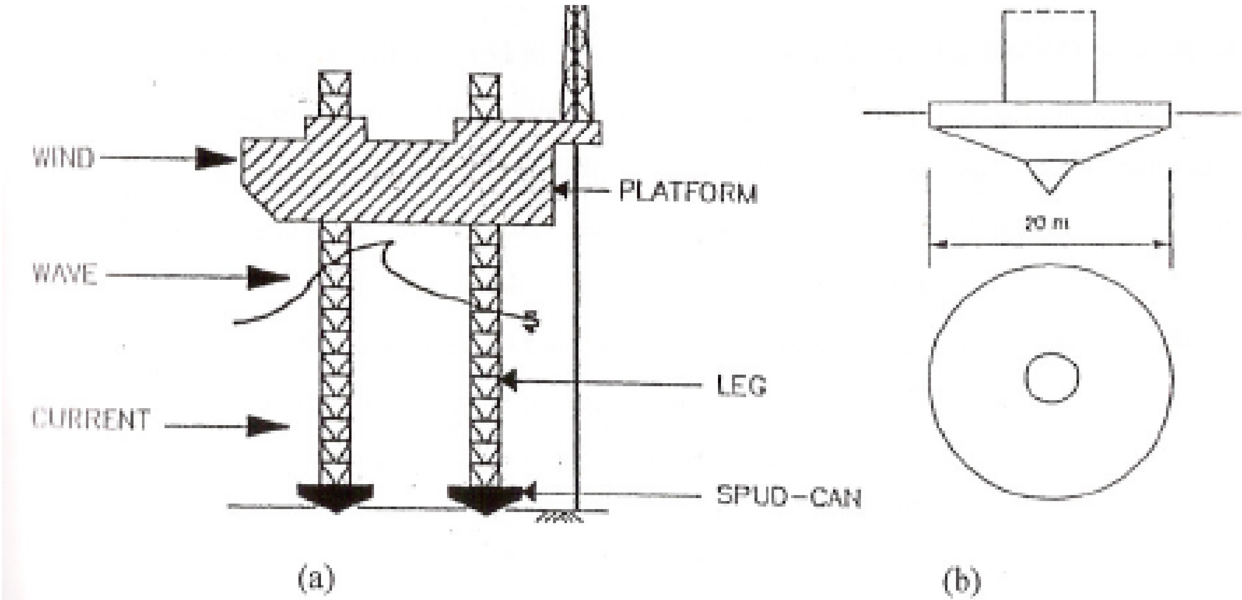

(a) (b)

Figures show (a) Jackup platform and environmental loads. (b) Spudcan footing.

The bearing capacity of spudcan footing increases with the depth of penetration below the seabed. The increase of bearing capacity with footing embedment is an important factor, since ever a small embedment can significantly increases the bearing capacity of such offshore footing. However this is not usually the case in coarse materials as penetration depth are typically very small.

The bearing capacity solution of Meyerhof (1953), Hansen (1970) and Vesic (1975) are commonly used to determine the ultimate bearing capacity of plane strain footing. These soil are modify by introducing shape factors to cover circular geometries [Hambly 1992; Dean et al. 1993]. In the case of spudcan footing, their embedded circular area in plane (i.e. plane area at ground surface) is used for the bearing capacity calculation. In order to investigate the applicability of the bearing capacity solutions to spudcan footing, analytical studied of conical shape footing using the Terzaghi's approach has been presented in the chapter three, by changing the cone angle (e.g., 0^o. 5^o, 10^o, 15^o). Also it is shone in the study that spudcan footing can be treated as equal cones enclosing the same volume. As per the past studies the load-displacement response of a spudcan footing and equal volume cone is almost equal.

Raft foundations are widely used in supporting structures for many reasons such as weak soil conditions or heavy columns loads. In many cases, some problems arise such as the construction is adjacent to an old building and/or the foundation depth is so great that the excavation needs to be braced during foundation construction (e.g., basement excavation). One of the available solutions is to sheet piles to support the excavation sides during construction. Due to the difficulty of removing these piles, they become part of the permanent structure and two problems arise. The first problem deals with the structural analysis of the raft if the piles are used as end supports for the raft. The second problem is the effect of these piles on the lateral movement of the soil underneath the raft and the effect of this confinement on the bearing capacity of the soil. While there are several solutions for the first problem, such as isolating the raft from the piles, the confining effect of these piles on the raft behavior is not clearly understood. Looking to the problem in a smaller scale, it can be modeled as a circular footing supported on a soil, which is surrounded by a confining cylinder. The strength of confined sand was studied by Rajagopal et al. (1999). They carried out a large number of triaxial compression tests to study the influence of geocell confinement on the strength and stiffness behavior of granular soils. Geocells fabricated by hand using different geotextiles were used to investigate the effect of the stiffness of the geocell on the overall performance of geocell–soil composite.

Several investigators have reported significant effect of soil confinement by using horizontal soil reinforcement to increase the bearing capacity of supporting soils. This was achieved by placing layers of geogrid at different depths and widths under the footing. The soil reinforcement is not only placed horizontally but also can be placed vertically besides the footing to resist the lateral deformation of the soil. The use of vertical reinforcement along with horizontal reinforcement was investigated as well. The reinforcement consists of a series of interlocking cells, constructed from polymer geogrids, which contain and confine the soil within its pocket geogrid. Rea and Mitchell (1978) conducted a series of model plate loading tests on circular footing supported over sand-filled square-shaped paper grid cell to identify different modes of failure and arrive at optimum dimensions of the cell. Dash et al. (2001a,b) performed an experimental study on the bearing capacity of a strip footing supported by a sand bed reinforced with a geocell mattress. Critical dimensions of reinforcement and depth of placement for mobilizing maximum bearing capacity improvement were presented.

The aim of this research is to investigate the effect of soil confinement by sheet piles on the behavior of soil foundation system. Also, the idea of improving the footing response by using confining cylinder around individual footing. To achieve this objective the analytical solution has been presented in the upcoming chapters four.

CHAPTER –2

LITERATURE REVIEW

Foundations, like the structures or equipment they support, are usually designed to meet certain serviceability and strength criteria. Serviceability conditions dictate that the foundation should perform such that under normal operating loads the structure or equipment it supports may fulfill its design purpose. These serviceability limitations are typically described by settlement or other motion limitations. The strength criteria have the purpose of ensuring that the foundation has sufficient reser4ve strength to resist the occasionally large load that may be experienced due to extreme environmental forces or other sources. In most, but not all cases, the serviceability or settlement criteria and the strength criteria may be treated as unrelated design tasks. Serviceability is a typically a long-term consideration for the foundation that may depend on time-dependent consolidation characteristics. Foundation strength, or bearing capacity, may be a short-termed problem such as an embankment construction on an untrained clay foundation or a long-term problem in which the maximum foundation load may appear at some unknown time.

A shallow foundation may be defined as one in which the embedment depth of the foundation is less than its least characteristic dimension. Usually, the bearing capacity of a foundation is determines by limit equilibrium, limit analysis, or slip-line solutions. The Varity of solutions available for a particular problem may lead to some uncertainty about which is the more appropriate procedure. In the following, the basic of these solution procedures will be summarized and method for their use presented.

2.1 METHODS OF ANALYSIS

At present time, the analysis of foundation can be made by employing one of the following four widely used methods:

1. Slip-line method
2. Limit equilibrium methods
3. Limit anal~~ysis metho~~ds
4. Finite-element methods

The first three methods are used in association with stability problems where the bearing capacity is sought. If, instead, the foundation settlement or stress distribution or stress distribution within the soil mass are of prime interest, then the fourth method must be used. Brief description of the first three procedures are given here.

The slip-line method involves construction of a family of shear or slip lines in the vicinity of footing load. These slip-lines, which represent the direction of maximum shear stress, form a network known as slip-line fields. The plastic slip-line fields are bounded by regions that are rigid. For plane equilibrium and one equation for the yield conditions available for solving for the three unknowns stresses. These equations are written with respect to curvilinear coordinates that coincide with slip-lines. If the foundation boundary conditions are given only in terms of stresses, these equations are sufficient to give the stress distribution without any references to the stress-strain relationship. However, if displacement or velocity are specified over part of the boundary, then the constitutive relation must be used to relate the stresses to the strain and the problem becomes much more complicated. Although solutions may be obtained analytically, numerical and graphical methods are often found necessary (see Sokolovskii, 1965; Brinch Hansen, 1961, 1970).

The method described in the well-known textbook by Terzaghi (1943) and by Taylor (1948), or the method developed by Meyerhof (1951) are all classified here as method of limit equilibrium. They can best be describing as approximate approach to constructing the slip-line fields. The solution requires that assumptions be made regarding the shape of the failure surface and the normal stress distribution along such a surface. The stress distribution usually satisfies the yield conditions and the equation of static equilibrium in an overall sense. By trial and error, it is possible to find a most critical location of the assumed slip surface from which the capacity of the footing can be calculated.

In addition to the yield condition, the limit analysis methods consider the soil stress-strain relationship in an idealized manner. This idealization, termed normality or the flow rule establishes the limit theorem on which limit analysis is based. The methods offer an upper and lower bound to the true solution. The upper-bond solution is calculated from a kinematically admissible velocity field that satisfies the velocity boundary conditions and is continuous except at certain discontinuity surface where the normal velocity must be continuous, but the tangential velocity may undergo a jump on crossing a boundary. Similarly, the lower-bond solution is determined from a statically admissible stress field that satisfy the stress boundary conditions, is in equilibrium, and nowhere violates the failure condition. If the two solutions coincide, then the method give the true answer for the problem considered. A good treatment of the subject is given by Chen (1975) and Chen and Liu (1990).

The method describe above are related in a manner. Most of the slip-line solution give kinematically admissible velocity fields and thus can be considered as an upper-bond solution provided that the velocity boundary conditions are satisfied. If the stress field within the plastic zone can be extended into the rigid region so that the equilibrium and yield conditions are satisfied, then the solutions may be the exact solutions. Shield (1995) has shown this for many cases. The extensive work that has been done on the stability analysis, including using the slip-line methods, is summarized in the book by Sokolovskii (1965).

Limit equilibrium method utilized the basic philosophy of the upper-bound rule, that is, a failure surface is assumed and the least answer is sought. However, it gives no consideration to soil kinematics and the equilibrium conditions are satisfied only in limited sense. Therefore, limit equilibrium solutions are not necessarily an upper bound or lower bound. However, any upper-bound solution from limit analysis will obviously be a limit equilibrium solution. Nevertheless, the method has been the most widely used owing to its simplicity and reasonably good accuracy.

The limit analysis method itself has many striking features that should appeal to researchers, as well as engineers. The problem formulation is generally simple and an analytically solution is always assured. In simple problems, it has been shown to yield reasonable answer when compared to limit equilibrium solutions. Its capability of providing a mean for bounding the true solution is noteworthy. Finally, the method is efficient and can be extended to solve more difficult footing problems for which other method is efficient and can be extended to solve more difficult footing problem for which other method have so far failed.

2.2 SOIL GOVERNING PARAMETERS

The bearing capacity of footing depends not only on the mechanical properties of the soil (cohesion c and friction angle ϕ), but also on the physical characteristics of the footing (width B, depth D, length L, and roughness δ). For a coulomb material, Cox (1962) has shown that for a smooth surface footing bearing on a soil subjected to no surcharge, the fundamental dimensionless parameters associated with the stress characteristics equations are ϕ and $G = \gamma B/2c$, where γ is the unit weight of the soil. When G is small, the soil behaves essentially as a cohesive weightless medium. If G is large, soil weight rather than cohesion is a principal source of bearing strength. For most practical cases, one can expect that ϕ lies in the range of 0^o to 40^o and G will range from 0.1 to 1.0. These limits assume that c ranges from 500 to 1000 psf, and that the footing width ranges from 3 to 10 ft. the dimensionless bearing capacity q/c depends only on the angle of internal friction of the soil ϕ, the dimensionless soil weight parameter G, footing base friction angle δ, surcharge depth ratio D/B, and the base dimensions B and L.

For the most part, the bearing capacity of footing on soils have in the past been calculated by a superposition method, suggested by Terzaghi (1943) in which the contributions to the bearing capacity from different soil and loading parameters are summed. These contributions are represented by the expression, $q_o = c\ N_c + qN_q + \gamma BN_\gamma/2$, where q_o is the average pressure over the footing contact area A, q is the overburden or surcharge pressure at the foundation base and the bearing capacity factors Nc, Nq and Ng represents the effect due to soil cohesion, surface loading, and soil unit weight, respectively. Above equation is valid for strip footing subjected to vertical center loads. However, other geometries are common. The parameters N are all functions of the angle of internal friction ϕ. Terzaghi's quasiempirical method assumed that these effects are directly superposable, where the soil behavior in the plastic region is nonlinear and thus superposition does not hold for general soil bearing capacities. The reason for using the simplified (superposition) method is largely the mathematical difficulties encountered when using conventional equilibrium method.

2.3 TERZAGHI'S BEARING CAPACITY THEORY

In 1948, Terzaghi proposed a well-conceived theory to determined the ultimate bearing capacity of shallow rough rigid continuous (strip) foundation supported by a homogeneous soil layer extending to a great depth. Terzaghi defined a shallow foundation as a foundation where the width, B, is equal to or less than its depth, D_f. The failure surface in soil at ultimate load (that is, q_u, per unit area of the foundation) assumed by Terzaghi is shown in Fig. 2.1. Referring to Fig. 2.1, the failure area in the soil under the foundation can be divided into three major zones. They are:

1. Zone abc. This is a triangular elastic zone located immediately below the bottom of the foundation. The inclination of sides ac and bc of the wedge with the horizontal is $\alpha = \phi$ (soil friction angle).
2. Zone bcf. This zone is the Prandtl's radial shear zone.
3. Zone bfg. This zone is the Rankinr passive zone. This slip lines in this zone make angles of $\pm(45\text{-}\phi/2)$ with the horizontal.

Note that a Prandtl's radial shear zone and a Rankine passive zone are also located to the left of the elastic triangular zone abc; however, they are not shown in Fig. 2.2.

Line cf is an arc of a log spiral, defined by the equation

$$\mathbf{r = r_o\, e^{\theta \tan\phi}} \qquad (2.1)$$

Lines bf and fg are straight lines. Lines fg actually extends up to the ground surface. Terzaghi assumed that the soil located above the bottom of the foundation could be replaced by surcharge $q = \gamma D_f$.

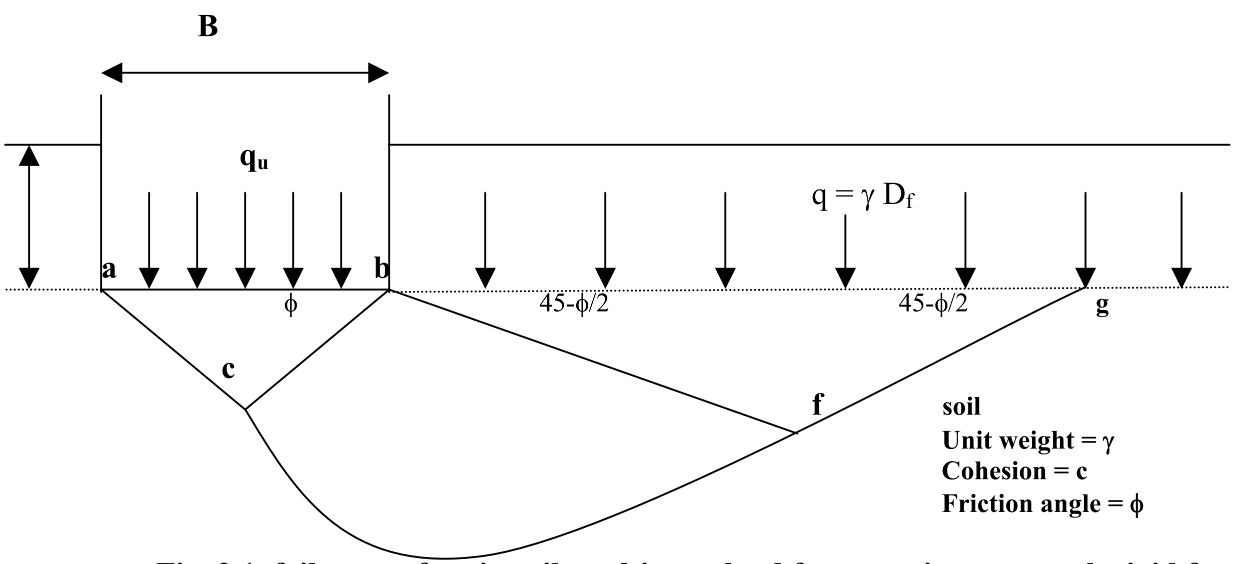

Fig. 2.1, failure surface in soil at ultimate load for a continuous rough rigid foundation as assumed by Terzaghi

The shear strength, s, of the soil can be given as

$$\mathbf{s = \sigma' \tan\phi + c} \qquad \mathbf{(2.2)}$$

Where σ' = effective normal stress

c = cohesion

The ultimate bearing capacity, q_u, of the foundation can be determined if we considered faces ac and bc of the triangle wedge abc and obtained the passive force on each face requires to cause failure. Note that the passive force P_p will be a function of the surcharge $q = \gamma\ D_f$. Cohesion c, unit weight γ, and angle of friction of the soil ϕ. So, referring to Fig. 2.2.

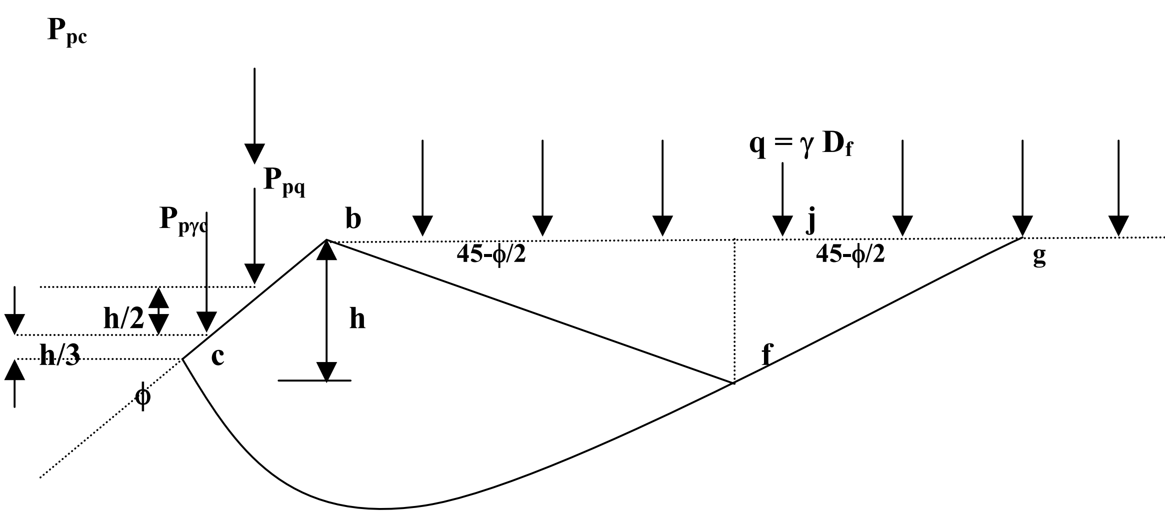

Fig. 2.2, Passive force on the face bc of wedge abc shone in figure 2.1

The passive force P_p on the face bc per unit length of the foundation at right to the cross section is

$$\mathbf{P_p = P_{pq} + P_{pc} + P_{p\gamma}} \qquad (2.3)$$

Where P_{pq}, P_{pc} and $P_{p\gamma}$ = passive force contributions of q, c and γ, respectively.

It is important to note that the directions of P_{pq}, P_{pc} and $P_{p\gamma}$ are vertical, since the face bc makes an angle ϕ with the horizontal, and P_{pq}, P_{pc} and $P_{p\gamma}$ must make an angle ϕ to the normal to bc. In order to obtain P_{pq}, P_{pc} and $P_{p\gamma}$, the method of superposition can be used; however, it will not be an exact solution.

Using the equilibrium analysis, Terzaghi express the ultimate bearing capacity in the form

$$\mathbf{q_u = cN_c + qN_q + \tfrac{1}{2}\,\gamma B N_\gamma} \text{ (strip foundation)} \qquad \textbf{(2.4)}$$

Where,

c = cohesion of soil

γ = unit weight of soil

$q = \gamma\, D_f$

N_c, N_q and N_γ = bearing capacity factors that are Nondimensional and only function of the soil friction angle, ϕ

The bearing capacity factors, N_c, N_q and N_γ are defined by

$$\mathbf{N_q = e^{2(3\pi/4 - \phi/2)\tan\phi} \Big/ 2\cos^2(45+\phi/2)} \qquad \textbf{(2.5)}$$

$$\mathbf{N_c = \cot\phi\,(N_q - 1)} \qquad \textbf{(2.6)}$$

$$\mathbf{N_\gamma = \tfrac{1}{2}\,(K_{p\gamma}/\cos 2\phi - 1)\tan\phi} \qquad (2.7)$$

Where , $K_{p\gamma}$ = passive pressure coefficient

The variation of bearing capacity factors defined by Eqs. 2.5, 2.6 and 2.7 are given in Table-2.1

Table- 2.1

Bearing-capacity factor for Terzaghi equations

Value of N_γ for f of 34 and 48° are orignal Terzaghi value and used to back-compute $K_{p\gamma}$

ϕ, deg	**N_c**	**N_q**	**N_γ**	**$K_{p\gamma}$**
0	5.7	1.0	0.0	10.8
5	7.3	1.6	0.5	12.2
10	9.6	2.7	1.2	14.7
15	12.9	4.4	2.5	18.6
20	17.7	7.4	5.0	25.0
25	25.1	12.7	9.7	35.0
30	37.2	22.5	19.7	52.0
34	52.6	36.5	36.0	59.5
35	57.8	41.4	42.4	82.0
40	95.7	81.3	100.4	141.0
45	172.3	173.3	297.5	298.0
48	258.3	287.9	780.1	650.6
50	347.5	415.1	1153.2	800.0

For estimating the ultimate bearing capacity of square or circular foundation Eq. (2.4) may be modified to (square footing) (circular footing)

$$q_u = 1.3\, cN_c + q\, N_q + 0.4\, \gamma\, B\, N_\gamma \quad \text{(square footing)} \qquad (2.8)$$

And

$$q_u = 1.3\, cN_c + q\, N_q + 0.4\, \gamma\, B\, N_\gamma \quad \text{(circular footing)} \qquad (2.9)$$

In Eq.(2.8), B equals the dimensions of each side of the foundation; in Eq. (2.9), B equals the diameter of the foundation.

For foundations that the local shear failure mode in soil, Terzaghi suggested modifications to Eqs. (2.4), (2.8) and (2.9) as follows:

$$\mathbf{q_u = 2/3\ cN'_c + q\ N'_q + \tfrac{1}{2}\ \gamma\ B\ N'_\gamma \qquad (strip\ foundation\ ) \qquad (2.10)}$$

$$\mathbf{q_u = 0.867\ cN'_c + q\ N'_q + 0.4\ \gamma\ B\ N'_\gamma \qquad (squar\ foundation) \qquad (2.11)}$$

$$\mathbf{q_u = 0.867\ cN'_c + q\ N'_q + 0.3\ \gamma\ B\ N'_\gamma \qquad (circular\ footing) \qquad (2.12)}$$

N'_c, N'_q and N'_γ are the modified bearing capacity factors. They can be calculated by using the bearing capacity factor equations (for N'_c, N'_q and N'_γ) by replacing ϕ by

$\phi' = \tan^{-1} (2/3 \tan \phi)$.

Terzaghi's bearing capacity equation have now been modified to take into account the effects of the foundation shape (B/L), depth of embedment (D_f), and the load inclination. This is given in tables in coming pages. Many design engineers, however, still use Terzaghi's equation, which provides fairly good results considering the uncertainty of the soil conditions at various sites.

2.3.1 ASSUMPTION AND LIMITATIONS IN TERZAGHI'S ANALYSIS

1. The soil is homogeneous and isotropic and its shear strength is represented by Coulomb's equation.
2. The strip footing has a rough base, and the problem is essentially two-dimensional.
3. The elastic zone has straight boundaries inclined at $\alpha = \phi$ to the horizontal, and the plastic zones fully develop.

4. Pp consists of three components, which can be calculated separately and added, although the critical surface for these components are not identical.
5. Failure zones do not extend the horizontal plane through the base of the footing, i.e. the shear resistance of soil above the base is neglected and the effect of soil around the footing is considered equivalent to a surcharge $\sigma = \gamma$ D.

LIMITATIONS

1. As the soil compressed, ϕ changes; slight downward movement of footing may not develop fully the plastic zones.
2. Error due to assumption 4 is small and on the safe side.
3. Error due to assumption 5 increases with depth of foundation, and hence the theory is suitable for shallow foundation only.

2.4 MEYERHOF'S BEARING CAPACITY EQUATION

Meyerhof (1951, 1963) proposed a bearing capacity equation similar to that of Terzaghi, but included a shape factor s_q for the depth term N_q. He also included depth factor d_i and inclination factor i_i for cases where the footing load is inclined from the vertical. This procedure equation of the general form shown on Table 2.1, with N factors in Table 2.4.

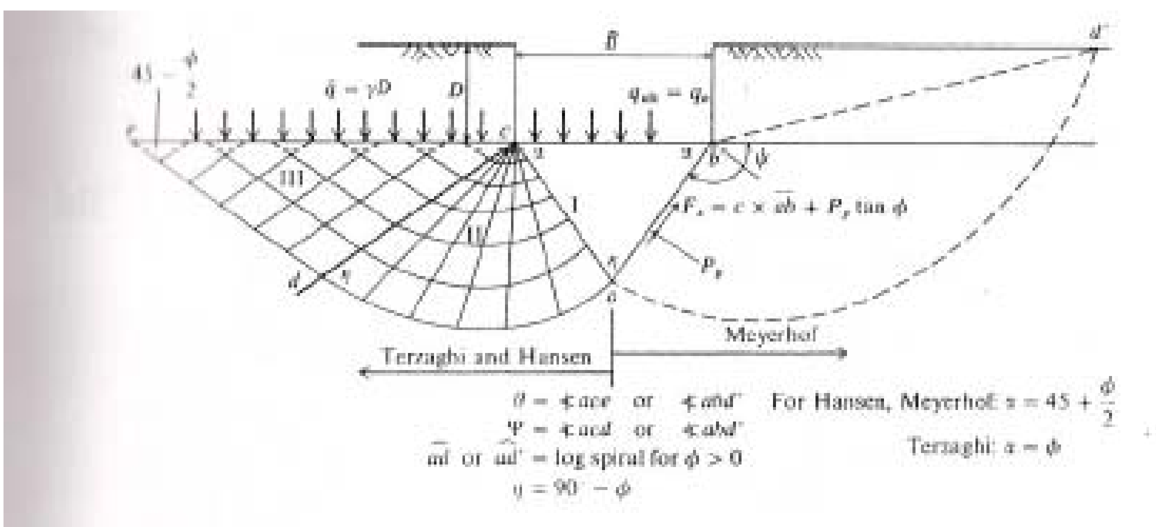

Fig2.3 General footing-soil interaction for bearing-capacity equations for strip footing- left side Terzaghi(1943), Hansen (1970), and right side Meyerhof (1951).

Meyerhof obtained his N factor by making trials of the zone abd' with arc ad', which includes an approximate for shear along cd of Fig 2.3a. The shape, depth and inclination factors in Table 2.3 are from Meyerhof (1963) and are somehow different from his 1951 valued. The shape factors do not greatly differ from those given by Terzaghi except for the addition of sq. observing that the shear effect along cd of Fig. 2.3a was being somewhat ignored, Meyerhof proposed depth factor d_i.

He also proposed using inclination factors to reduce the bearing capacity when the load resultant was inclined from the vertical by the angle θ.

Up to about D = B of Fig. 2.3a Meyerhof's q_u is not greatly differ from the Terzaghi value. The difference is more pronounced at larger D/B ratios.

Table 2.2 Bearing capacity equations by several authors indicated

TERZAGHI :

$$\mathbf{q_u = cN_c + qN_q + 0.5\gamma BN_\gamma\, s_\gamma}$$

$$N_q = a^2 / 2\cos^2(45+\phi/2)$$

$$a = e^{(0.75\pi-\phi/2)\tan\phi}$$

$$N_c = (N_q - 1)\cot\phi$$

$$N_\gamma = \tan\phi/2\ (K_{p\gamma}/\cos^2\phi \ - 1)$$

For:	strip	round	square
s_c =	1.0	1.3	1.3
s_γ =	1.0	0.6	0.8

MEYERHOF :

Vertical load : $\mathbf{q_u = cN_c\, s_c\, d_c + qN_q\, s_q\, d_q + 0.5\gamma BN_\gamma\, s_\gamma\, d_\gamma}$

Inclined load: $\mathbf{q_u = cN_c\, d_c\, i_c + qN_q\, d_q\, i_q + 0.5\gamma BN_\gamma\, d_\gamma\, i_\gamma}$

$$N_q = e^{\pi\tan\phi}\tan^2(45+\phi/2)$$

$$N_c = (N_q - 1)\cot\phi$$

$$N_\gamma = (N_q - 1)\tan(1.4\phi)$$

HANSEN :

General : $\mathbf{q_u = cN_c\, s_c\, d_c\, i_c\, g_c\, b_c + qN_q\, s_q\, d_q\, i_q\, g_q\, b_q + 0.5\gamma BN_\gamma\, s_\gamma\, d_\gamma\, i_\gamma\, g_\gamma\, b_\gamma}$

When $\phi = 0$

Use $q_u\ 5.14s_u(1 + s'_c + d'_c - I'_c - b'_c - g'_c) + q$

N_q = same as Meyerhof above

N_c = same as Meyerhof above

$N_\gamma = 1.5\,(N_q - 1)\tan\phi$

VESIC:

Use Hansen's equation above

N_q = same as Meyerhof above

N_c = same as Meyerhof above

$N_\gamma = 2(N_q + 1)\tan\phi$

Table 2.3 Shape, Depth and inclination factors for the Meyerhof bearing –capacity equation of Table –2.2

Factors	**value**	**for**
Shape :	$s_c = 1 + 0.2\,K_p\,B/L$	Any ϕ
	$s_q = s = 1 + 0.1\,K_p\,B/L$	$\phi > 10^o$
	$s_q = s_\gamma = 1$	$\phi = 0$
Depth:	$d_c = 1 + 0.2\,(K_p)^{1/2}\ D/B$	Any ϕ
	$d_q = d_\gamma = 1 + 0.1\,(K_p)^{1/2}\,D/B$	$\phi > 10$
	$d_q = d_\gamma = 1$	$\phi = 0$
Inclination:	$i_c = i_q = (1 - \theta^o/90^o)^2$	Any ϕ
	$i_\gamma = (1 - \theta^o/\phi^o)2$	$\phi > 0$
	$i_\gamma = 0$	$\phi = 0$

$K_p = \tan^2(45 + \phi/2)$

θ = angle of resultant measured from vertical without a sign

2.5 HANSENE'S BEARING CAPACITY METHOD

Hansen (1970) proposed the general bearing capacity case and N factor equation shown in Table 2.2. It can be readily seen that this equation is a further extension of the earlier Meyerhof (1951) work. Hansene's shape, depth, and other factors making up the general bearing capacity equation proposal in 1957 and 1961. The extension includes a factor for the footing being tilted from the horizontal b_i and for the possibility of the footing being on a slope g_i. Table 2.4 give selected N values for the Hansen equation together with the more difficult shape and depth factor aids.

Any of the equation not subscripted with a (V) may be used as appropriate (limitations and restriction are noted in the Table). When the value used in the inclination equation has the horizontal load component H parallel to B one should use B' with the N_γ term in the bearing capacity equation and if H is parallel to L use L' with N_γ. A further restriction is $i_i>0$ since a value of $i_i \leq 0$ is an unstable footing that requires resizing before proceeding. For a footing on clay with $\phi = 0$ compute i_c using H parallel to B and/or L as appropriate and note it is a subtractive constant in the modified bearing capacity equation.
We note that when the base is tilted V and H are perpendicular and parallel, respectively, to the base as compared with when it is horizontal.

For footing on a slope g_i factor are used to reduce the bearing capacity, however, these- as with the factor of Table 2.5 should be used cautiously as here is little experimental data available other than the work of Shields et. al. (1977) who used model footing on a sand box slope. It is difficult to see a field case where one would use a spread footing in a cohesionless soil slope unless the slope angle β is very and the footing depth D very large. In any case, since there are already shear stresses in the slop soil (holding the slop in place) one should not adjust any ϕ_{tr} to the large plane strain value and, additionally, one should use a large safety factor.

The Hansen equation implicitly allows ant D/B and thus can be used for both shallow (footing) and deep (piles, drill caisson) bases. Inspection of the qN_q term implies a great increase in q_{ult} with great depth. To place modest limits on this Hansen used

$$\left.\begin{aligned} d_c &= 1 + 0.4D/B \\ d_q &= 1 + 2\tan\phi(1 - \sin\phi)^2\, D/B \end{aligned}\right\} D/B \leq 1$$

$$\left.\begin{aligned} d_c &= 1 + 0.4 \tan^{-1} D/B \\ d_q &= 1 + 2\tan\phi(1 - \sin\phi)^2 \tan^{-1} D/B \end{aligned}\right\} D/B > 1$$

This gives a discontinuity at D/B = 1; however, note the use of ≤ and>. For f = 0, we have

D/B =	0	1	1.1	2	5	10	20	100
d_c' =	0	0.40	0.33	0.44	0.55	0.59	0.61	0.62

We can see that use of $\tan^{-1}$ D/B for D/B > 1 controls the increase in d_c and d_q in line with observation that q_{ult} appears to reach some limiting value at some depth ratio D/B where this value of D is often termed the critical depth.

2.6 VESIC'S BEARING CAPACITY EQUATIONS

The Vesic (1973, 1974) procedure that is essentially the Hansen method will be briefly noted. Essentially differences in this method are in using a slight difference N_γ (see table 2.4) and a variation on some of Hansen's i_i, b_i, and g_i factor as noted with the subscript (V) in Table 2.5. Any of the factor not subscribed with an (H) can be used for a Vesic solution. Note that some of the Vesic factors are less conservative than those of Hansen and since none of the methods have been extensively verified with full-scale field test one should exercise caution in their use.

Table 2.4

Bearing-capacity factors for the Meyerhof, 1951; Hansen, 1970; and Vesic, 1973 Bearing-capacity equations

Note that N_c and N_q are same for all three methods; subscript identify auther for N_γ

ϕ	N_c	N_q	$N_{\gamma(H)}$	$N_{\gamma(M)}$	$N_{\gamma(V)}$
0	5.14	1.0	0.0	0.0	0.0
5	6.49	1.6	0.1	0.1	0.4
10	8.34	2.5	0.4	0.4	1.2
15	10.97	3.9	1.2	1.1	2.6
20	14.83	6.4	2.9	2.9	5.4
25	20.71	10.7	6.8	6.8	10.9
26	22.25	11.8	7.9	8.0	12.5
28	25.79	14.7	10.9	1.2	16.7
30	30.13	18.4	15.1	5.7	22.4
32	35.47	23.2	20.8	22.0	30.2
34	42.14	29.4	28.7	31.1	41.0
36	50.55	37.7	40.0	44.4	56.2
38	61.31	48.9	56.1	64.0	77.9
40	75.25	64.1	79.4	93.6	109.3
45	133.73	134.7	200.5	262.3	271.3
50	266.50	318.5	567.4	871.7	761.3

Table 4-5

Shape, depth, inclination, ground and base factors for use in either the Hansen (1970) or Vesić (1973) bearing-capacity equations of Table 4-1. Factors apply to either method unless subscripted with (H) or (V). Use primed factors when $\phi = 0$

Shape factors	Depth factors	Inclination factors	Ground factors (base on slope)
$s'_c = 0.2 \cdot \dfrac{B}{L}$ $s_c = 1 + \dfrac{N_q}{N_c} \cdot \dfrac{B}{L}$ $s_c = 1$ for strip	$d'_c = 0.4k$ $d_c = 1 + 0.4k$	$i'_{c,H} = 0.5 - 0.5\sqrt{1 - \dfrac{H}{A_f c_a}}$ $i'_{c,V} = 1 - \dfrac{mH}{A_f c_a N_c}$ $i_c = i_q - \dfrac{1 - i_q}{N_q - 1}$ (Hansen and Vesić)	$g'_c = \dfrac{\beta^\circ}{147^\circ}$ for Vesić use $N_\gamma = -2 \sin \beta$ for $\phi = 0$ $g_c = 1 - \dfrac{\beta^\circ}{147^\circ}$
$s_q = 1 + \dfrac{B}{L} \tan \phi$	$d_q = 1 + 2 \tan \phi (1 - \sin \phi)^2 k$		$g_{q,H} = g_{\gamma,H} = (1 - 0.5 \tan \beta)^5$
		$i_{q,H} = \left(1 - \dfrac{0.5H}{V + A_f c_a \cot \phi}\right)^5$	$g_{q,V} = g_{\gamma,V} = (1 - \tan \beta)^2$
$s_\gamma = 1 - 0.4 \cdot \dfrac{B}{L}$	$d_\gamma = 1.00$ for all ϕ		**Base factors (tilted base)**
	$k = \dfrac{D}{B}$ for $\dfrac{D}{B} \le 1$ $k = \tan^{-1} \dfrac{D}{B}$ for $\dfrac{D}{B} > 1$ (rad)	$i_{q,V} = \left(1 - \dfrac{H}{V + A_f c_a \cot \phi}\right)^m$	$b'_c = \dfrac{\eta^\circ}{147^\circ}$ $b_c = 1 - \dfrac{\eta^\circ}{147^\circ}$
Where A_f = effective footing area $B' \times L'$ (see Fig. 4-4) c_a = adhesion to base = cohesion or a reduced value D = depth of footing in ground (used with B and not B') e_B, e_L = eccentricity of load with respect to center of footing area H = horizontal component of footing load with $H \le V \tan \delta + c_a A_f$ V = total vertical load on footing β = slope of ground away from base with downward = (+) δ = friction angle between base and soil—usually $\delta = \phi$ for concrete on soil η = tilt angle of base from horizontal with (+) upward as usual case General: 1. Do not use s_i in combination with i_i 2. Can use s_i in combination with d_i, g_i, and b_i 3. For $L/B \le 2$ use ϕ_{tr} For $L/B > 2$ use $\phi_{ps} = 1.5\phi_{tr} - 17$ For $\phi \le 34^\circ$ use $\phi_{ps} = \phi_{tr}$		$i_{\gamma,H} = \left(1 - \dfrac{0.7H}{V + A_f c_a \cot \phi}\right)^5$ $(\eta = 0)$ $i_{\gamma,H} = \left(1 - \dfrac{(0.7 - \eta^\circ/450^\circ)H}{V + A_f c_a \cot \phi}\right)^5$ $(\eta > 0)$ $i_{\gamma,V} = \left(1 - \dfrac{H}{V + A_f c_a \cot \phi}\right)^{m+1}$	$b_{q,H} = \exp(-2\eta \tan \phi)$ $b_{\gamma,H} = \exp(-2.7\eta \tan \phi)$ $b_{q,V} = b_{\gamma,V} = (1 - \eta \tan \phi)^2$
		$m = m_B = \dfrac{2 + B/L}{1 + B/L}$ H parallel to B $m = m_L = \dfrac{2 + L/B}{1 + L/B}$ H parallel to L	Notes: $\beta + \eta \le 90^\circ$ $\beta \le \phi$ 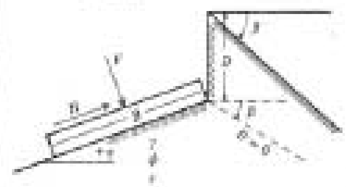
		Note: $i_q, i_\gamma > 0$	

2.7 NUMERICAL EVALUATION OF TERZAGHI'S N_γ

While developing the solution, Eq.2.4 and Fig.2.4, Terzaghi (1943) makes a series of assumptions (e.g., replacement of the soil located above the base of the footing by a uniform surcharge, limit equilibrium), separates contributions of c, q, and γ, and calculates q, by superposition. Key details of his procedure relevant to the present paper are briefly summarized here. Fig. 2.5(a) (after Terzaghi 1943) shows a shallow, strip footing with rough base resting on a horizontal surface. The soil below the footing is in a state of plastic equilibrium under general shear failure. Terzaghi uses Prandtl's mechanism to divide the body of soil *iecdh* into an elastic zone *abc,* I, and symmetric radial shear, II, and passive Rankine zones, III, and assumes that the radial shear zone is bounded by a log-spiral, $r = r_o e^{\theta \tan\phi}$ (*cd* in Fig. 2.5) failure surface. While calculating Arc and N_q, the log spiral is unique.

It is centered at the footing edge (point a in Fig. 2.5) and spans between *ac* and *ad,* which, respectively, make angles ϕ and 45 - ϕ/2 with the horizontal. Closed-form expressions for N_c and N_q are therefore easily obtained by taking moments of the forces acting on the block *acdf* about a. This log spiral proves unsatisfactory for calculating N_γ. Terzaghi therefore assumes that the center of the unknown failure surface spanning between *ac* and *ad* lies on *ad.* From the family of log spirals, he finds the critical failure surface, one which yields minimum passive pressure P_γ on the wedge *acdf,* Fig. 2.5(c), graphically by trial and error for a series of ϕ values, and provides a ϕ versus N_γ (Fig. 2.4) relation. The procedure, although tedious, is logical, since mathematical expression for obtaining the critical surface and its solution become formidable. Modifications to the original solution that enhance accuracy of (2.4) in many respects, still use the trial-and-error procedure for calculating N_γ. Graphical procedures in general have inherent limitations regarding accuracy and, the extent of accuracy of Terzaghi's solution is not known. The objective of this technical note is to present explicit analytical expressions for calculating N_γ, to provide results of their numerical solution and compare them with those of the graphical method.

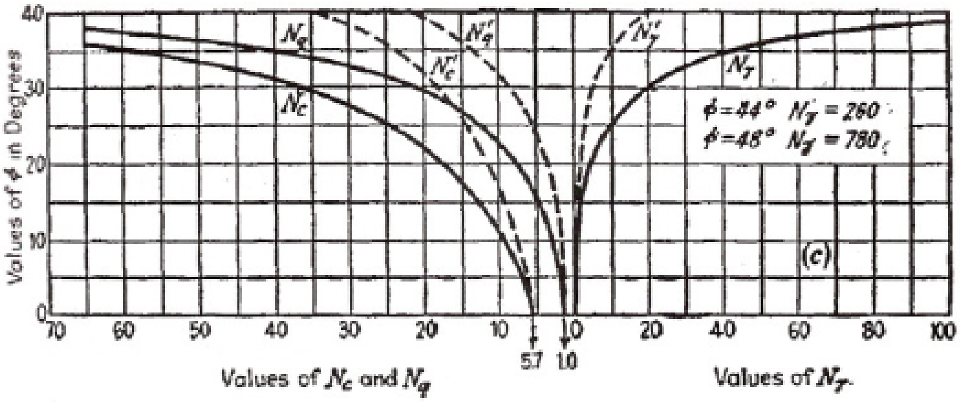

Fig. 2.4 Relation between f and Bearing-capacity Factor (After Terzaghi 1943)

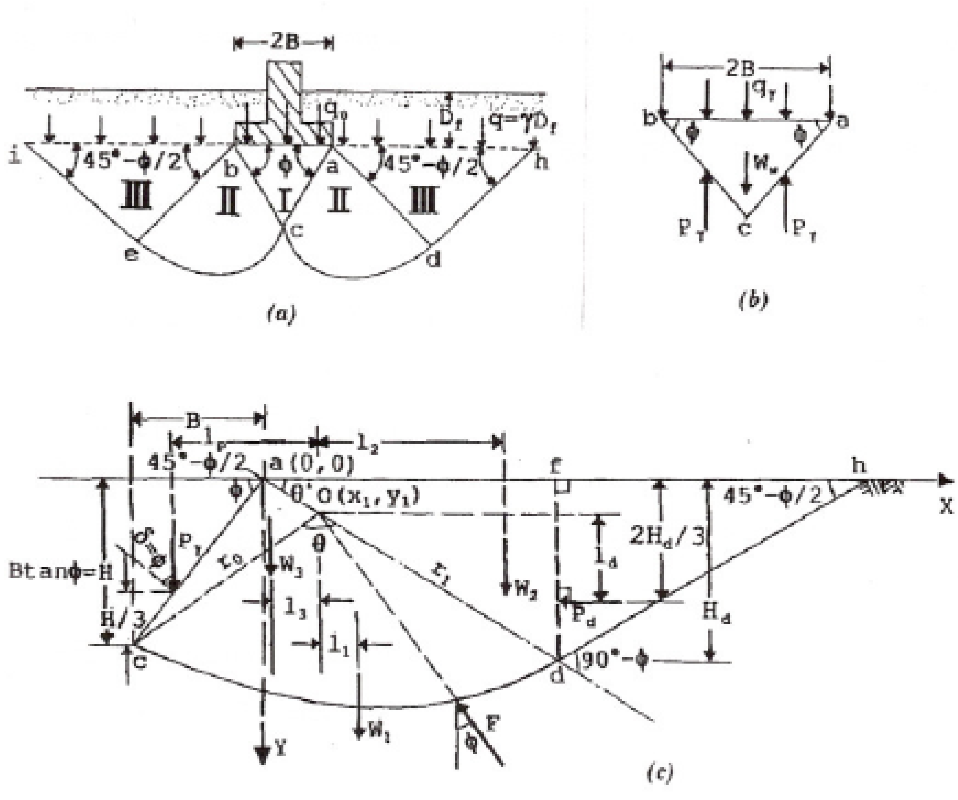

Fig. 2.5 Determination of P_γ ($\phi \neq 0$, $g \neq 0$, $q = 0$, $c = 0$) to calculate N_γ: (a) Geometry of strip footing and adjacent soil in limit equilibrium; (b) forces acting on elastic wedge due to self weight; (c) free-body diagram of wedge acdf.

2.7.1 NUMERICAL SOLUTION FOR N_γ (by kumbhojkar)

The condition for finding a log spiral that gives minimum P_γ can be easily described as $\partial P_\gamma/\partial \nu = O$, where v is any characteristic variable related to the log-spiral geometry such as a coordinate of the center of the log spiral or θ. Fig. 2.5, shows a trial log spiral *cd* with center $O(x_1,y_1)$ and angle *doc* = θ. The wedge *acdf* is in equilibrium under the forces W_1, W_2, W_3, P_d, F, and P_γ (per unit length of the footing) where

$$W_1 = \text{weight of the block ocd} = \gamma\ r_1^2 - r_o^2 / 4.\ \tan\phi \qquad (2.13)$$

$$W_2 = \text{weight of the triangle afd} = \gamma\ (r_1^2\cos\phi + 4\ r_1 x_1 \sin\theta^* + 2x_1^2\tan\theta^*)/4 \qquad (2.14)$$

$$W_3 = \text{weight of the triangle aco} = \gamma\ (\tan\phi + \tan\theta^*)x_1\ B/2 \qquad (2.15)$$

$$P_d = \text{Rankine passive earth pressure} = \gamma\ (x_1 + r_1\cos\theta^*)^2 / 2 \qquad (2.16)$$

F = resultant reaction of frictional force acting along the arc cd, which passes through O. P_γ = passive force component due to γ.

Taking moment about O, one gets P_γ as

$$P_\gamma = (W_1\ l_1 + W_2 l_2 - W_3 l_3 + P_d l_d) / l_p \qquad (2.17)$$

Where the lever arm l_1(Das 1987), l_2, l_3, l_d, and l_p are given by

$$l_1 = 4\tan\phi\{r_1^3(3\tan\phi\ \cos\theta^* - \sin\theta^*) + r_o^3[\sin(\theta+\theta^*) - 3\tan\phi\cos(\theta^* + \theta)]\}\ / 3(9\tan^2\phi + 1)(r1^2 - r_o^2) \qquad (2.18)$$

$$l_2 = 2r_1\cos\theta^* - x_1 / 3 \qquad (2.19)$$

$l_3 = x_1 – 2/3\ (x_1 – B)/2\ = 2x_1 + B/3$ (2.20)

$l_d = 2r_1 \sin\theta^* - x_1 \tan\theta^* / 3$ (2.21)

$l_p = x_1 + 2B/3$ (2.22)

All the quantities on the right-hand side of (2.17) are a function of variables x_1, the x-coordinate of the center of the log spiral, and r_o and r_l, the radii of the log spiral for $\theta = 0$ and $\theta = 0$. The quantities x_1, r_0, and r_l, in turn, can be expressed as a function of θ using geometrical relations.

$x_1 = -B/2 – (1+\sin\phi)\cot\theta B/2\cos\phi$ (2.23a)

$r_1 = (\tan\phi \cos\theta^* + \sin\theta^*)B\ e^{\theta\tan\phi} / \sin\theta$ (2.23b)

Substituting these values in (2.17) and rearranging the terms we get the following explicit expression:

$P_\gamma / \gamma B^2\ = \sum c_i\ t_i / c_8\ t_6 + c_9\ t_7$ (2.24)

$\partial Pg/\partial q\ = \ \gamma B^2/(c_8\ t_6 + c9\ t_7)^2 \sin^3\theta \quad \sum d_i\ u_i$ (2.25)

Coefficient c_i and terms t_i and terms d_i and u_i are respectively given in Table 2.6 and 2.7. The equations $\partial P_\gamma/\partial q\ =\ 0$ is solved numerically to obtained θ for $P_{\gamma min}$ $P_\gamma / \gamma B^2$ is obtained from (2.24) and Ng using Terzaghi;s equation

$N_\gamma = P_{\gamma min} / \gamma\ B^2\ - \tan\phi / 2$ (2.26)

Tables 2.8 and 2.9 provide values of N_γ along with the coordinates of the center and angles of the log-spiral for $\phi = 0^o$ to 53^o When ϕ becomes larger, N_γ becomes highly sensitive to ϕ; for $\phi > 35^o$ results are therefore given with an increment of 0.5^o.

Table 2.6, Terms and their Coefficients in Eq. (2.24)

Solution number (1)	Coefficient C_i (2)	Term t_i (3)
1	$c_1 = 3\tan\phi \cos^4\theta^* - \sin\theta^* \cos^3\theta^* / 3(8\sin^2\phi + 1) + \cos^4\theta^*/3 \cos\phi$	$t_1 = e^{3\theta\tan\phi}/ \sin^2\theta$
2	$c_2 = - \cos^2\theta^* /4$	$t_2 = e^{2\theta\tan\phi}/\sin\theta$
3	$c_3 = -(1 + \sin\phi) \cos^2\theta^* / 4\cos\phi$	$t_3 = e^{2\theta\tan\phi} \cos\theta/\sin^2\theta$
4	$c_4 = 2 \cos^4\theta^* + 3 \sin \phi \cos^2\theta^*/ 6(8\sin^2\phi + 1) + (1+\sin\phi)/8 - (1+\sin\phi)2/12\cos^2\phi$	$t_4 = 1/ \sin\theta$
5	$c_5 = \sin\theta^* \cos3\theta^* - 3 \tan\phi \cos^4\theta^* / 3(8 \sin^2\phi + 1) + (1+\sin\phi)2/ 24 \cos\phi$	$t_5 = \cos\theta/\sin^2\theta$
6	$c_6 = (1+ \sin\phi)2 / 12 \cos^2\phi + \cos^2\phi / 24(1+\sin\phi) - (1+\sin\phi)/8$	$t_6 = \sin\theta$
7	$c_7 = - (1+\sin\phi)/12 \cos\phi + \cos\phi/8 – (1+\sin\phi)2/ 24\cos\phi$	$t_7 = \cos\theta$
8	$c_8 = \cos\phi/6$	-
9	$c_9 = - (1+\sin\phi)/2$	-

Table- 2.7, Coefficients and Terms in Equation $\sum d_i u_i$

Solution no. (1)	Coefficient d_i (2)	Term u_i (3)
1	$d_1 = 3c_1 c_8 \tan\phi + c_1 c_9$	$u_1 = \sin^2\theta e^{3\theta\tan\phi}$
2	$d_2 = 3 c_1 c_9 \tan\phi – 3 c_{1\ c8}$	$u_2 = \sin\theta \cos\theta e^{3\theta\tan\phi}$
3	$d_3 = -2 c_1 c_9$	$u_3 = \cos2\theta e^{3\theta\tan\phi}$
4	$d_4 = 2 c_2c_8 \tan\phi – c_3c_8 + c_2c_9$	$u_4 = \sin^3\theta e^{2\theta\tan\phi}$
5	$d_5 = 2c_3c_8 \tan\phi + 2 c_2 c_9 \tan\phi – 2 c_2c_8$	$u_5 = \sin2\theta \cos\theta e^{2\theta\tan\phi}$
6	$d_6 = 2c_3 c_8 \tan\phi – c_2 c_9 – 3 c_3c_8$	$u_6 = \sin\theta \cos^2\theta e^{2\theta\tan\phi}$
7	$d_7= -2 c_{3\ c9}$	$u_7 = \cos^3\theta e^{2\theta\tan\phi}$
8	$d_8 = 2c_4 c_9 + 2c_5 c_8 – c_7 c_8 + c_6 c_9$	$u_8 = \sin^3\theta$
9	$d_9 = -3c_5 c_8 – c_4 c_9$	$u_9 = \sin\theta$
10	$d_{10} = -2 c_4 c_8$	$u_{10} = \cos\theta$
11	$d_{11} = 2 c_4 c_8 – 2 c_5 c_9$	$u_{11} = \cos^3\theta$

2.7.2 COMMENTS

The values given in Tables 2.8 and 2.9 match the plot in Fig. 2.4 exactly over its entire range: $\phi = 0^o$ to 39^o It is, however, a crude way of comparing since precision of this plot is lower than that of the numerical solution. With the exception of $N_\gamma = 36$, 260, and 780, respectively, for $\phi = 34^o$, 44^o and 48^o (Terzaghi 1943), it is not known whether explicit numerical values of N_γ used to plot Fig. 2.4 exist. The results presented in the present paper, therefore, can be compared with only these three values. For $\phi = 3^{4o}$ (38^o versus 36^o) and 44^o, the difference 261 versus 260 is negligibly small and accuracy of the graphical solution is excellent. The large difference, 650 versus 780, in N_γ for $\phi = 48^o$ is probably due to some small error in the graphical analysis magnified by the sensitivity of N_γ to ϕ since the angle that gives $N\gamma = 780$ is about 48.6^oAny interpolation between $\phi = 44^o$ and 48^o and extrapolation beyond $\phi = 48^o$ in Fig. 2.4 on the basis of $N_\gamma = 780$ are likely to include relatively large errors. Use of approximate methods similar to the graphical method to obtain N_γ are also likely to provide only approximately accurate answers. Bowles (1968), using a curve-fitting method, provides the only other set of numerical values of Terzaghi's N_γ for $\phi = 5^o$, 10^o . . . 50^o For $\phi < 20^o$ his values are approximately double of those given in Table 2.9 and for $\phi > 35$ they become smaller than those given in Table 4, although their accuracy is comparable to that of Fig. 2.4. Beyond providing explicit values and enhancing accuracy of N_γ, the analysis given here provides another distinct benefit: it defines log spirals demarking the radial shear zone for each qb.

A numerical solution for Terzaghi's bearing-capacity factor N_γ was presented. In addition to providing values of N_γ up to $\phi) = 53^o$ it also defined the geometry of the log spiral for each value of ϕ. The results showed that within the limits of accuracy of graphical method, Terzaghi's N_γ calculations agree with the almost-exact numerical results.

Table 2.8, Bearing Capacity Factor N_γ and Geometry Details of Log-Spiral Providing for $\phi = 0^o$ to 35^o

Solution Number	Friction Angle ϕ	Log-spiral Angle θ	Coordinate of center of log-spiral x_1/B	y_1/B	N_γ
1	0.0	-	-		0
2	1.0	88.833	-0.510	-0.502	0.014
3	2.0	90.910	-0.492	-0.475	0.035
4	3.0	92.494	-0.477	-0.453	0.063
5	4.0	93.753	-0.465	-0.434	0.099
6	5.0	94.782	-0.454	-0.416	0.144
7	6.0	95.637	-0.445	-0.401	0.200
8	7.0	96.356	-0.437	-0.387	0.267
9	8.0	96.966	-0.430	-0.374	0.348
10	9.0	97.486	-0.423	-0.361	0.444
11	10.0	97.931	-0.417	-0.350	0.559
12	11.0	98.311	-0.411	-0.339	0.694
13	12.0	98.637	-0.406	-0.329	0.854
14	13.0	98.916	-0.401	-0.319	1.041
15	14.0	99.152	-0.397	-0.310	1.262
16	15.0	99.352	-0.393	-0.301	1.520
17	16.0	99.519	-0.389	-0.293	1.822
18	17.0	99.656	-0.385	-0.285	2.175
19	18.0	99.768	-0.382	-0.277	2.589
20	19.0	99.855	-0.378	-0.270	3.074
21	20.0	99.921	-0.375	-0.263	3.641
22	21.0	99.968	-0.372	-0.256	4.305
23	22.0	99.996	-0.369	-0.249	5.085
24	23.0	100.009	-0.367	-0.243	6.000
25	24.0	100.006	-0.364	-0.237	7.076
26	25.0	99.989	-0.362	-0.231	8.342
27	26.0	99.960	-0.360	-0.225	9.836
28	27.0	99.918	-0.357	-0.219	11.602
29	28.0	99.866	-0.355	-0.214	13.636
30	29.0	99.804	-0.353	-0.208	16.175
31	30.0	99.732	-0.352	-0.203	19.129
32	31.0	99.652	-0.350	-0.198	22.653
33	32.0	99.563	-0.348	-0.193	26.871
34	33.0	99.467	-0.346	-0.188	31.035
35	34.0	99.363	-0.345	-0.183	38.035
36	35.0	99.253	-0.344	-0.179	45.410

Table 2.9, Bearing Capacity Factor N_γ and Geometry Details of Log-Spiral Providing for ϕ = 35.5^o to 53^o

Solution	Friction	Log-spiral	Coordinate of center of log-spiral		
Number	Angle ϕ	Angle θ	x_1/B	y_1/B	N_γ
1	35.5	99.196	-0.343	-0.177	49.666
2	36.0	99.137	-0.342	-0.174	54.360
3	36.5	99.077	-0.342	-0.172	59.541
4	37.0	99.015	-0.341	-0.170	65.266
5	37.5	98.952	-0.340	-0.168	71.599
6	38.0	98.888	-0.340	-0.166	78.614
7	38.5	98.822	-0.339	-0.164	86.392
8	39.0	98.755	-0.338	-0.162	95.028
9	39.5	98.687	-0.338	-0.159	104.627
10	40.0	98.618	-0.337	-0.157	115.311
11	40.5	98.548	-0.337	-0.155	127.219
12	41.0	98.477	-0.336	-0.153	140.509
13	41.5	98.404	-0.336	-0.151	155.363
14	42.0	98.331	-0.335	-0.149	171.990
15	42.5	98.257	-0.335	-0.148	190.628
16	43.0	98.181	-0.334	-0.146	211.556
17	43.5	98.105	-0.334	-0.144	235.091
18	44.0	98.028	-0.334	-0.142	261.603
19	44.5	97.951	-0.333	-0.140	291.521
20	45.0	97.872	-0.333	-0.138	325.342
21	45.5	97.793	-0.332	-0.136	363.647
22	46.0	97.712	-0.332	-0.134	407.113
23	46.5	97.632	-0.332	-0.133	456.532
24	47.0	97.550	-0.332	-0.131	512.836
25	47.5	97.468	-0.331	-0.129	577.119
26	48.0	97.385	-0.331	-0.127	650.673
27	48.5	97.302	-0.331	-0.125	735.026
28	49.0	97.218	-0.331	-0.124	831.990
29	49.5	97.133	-0.330	-0.122	943.723
30	50.0	97.048	-0.330	-0.120	1072.797
31	50.5	96.962	-0.330	-0.119	1222.294
32	51.0	96.876	-0.330	-0.117	1395.915
33	51.5	96.790	-0.330	-0.115	1598.120
34	52.0	96.703	-0.329	-0.113	1834.301
35	52.5	96.615	-0.329	-0.112	2111.003
36	53.0	96.528	-0.329	-0.110	2436.199

2.8 COMPUTATION OF BEARING CAPACITY FACTOR N_γ BY USING KOTTERS EQUATION

The analysis is primarily based on the computation of vertical (R_V) and horizontal (R_H) components of reaction R that acts on the curved part CD of the failure surface [Fig. 1(a)]. For this purpose, Kotter's equation (1903) is used.

2.8.1 KOTTER'S EQUATION

For a cohesionless soil medium, in passive state of equilibrium, Kotter's equation gives a solution for determining the distribution of soil reaction pressure p along the arc of the failure surface in the following form (Fig.2):

$$dp/ds + 2p \tan \phi \, d\alpha/ds - \gamma \sin(\alpha+\phi) = 0 \qquad (2.27)$$

in which dp = differential reactive pressure on the elemental length ds of the failure surface; α = angle made by the tangent to the failure surface at the point of interest with the horizontal; and ϕ = angle of soil internal friction. The applicability of Kotter's equation to the analysis of limit equilibrium problems has been demonstrated for a retaining wall problem (Coulomb's mechanism) for the case of a ponderable cohesionless soil by Dewaikar and Halkude (2002).

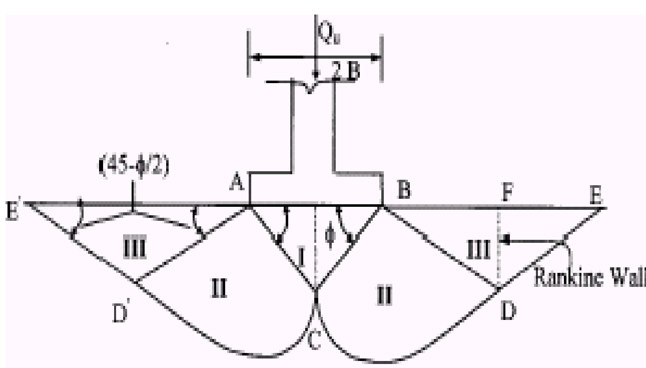

Fig. 2.6, Failure mecanisum-Terzaghi's analysis

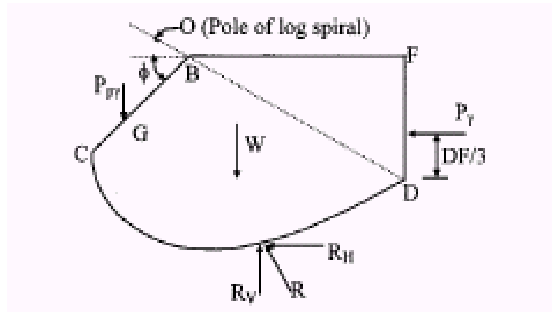

(b)

Fig. 2.7, Free body diagram of wedge CDFB

2.8.2 OUTLINE OF PROPOSED ANALYSIS

As shown in Fig.2.7, the known forces that act on the failure wedge CDFB are R_H, R_V, P_γ (passive Rankine thrust), W (weight of wedge CDFB), and unknown is only one force, i.e., the passive thrust $P_{p\gamma}$. Now, if the pole of the log spiral CD is correctly located, the calculated forces P_γ and R_H will be exactly equal to each other so as to satisfy horizontal force equilibrium, otherwise, they will be different. If they are different, the trial location of the pole along the line BD is changed and for this new location of the pole, R_H, R_V, W, and P_γ are again computed. Iterations are thus continued until the horizontal force equilibrium condition is satisfied to a specified decimal accuracy. After satisfying this condition, vertical force equilibrium condition is used to compute the desired value of $P_{p\gamma}$, from which N_γ is calculated.

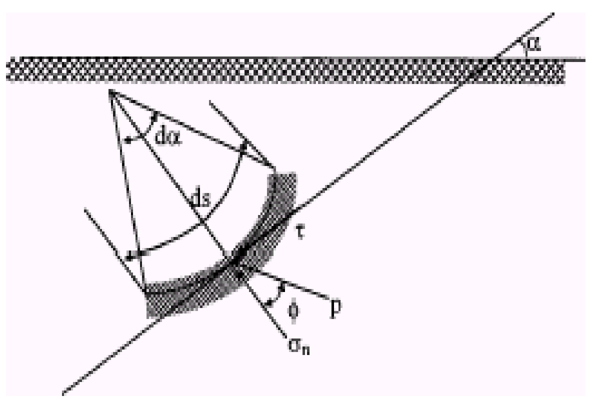

Fig. 2.8, Kotter's equation for cohesionless soil in passive state of equilibrium

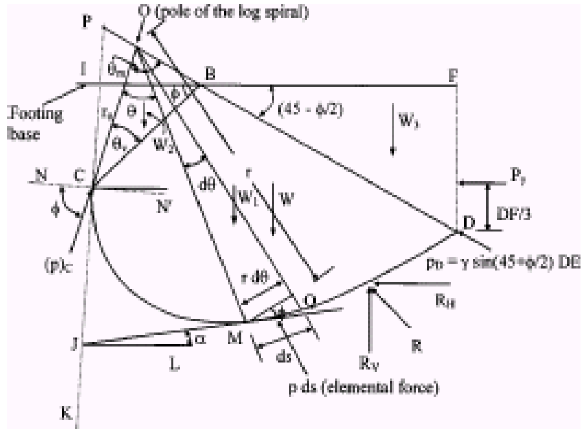

Fig. 2.9, Geometrical relationships for pole above footing.

2.8.3 INTEGRATION OF KOTTER'S EQUATION

As seen earlier [Fig. 2.6], the failure surface has two parts, namely, CD being part of the log spiral and DE its tangent.

2.8.3.1 INTEGRATION OVER PART DE OF FAILURE SURFACE

This part of the failure surface being straight, $d\alpha/ds = 0$ and Eq.(2.27) reduces to the following form:

$$\boldsymbol{dp/ds = \gamma \sin(\alpha+\phi)} \qquad (2.28)$$

Integration of the above equation gives the pressure distribution over the plane failure plane DE and the value of p at point D is calculated as

$$p_D = \gamma \sin(45+\phi/2)DE \qquad (2.29)$$

The distance DE depends upon the location of pole of the log spiral as shown in Fig. 2.6. Referring to Figs. 2.7 and 2.9, DE is calculated from the geometry of the failure wedge. With this substitution, Eq. (2.29) becomes

$$p_D = \gamma \sin(45+\phi/2)\, K r_o e^{\theta m \tan\phi} \qquad (2.30)$$

in which, r_o, θ_m, and θ_v are as shown in Fig. 3 and K is as given by the following expression:

$$K = [1 - \sin\theta_v/\sin(45+f/2)\, e^{\theta m \tan\phi}] \qquad (2.31)$$

2.8.3.2 COMPUTATION OF VERTICAL AND HORIZONTAL COMPONENTS OF REACTION R ON CURVED FAILURE SURFACE CD

For this purpose, wedge CDFB as shown in Fig. 2.7 is referred. The magnitude of passive Rankine thrust P_γ is given as

$$P_\gamma = 1/2\ \gamma(DF)^2\ (1+\sin\phi/1-\sin\phi) \quad (2.32)$$

The forces, R_H and R_V are calculated using Kotter's equation for a curved failure surface. For this purpose, Fig. 2.9 is referred.

Integration of Kotter's equation [Eq. (2.27)] gives the pressure distribution on the curved failure surface (Mohapatro 2001) and is given as

$$\begin{aligned}\mathbf{p} = \{&\gamma r_o K \sin(45+\phi) e^{(3\theta m - 2\theta \tan\phi)}\} + \\ &+\{(\gamma r_o \sec\phi e^{\theta\tan\phi} / 1 + 9\tan^2\phi)\ [3\tan\phi \sin(\theta - \theta_L + \phi) - \cos(\theta - \theta_L + \phi)]\} \\ &-\{\gamma r_o \sec\phi e\ (3\theta_m - 2\theta)\tan\phi / (1 + 9\tan^2\phi) \\ &X\ \{3\tan\phi \sin(\theta - \theta_L + \phi) - \cos(\theta - \theta_L + \phi)\}] \qquad (2.33)\end{aligned}$$

Where θ_L=(90-θ_v) and θ is as shown in Fig. 2.9. In deriving the above expression, reactive pressure at point D as given by Eq. (2.30) is used as a boundary condition.

2.8.3.3 COMPONENTS OF RESULTANT REACTION ON FAILURE SURFACE

The resultant reaction R on the failure surface is given as

$$R = \int p\, ds \qquad (2.34)$$

The vertical component R_V of the reaction is obtained as (Fig. 2.9)

$$R_V = \int p \cos(\theta - \theta_L + \phi)\, ds \qquad (2.35)$$

After substituting the value of p from Eq. (2.33) and value of ds from Fig. 2.9, R_V is obtained in the following form:

$$R_V = f_1 + f_2 + f_3 \qquad (2.36)$$

Similarly, the horizontal component R_H of the resultant reaction is given as (Fig. 2.9)

$$R_H = \int p \sin(\theta - \theta_L + \phi)\, ds$$

After substituting the value of p from Eq. (2.33) and performing integration R_H is obtained as

$$R_H = f_4 + f_5 + f_6 \qquad (2.37)$$

Where, f_1, f_2, f_3, f_4, f_5, and f_6 are –

$$f_1 = \gamma r_0^2 K \sin\left(45 + \frac{\phi}{2}\right) e^{3\theta_m \tan\phi}\left[e^{-\tan\phi\,\theta_m}\sin\left(45 - \frac{\phi}{2}\right) - \sin\left(45 - \theta_m - \frac{\phi}{2}\right)\right] \tag{21}$$

$$f_2 = \left[\frac{\gamma r_o^2 \sec\phi}{4(1+9\tan^2\phi)} 3\tan\phi\{e^{2\theta_m \tan\phi}\sin 2\phi + \sin 2(\theta_m - \phi)\}\right] - \left[\frac{\gamma r_o^2 \sec^2\phi}{4(1+9\tan^2\phi)}\left\{\begin{matrix} \frac{1}{\tan\phi}[e^{2\theta_m \tan\phi} - 1] \\ + \frac{1}{\sec\phi}[e^{2\theta_m \tan\phi}\cos 2\phi - \cos 2(\phi - \theta_m)] \end{matrix}\right\}\right] \tag{22}$$

$$f_3 = \frac{\gamma r_0^2 \sec\phi\, e^{3\theta_m \tan\phi}}{(1+9\tan^2\phi)}\left\{e^{-\theta_m \tan\phi}\left\{\sin\left(45 - \frac{\phi}{2}\right) - \sin\left(45 - \theta_m - \frac{\phi}{2}\right)\right\}\right\}\left\{3\tan\phi\sin\left(45 + \frac{\phi}{2}\right) - \cos\left(45 + \frac{\phi}{2}\right)\right\} \tag{23}$$

$$f_4 = \gamma r_o^2 K \sin\left(45 + \frac{\phi}{2}\right) e^{3\theta_m \tan\phi}\left\{\cos\left(45 - \theta_m - \frac{\phi}{2}\right) - e^{-\theta_m \tan\phi}\cos\left(45 - \frac{\phi}{2}\right)\right\} \tag{24}$$

$$f_5 = \left\{\frac{\gamma r_o^2 \sec^2\phi \tan\phi}{4(1+9\tan^2\phi)}\left[\begin{matrix} \frac{1}{\tan\phi}(e^{2\theta_m \tan\phi} - 1) \\ - \frac{1}{\sec\phi}(e^{2\theta_m \tan\phi}\cos(2\phi) - \cos(2\phi - 2\theta_m)) \end{matrix}\right]\right\} - \left\{\frac{\gamma r_o^2 \sec\phi}{4(1+9\tan^2\phi)}\{e^{\theta_m \tan\phi}\sin 2\phi + \sin(2\theta_m - 2\phi)\}\right\} \tag{25}$$

$$f_6 = -\frac{\gamma r_0^2 \sec\phi\, e^{3\theta_m \tan\phi}}{(1+9\tan^2\phi)}\left\{3\tan\phi\sin\left(45 + \frac{\phi}{2}\right) - \cos\left(45 + \frac{\phi}{2}\right)\right\}\left\{\cos\left(45 - \theta_m - \frac{\phi}{2}\right) - e^{-\theta_m \tan\phi}\cos\left(45 - \frac{\phi}{2}\right)\right\} \tag{26}$$

2.8.4 SELF WEIGHT OF WEDGE CDFB

This is obtained by calculating weight, W_1 of part OCD, W_2 of part OCB, and W_3 of part BDF as shown in Fig. 2.9. The required weight W (of part CDFB) is given as

$W = (W_1 - W_2 + W_3)$ (2.38)

In which

$W_1 = (\gamma r_o^2 / 4 \tan\phi)\,[e^{2\theta m \tan\phi} - 1]$ (39*a*)

$W_2 = 1/2\, \gamma r_o^2 \sin\theta_v \sin\theta_m / \sin(45+\phi/2)$ and (39*b*)

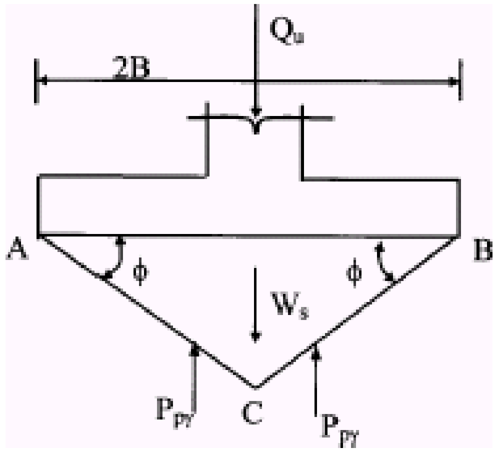

Fig. 2.10, Free body diagram of triangular wedge ABC for the determination of N_γ

$W_3 = 1/4\ \gamma r_o^2 K^2 e^{2\theta m \tan\phi} \cos\phi$ (39*c*)

2.8.5 COMPUTATION OF PASSIVE THRUST $P_{P\gamma}$

The passive thrust is obtained by using the two equations of force equilibrium (Fig.3) Vertical force equilibrium

$R_V - P_{p\gamma} - W = 0$ (40*a*)

Horizontal force equilibrium

$-R_H - P_\gamma = 0$ (40*b*)

The procedure of obtaining the desired value of $P_{p\gamma}$ has been described in the outline of the proposed analysis. The iterations were carried out till the computed values of $P\gamma$ and R_H matched with each other up to four decimal places. The computed values of $P_{p\gamma}$ and $N\gamma$ are therefore correct up to four decimal places. The computation further showed that the pole of the log spiral was located very close to the footing edge.

2.8.6 COMPUTATION OF N_γ

For this computation, Fig. 2.10 is referred, which shows the free body diagram of triangular wedge ABC (of Fig.2.6), subjected to forces Q_u (ultimate load), W_s (weight of the triangular soil wedge ABC), and $P_{p\gamma}$, the passive thrust.

The vertical force equilibrium gives

$Q_u + W_s = 2\ P_{p\gamma}$ (2.41)

After substituting the value of W_s, Eq. (2.41) becomes

$Q_u = 2\ P_{p\gamma} - \gamma B^2 \tan\phi$ (2.42)

Dividing the above expression throughout by 2B (footing width) yields the ultimate bearing pressure q_u, *which* is given as

$q_u = P_{p\gamma} / B - \gamma B/2\ \tan\phi$ (2.43)

On comparing Eq. (19) with Eq. $q_u = \gamma$ B N_γ, the bearing capacity factor N_γ is finally obtained as

$N_\gamma = P_{p\gamma} / \gamma B^2 - \tan\phi /2$ (2.44)

2.8.7 THE FOLLOWING MAIN CONCLUSIONS ARE DRAWN FROM THE PROPOSED ANALYSIS:

1. The concept of force equilibrium condition coupled with Kotter's equation identifies the unique failure surface, consistent with the specified failure mechanism.
2. Application of Kotter's equation makes the analysis statically determinate.
3. The $N\gamma$ values that are obtained from the proposed analysis based on Terzaghi's failure mechanism with the limit equilibrium approach are the unique values since; no other simplifying assumptions are made to evaluate them.
4. The $N\gamma$ values as obtained from the proposed analysis show a good agreement with experimental values and this establishes reliability of the proposed method of analysis.

Table – 2.10, Comparision of bearing capacity Factor, N_γ with other theories and Experimental results.

ϕ	Proposed analysis	Ingra & becher (1983)	Zadroga (1994)	Meyerhof (1963)	Baki & Beik (1970)	Hansen (1970)	Chen (1975)	Kumbh-ojkar (1993)	Frydman & Burd (1997)	Michal-owski (1997)	Soubra (1999)
25	8.363	14.570	22.307	6.764	12.8	6.758	12.409	8.342	-NA-	9.765	9.81
30	21.404	34.605	45.147	15.676	27	15.069	26.702	19.129	21.7	21.394	21.51
35	53.844	82.187	91.371	37.168	60	33.920	60.236	45.410	54.2	58.681	49.00
40	141.32	195.19	184.921	93.712	149	79.54	146.76	115.311	147.0	118.827	119.81
45	407.14	463.58	374.251	262.793	400	200.81	400.47	325.342	422.0	322.835	326.59

2.9 BEHAVIOR OF CIRCULAR FOOTINGS RESTING ON CONFINED GRANULAR SOIL

Raft foundations are widely used in supporting structures form any reasons such as weak soil conditions or heavy columns loads. In many cases, some problems arise such as the construction is adjacent to an old building and/or the foundation depth is so great that the excavation needs to be braced during foundation construction (e.g., basement excavation). One of the available solutions is to use sheet piles to support the excavation sides during construction. Due to the difficulty of removing these piles, they become part of the permanent structure and two problems arise. The first problem deals with the structural analysis of the raft if the piles are used as end supports for the raft. The second problem is the effect of these piles on the lateral movement of the soil underneath the raft and the effect of this confinement on the bearing capacity of the soil. While there are several solutions for the first problem, such as isolating the raft from the piles, the confining effect of these piles on the raft behavior is not clearly understood. Looking to the problem in a smaller scale, it can be modeled as a circular footing supported on a soil, which is surrounded by a confining cylinder. The strength of confined sand was studied by Rajagopal et al. (1999). They carried out a large number of triaxial compression tests to study the influence of geocell confinement on the strength and stiffness behavior of granular soils. Geocells fabricated by hand using different geotextiles were used to investigate the effect of the stiffness of the geocell on the overall performance of geocell soil composite.

The aim of this research is to model and investigate the effect of soil confinement by piles on the behavior of soil foundation system. Also, we studied the idea of improving the footing response by using confining cylinders around each individual footing. To achieve that objective, more than 35 tests were carried out with a wide range of variables as detailed in Table 2.11.

Table 2.11, Model Test Program

Test series	Constant parameter	Varible parameters
A	Test on unconfined sand	Test is repeated three times
B	d/D = 0.66 and u/D = 0.0	h/D = 0.5, 1.00, 1.5, 2.00
C	d/D = 1.07 and u/D = 0.0	h/D = 0.5, 1.00, 1.5, 2.00
D	d/D = 1.33 and u/D = 0.0	h/D = 0.5, 1.00, 1.5, 2.00
E	d/D = 1.60 and u/D = 0.0	h/D = 0.5, 1.00, 1.5, 2.00
F	d/D = 2.00 and u/D = 0.0	h/D = 0.5, 1.00, 1.5, 2.00
G	d/D = 2.66 and u/D = 0.0	h/D = 0.5, 1.00, 1.5, 2.00
H	d/D = 1.33 and h/D = 1.0	u/D = 0..0, 0.07, 0.13, 0.50, 1.0
I	d/D = 1.33 and h/D = 1.5	z/D = 0.0, 0.17, 0.33, 0.50, 0.67

2.9.1 LABORATORY MODEL TESTS

Model Box and Footing

Nine series of laboratory model tests were conducted in a test box, having inside dimensions of 0.90m x 30.50m in plan and 0.5 m in depth. The tank is made from steel with the front wall made of 20 mm thick glass and is supported directly on two steel columns as shown in Fig. 2.11. These columns are firmly fixed in two horizontal steel beams, which are firmly clamped in the lab ground using four pins. The loading system is mounted by a horizontal Standard I beam steel beam supported on the two columns. It consists of a hand-operated hydraulic jack and precalibrated load ring. Since the sand raining technique is used to deposit the sand inside the tank, the beam was designed to swing about one end. Therefore, the beam can be swung out during deposition of the sand from the sand raining box and returned back, when sand deposition is completed, to the original loading position above the tank. The sand-raining box is made from wood and is 0.85 m 30.38 m in plan and 0.10 m in depth. The sand particles rain from the box through a square grid of holes (4 mm diameter and 20 mm spacing) in the base plate. The height of sand raining, measured from the bottom of the box to sand surface in the tank, can be changed up or down by using a manual winch. A circular model footing made of steel with a hole at its top center was used. The footing is 75 mm in diameter and 10 mm in thickness. A rough base condition was achieved by fixing a thin layer of sand onto the base of the model footing with epoxy glue. The load is transferred to the footing through a ball bearing, which was placed, between the footing and the proving ring. Such an arrangement produced a hinge, which allowed the footing to rotate freely as it approached failure and eliminated any potential moment transfer from the loading fixture. An overall view of the apparatus is illustrated in Fig. 2.11.

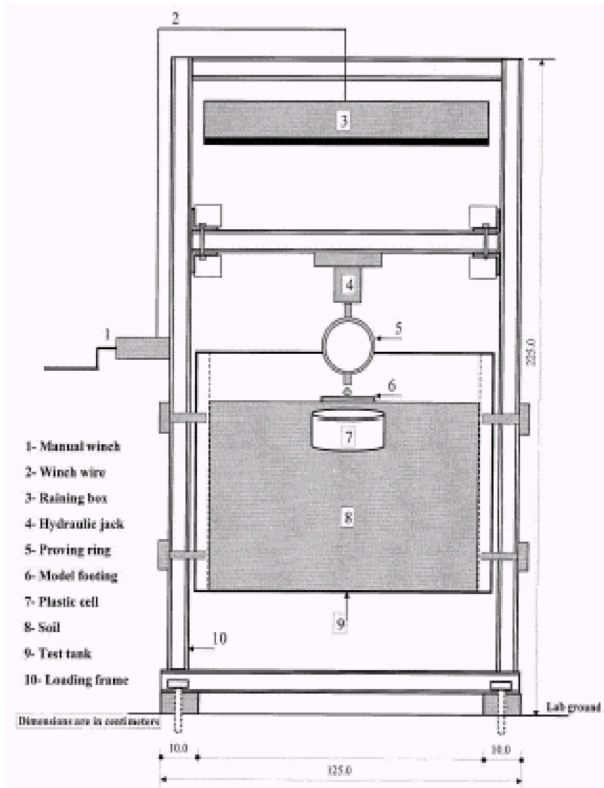

Fig. 1. Schematic view of the experimental apparatus

Fig.2.11, Schematic view of the experimental apparatus

2.9.2 TEST MATERIAL

The sand used in this research is medium to coarse sand, washed, Dried, and sorted by particle size. It is composed of rounded-to sub rounded particles. The specific gravity of the soil particles was determined by the gas jar method. Three tests were carried out producing an average value of 2.654. The maximum and the minimum dry densities of the sand were found to be 19.95 and 16.34 kN/m^3 and the corresponding values of the minimum and the maximum void ratios are 0.305 and 0.593, respectively. The particle size distribution was determined using the dry sieving method and the results are shown in Fig. 2.12. The effective size (D_{10}), uniformity coefficient (C_u), and coefficient of curvature (C_c) for the sand were 0.152 mm, 4.071, and 0.771, respectively. In order to set up a sample, the sand was poured in 50 mm in height layers by raining technique in which sand is allowed to rain through air at a controlled discharge rate and height of fall to give uniform densities. A series of tests were carried out to check the relative density obtained and uniformity of the sand samples by using three density molds placed at different locations in the test box. After pouring, each mold was carefully excavated and the density of the sample calculated. The raining technique adopted in this study provided a uniform relative density of approximately 75.8% with a unit weight of 18.94 kN/m^3. The results also showed that the obtained relative densities from the three samples did not depend on the position of the mold. A series of direct shear tests were performed at the same relative density of the sand and the estimated internal friction angle was approximately 42°.

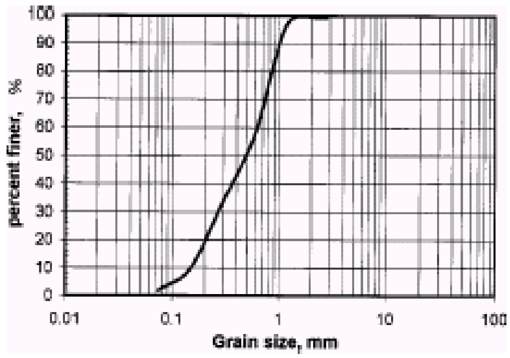

Fig. 2. Grain size distribution of the sand

Fig. 2.12, Grain size distribution of the sand

The confining elements were made of unplasticized polyvinylchloride (UPVC) Cylinders with different diameters and heights. The used diameters were 50, 80, 100, 120, 150, and 200 mm. UPVC is produced from the polymerization of a vinyl chloride monomer with certain additives including heat stabilizers and lubricants. Its actual strength for any situation depends on the wall thickness uniformity, the rate of loading, and the temperature of plastic materials. The interior and exterior surfaces of the cylinders were made very smooth. The thickness of the cylinder wall is 2.5 mm and its properties as given by the manufacturer are shown in Table 2.12. Some of the tests were carried out by introducing the UPVC cylinders initially in position and then a sand bed was placed by raining. The ultimate loads were determined and compared with those of tests performed with cylinders installed vertically after setting sand samples. The difference of the ultimate loads in the two cases was found to be less than 1.5% and load–settlement relationships were approximately of the same pattern. Therefore, it was decided to carry out the entire test program using only one method by installing the cylinders vertically after setting sand beds, and considering the difference in the relative densities of the samples resulting from installing cells with different diameters and heights to be small and negligible.

Table 2.12, Properties of the Unplasticized Polyvinyle Chloride Cylinder

Maximum hydraulic pressure for 1 h at 23°C Bar	23
Specific gravity	1.4
Tensile strength, 10^3 Kpa	55
Tensile modulus, 10^5 Kpa	28
Water adsorption at 100°C for 24 h, mg/cm^2	4

2.9.3 EXPERIMENTAL SETUP AND TEST PROGRAM

After the sand surface was set up, the cells were pushed vertically into the sand at the design place, the footing was placed on position, and the load was applied on it by the hydraulic jack. The load was applied in small increments until reaching failure. Each load increment was maintained constant until the footing settlement had stabilized. The settlements of the footing were measured using two dial gauges placed on opposite sides of the footing. The geometry of the soil, model footing, and confining cylinder are shown in Fig. 2.13. The test program consisted of carrying out nine series of tests on the circular model footing to study the effect of soil confinement on the soil–foundation response as shown in Table 1. Initially, the behavior of the footing supported on the unconfined conditions was determined. Then, each series of the tests was carried out to study the effect of one parameter while the other variables were kept constant. The studied variables are the cell height (*h*) and cell diameter (*d*) for cases when the cells are placed under the foundation level and the embedded depth (*z*) for cases when the foundation level is lower than the cell top. Several tests were repeated at least twice to verify the repeatability and the consistency of the test data.

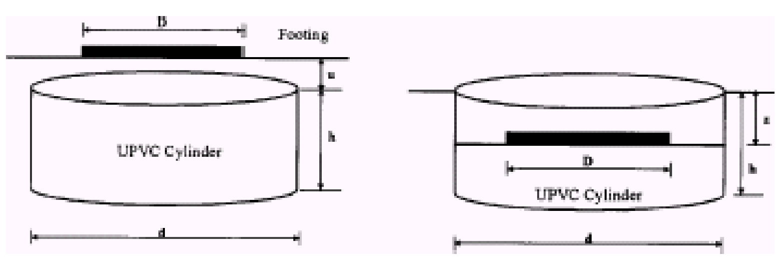

Fig. 3. Geometric parameters of confined sand-foundation model

Fig. 2.13, Geometric parameters of confined sand-foundation model

2.9.4 RESULTS AND DISCUSSION

The load–settlement relationship and the ultimate bearing capacity of the footing with and without confinement were obtained. The bearing capacity improvement due to the soil confinement is represented using a nondimensional factor, called the bearing capacity ratio (BCR). This factor is defined as the ratio of the footing ultimate load with soil confinement to the footing ultimate load in tests without confinement. The footing settlement (*S*) is also expressed in nondimensional form in terms of the footing diameter (*D*) as the ratio (*S*/*D*,%). The measured ultimate load and the associated ultimate displacement for the nonconfined case are 250 N and 5.24 mm, respectively. The theoretical ultimate bearing capacity can be calculated from the equation $q_o = 0.5\ \gamma\ D\ \zeta_\gamma N$. Using the shape factor proposed for circular footing by De Beer (1970) (ζ_γ=0.6) and the values of the bearing capacity factor $N\gamma$ taken from Meyerhof (1963) (N_γ=139.3) or Hansen (1968) (N_γ =136.7), the theoretical bearing capacities are 59.36 kPa (262 N) and 58.25 kPa (257 N), respectively. These data show a close agreement between both the theoretical values and the experimental results. Typical variations of bearing pressure with footing settlement ratios (*S*/*D*) with and without soil confinement for different heights of confining cells are presented in Fig. 2.14. It can be seen that the installation of confining cylinders appreciably improves the bearing capacity of the footing as well as the stiffness of the foundation bed. It is apparent from the curves that the mode of failure is a general shear failure in which a pronounced peak can be observed in the load–settlement curve, after which the footing collapses and the load decreases (Vesic 1973). Also, the value of the settlement ratio *S*/*D* at the ultimate load in the confined tests varied from about 12% to 18%. The observed improvement in the bearing capacity loads due to soil confinement along with the increase in the settlement ratio was reported by many investigators when using soil reinforcement (Omar et al. 1993a,b; Das et al. 1996). Comparing the curves of Fig. 4 at the ultimate *S*/*D* ratio of the unconfined case (the values across the dotted line, *S*/*D* = 7%), it can be seen that soil confinement improved the bearing load from 56.59 kPa for the unconfined case to 562.5 kPa for the confined soil using cells with a *d*/*D* ratio of 1.33 and *h*/*D* ratio of 2.0. Therefore, it can be concluded that, in cases when the excessive settlement is the controlling factor in determining the allowable bearing capacity, using confining cells may significantly decrease the settlement ratio for the same level of bearing load.

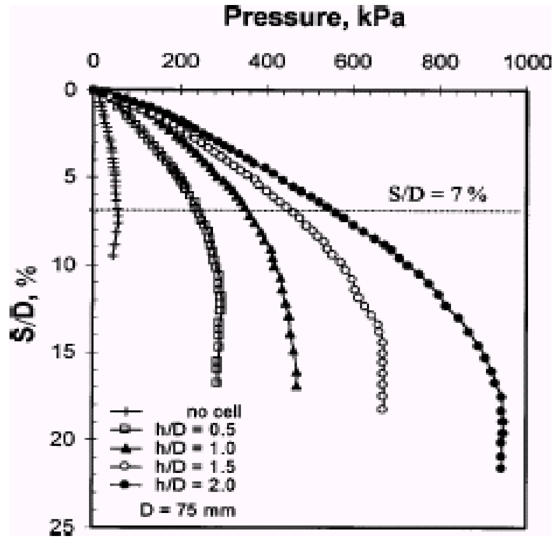

Fig. 4. Variation of bearing pressure with (S/D) ratio for different cell heights (Series D)

Fig. 2.14, Variation of bearing pressure with (S/D) ratio for different cell heights (Series D)

2.9.5 EFFECT OF CELL DIAMETER

In order to investigate the effect of cell diameter on the footing behavior, six cells with diameters of 50, 80, 100, 120, 150, and 200 mm were used. Fig. 5 shows the variation of BCR with normalized cell diameter for different cell heights with a constant footing diameter of 75 mm. A significant increase in the bearing capacity of the model footing supported on confined sand with the increase of normalized cell diameter d/D is observed until a specific value of d/D after which the BCR decreases with an increase in the d/D ratio. While conducting the model tests, it was observed that as failure approached in tests carried out with small cell diameters, sand inside the cell and the cell behaved as one unit (when the load was increased, the cell, sand, and footing settled altogether). In tests carried out with large cell diameters, this behavior was noticed initially,

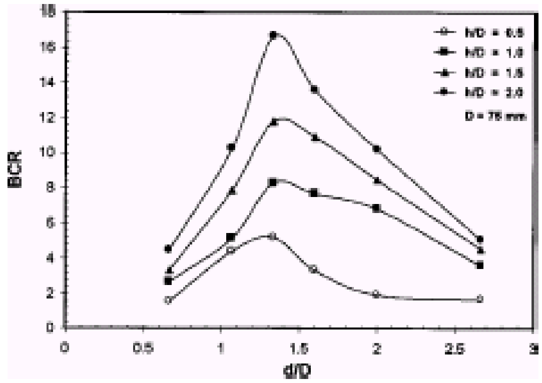

Fig. 5. Variation of bearing capacity ratio with normalized cell diameter (d/D) for different cell heights

Fig. 2.15, Variation of bearing capacity ratio with normalized cell diameter (d/D) for different cell height.

But as the load was increased it was no longer observed (the footing settled down while the cell was unaffected with the increase of the load). Fig. 2.15 also shows that using soil confinement could result in an improvement in bearing capacity as high as 17 times more than that without soil confinement. It is clear that the best benefit of soil confinement could be obtained with a (d/D) ratio between 1.0 to 2.0 with the maximum improvement in the bearing capacity at a ratio of about 1.4 for different heights of confining cells. This significant increase in the bearing capacity of the footing can be explained with the aid of Fig. 6 as follows. When the footing is loaded, such confinement resists the lateral displacements of soil particles underneath the footing and confines the soil leading to a significant decrease in the vertical settlement and hence improving the bearing capacity. For small cell diameters, as the pressure is increased, the plastic state is developed initially around the edges of the footing and then spreads downward and outward. The mobilized vertical frictions between the sand and the inside wall of the cylinder increase with the increase of the acting active earth pressure until the point when the system (the cylinder, sand, and footing) starts to behave as one unit. The behavior is similar to that observed in deep foundations (piles and caissons) in which the bearing load increases due to the shear resistance of cell surface. This illustrates the increase of the bearing load with the increase of the cell diameter and cell height. Based on tests performed with cells made with very smooth surfaces, it can be concluded that increased surface roughness results in greater bearing load improvement. In comparison to this response, sand beds at relative density of 70% and reinforced with a geocell mattress carried out by Dash et al. (2001b) mobilized bearing capacity pressure as high as eight times the ultimate capacity of the unreinforced sand. Also, tests on sand beds at a relative density of 75% and reinforced with planar reinforcement carried out by Omar et al. (1993a,b) and Khing et al. (1993) failed with clearly pronounced peak loads of about five times the ultimate capacity of unreinforced soil at settlements equal to about 20% of the footing width.

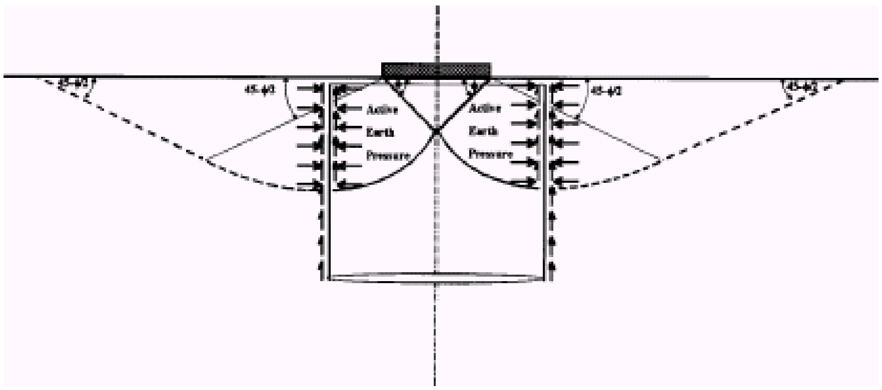

Fig. 6. Intersection of failure surface with the cylinder

Fig. 2.16, Interaction of failure surface with the cylinder

2.9.6 EFFECT OF CELL HEIGHT

In order to investigate the effect of cell height on the footing response, tests were carried out using four different heights for each cell diameter. The variation of BCR with normalized cell height (*h*/*D*) is shown in Fig. 7 for different normalized cell diameters (*d*/*D*). The figure shows the same pattern of behavior for the different cell diameters. Increasing cell heights results in a greater improvement in the BCR. This increase in cell height results in the enlargement in the surface area of the cell–model footing leading to a higher bearing capacity load. The slope of the BCR versus *h*/*D* curves for *d*/*D* ratios of 0.67 and 2.67 are less than the comparable slopes for *d*/*D* ratios of 1.33 and 1.6. This trend confirms the previous conclusion that the greatest benefit of cell confinement can be obtained at a *d*/*D* ratio of about 1.4.

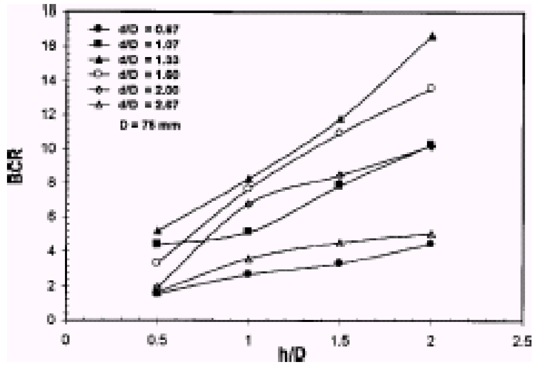

Fig. 7. Variation of bearing capacity ratio with normalized cell height (h/D) for different cell diameters (d)

Fig. 2.17, Variation of bearing capacity ratio with normalized cell height (h/D) for different cell diameter(d)

2.9.7 EFFECT OF THE SOIL PRESSURE ON THE CELL

One of the proposed parameters to be investigated was the thickness of the cell wall to study the effect of the cell rigidity on the footing–cell system behavior and also to study the hoop tension in the cell wall due to the pressure under the footing. However, according to the manufacturer data, the supplied cell with a wall thickness of 2.5 mm can withstand internal hydraulic pressure of 23 bars (2,300 kPa) with maximum tensile strength of the wall of 55,000 kPa. In the model tests, the most critical case occurs with h/D=2 and d/D=1.33 at failure vertical pressure of 950 kPa. The horizontal pressure acting on the sidewall of the cell is equal to the vertical pressure multiplied by the coefficient of lateral earth pressure. It can be seen that the maximum estimated horizontal earth pressures on the sidewalls of the cell are very small in comparison to the allowable hydraulic pressure. Another point is that the given allowable value is the net inside pressure while the cell in the model is subjected to both internal and external pressures. Checks were performed after each test to observe any change in the cell wall and measurements were taken to check the internal diameter as well as the thickness of the cell wall. There was no noticeable change in the cell or its dimension. Therefore, it was concluded that for the given model and dimensions, the pressures under the footing have no disturbing effects on the cell wall and, therefore, it was decided to use them again.

2.9.8 CONCLUSIONS

Soil confinement has a significant effect on improving the behavior of circular footing supported on granular soil. The ultimate capacity was found to increase by a factor of 17 as compared to the unreinforced case. Therefore, it can be concluded that the piles (or sheet piles) used to brace cuts have a significant effect on improving the bearing capacity of soils under raft foundations. However, more research in this area is required to study cases in which piles are constructed only on one, two, or three sides. Also, theoretical analysis is needed to modify the bearing capacity equation to consider the effect of pile confinement. Based on the experimental results, soil confinement could be considered as a method to improve the bearing capacity of isolated footings bearing on medium to dense sand. UPVC cells with different heights, diameters, and thickness could be easily manufactured and placed around the individual footings leading to a significant improvement in their response.

2.10 BEARING CAPACITY OF A JACKUP SPUDCAN FOOTING

The ultimate bearing capacity of a flat surface footing, as discussed in the previous articles is depend upon the footing soil interaction under vertical, horizontal and inclined loading which governs the stability of the footing. In this article we shall consider the stability of jackup spudcan footing and calculate its ultimate bearing capacity.

The growing use of mobile jackup units on spudcan footing in deep offshore waters has raised a great deal of concern about the overall stability of jackup unit in hostile environmental forces. The stability of a jackup unit is greatly influenced by the performance of a typical spudcan footing under storm loading conditions. Therefore, as a result, much research has been focused towards the study of a spudcan footing behavior subjected to combined vertical and horizontal loading. Recently, over a period of several years, a joint industry study coordinated by Noble Denton Association has been considered many aspects of jackup stability including the soil-structure interaction (Houlsby and James, 1991).

Mobile jackup units consist of a floatable drilling platform, supported on three or more legs, which can be raised or lowered (see figure 2.18). A detailed description of the installation procedure is given by Tan (1990). The platform legs can either be supported separately as shown in Figure 8.1a or they can be supported on a single shared mat.

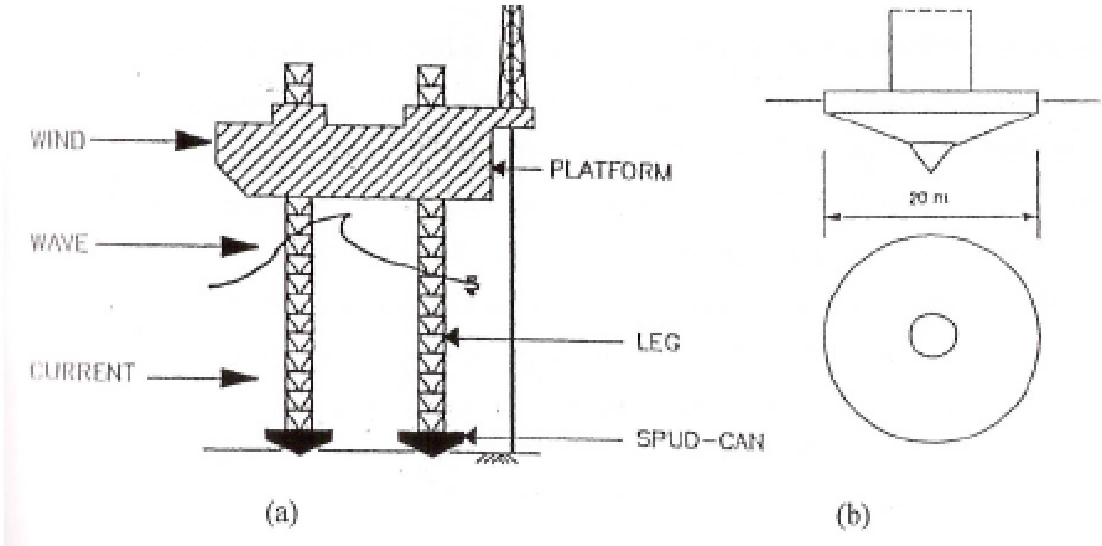

Figures show (a) Jackup platform and environmental loads. (b) Spudcan footing.

Most modern jackup unit platforms are former type and have approximately conical shaped footing with a protruding tip at the center. These are commonly referred to as ‘spudcan’ footings (see Fig. 2.18 b)

The mobility of jackup units allows for relocating and reuse of platforms. Before actual oil and gas exploration activity begins, the legs of the platform are preloaded to almost twice the working load. During this loading operation, spudcan footing moves into the seabed to a depth of almost twice its diameter. In soft clays, a 30m penetration of a 15m-diameter spudcan is not uncommon. The bearing capacity with footing embedment is an important factor, since even a small embedment can significantly increase the bearing capacity of such offshore footing (Houlsby and Martin (1993)). However, this is not usually the case in coarse material as penetration depths are typically very small (see e.g. Dean et al. (1993)).

In addition to the vertical load of the jackup structure, a spudcan footing is also subjected to large horizontal forces due to severe environmental conditions reaching, in stormy weather, up to 30% of the total vertical load and thereby producing a corresponding large moment (Poulos (1988)).

In this article we are making a conventional assumption, that a jackup leg is pinned at the foundation level and that therefore a spudcan footing offers no moment restraint to the leg (see Fig. 2.19a). This means that, only the interaction between horizontal and vertical loading need to be studied. Although, in recent studies moment restraint at the footing has also been considered which would reduce the bending moment in the lower leg guide (see Fig. 2.19b), which is often a critical feature of the structure in extreme loading conditions: a full interaction between vertical, horizontal and moment loading has been studied by e.g. Houlsby and Martin (1993) for clays, and Dean et al. (1993) for sands.

We discuss here the ultimate bearing capacity of a partially penetrated spudcan footing subjected to combined vertical and horizontal loading.

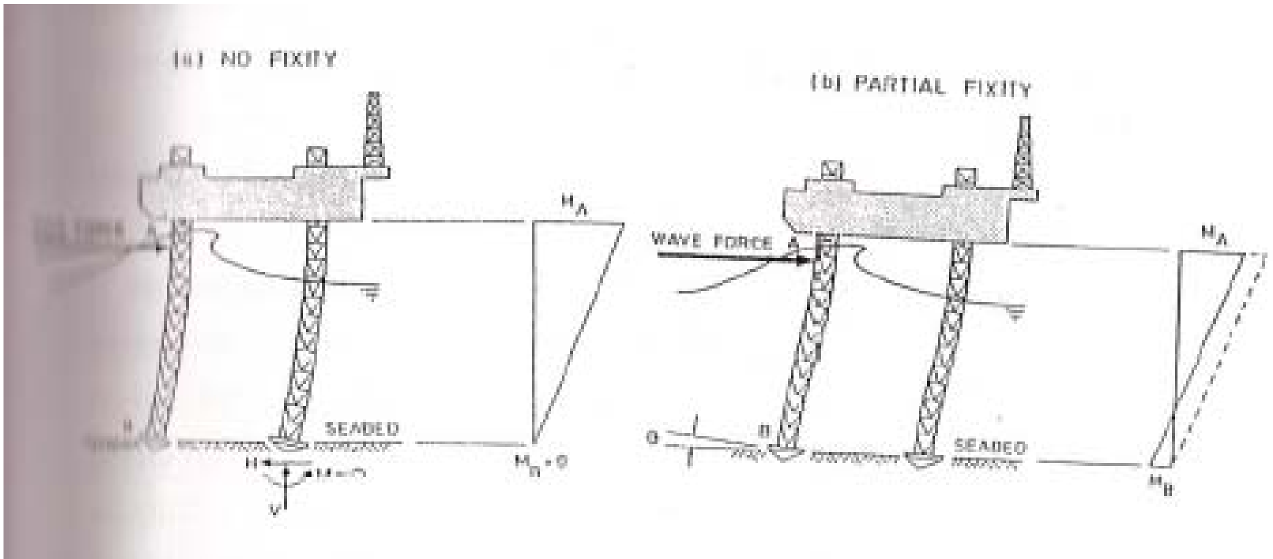

Fig 2.19: Bending moment in the legs of Jack-up units

2.10.1 BACKGROUND

The bearing capacity solution of Meyerhof (1953), Hansen (1970) and Vesic (1975) are commonly used to determine the ultimate bearing capacity pf plan strain footing. These solutions are modified by introducing shape factors to cover circular geometries (see e.g. (1992), Dean et al. (1993)). In the case of spudcan footings, their embedded circular area in plane (i.e. plan area at ground surface) is used for the bearing capacity solutions to spudcan footings, theoretical and experimental studies of conical shaped footings (based on centrifuge model tests) have been undertaken by Cambridge University Engineering Department over a several years. In this study, a series of test of cone angle O^o (flat), 13^o, 20^o, 25^o and 35^o was conducted on sand at 28.3mm diameter model footing at 56.6g, repressing 1.6m prototype in the drum centrifuge. It is shown in the study that spudcan footing can be treated as equivalent cones enclosing the same volume. The load displacement response of a spudcan footing and an equal volume cone is almost identical. The ultimate bearing capacity of these footings for vertical loading only, combined horizontal-vertical (inclined) loading, vertical-moment (eccentric) loading and lateral-moment loading has been determined. The results are compared with existing bearing capacity theories and analytical solutions were possible. The study show that the vertical bearing capacity does not vary much for cone angles between O^{o}-20^{o}. However, foe flat circular footings under combined vertical – horizontal loading (referred as shear sidewipe tests at constant penetration), most of the experimental data lies outside the curve proposed by Meyerhof (1953), Hansen (1970) and Dean et al. (1993).

Hambly (1992) carried out laboratory tests in sand on two model footing – flat and spudcan. The purpose of this investigation was to compare the ultimate bearing capacity of flat and spudcan footing. In the series of test performed by Hambely (1992), the footing were preloaded until the penetration for the flat footing was 10% of its diameter (Vesic (1975)) and for the spudcan footing, a penetration of its bearing area at the ground surface equivalent to the bearing capacity of the sand under the flat circular footing was insufficient to mobilized the ultimate bearing capacity of the sand under the spudcan footing. Hambly (1992) showed that the ultimate bearing capacity of a partially penetrated spudcan footing is twice the preload forces required for the flat footing. He obtained enhanced sliding resistance of the spudcan footing using twice the preload force for the flat footing with Hansen’s (1970) theory. He attributed the difference between the preload and the ultimate bearing capacity to the much greater volume of sand displacement by flat footing mobilization ultimate bearing resistance, as compared to the volume displaced by partially penetrated cone of the spudcan. He suggested ‘partial penetration factor’ to determined the ultimate bearing capacity from the vertical preload force. He concluded in his study that a further laboratory investigation is needed to validate his results. Although, in the absence of such an investigation it is difficult to comprehend Hambly’s (1992) results, the experimental results described by Tan (1990) resembles more closely the actual preload operation of the spudcan footing. The footing penetrates into the seabed as the load is applied and continues to penetrate until there is no further penetration into the seabed as the load is applied and continues to penetrate until there is no further penetration i.e. the footing is locked vertically. The final value of the load, thus, represents the ultimate bearing capacity of the footing.

2.10.2 VERTICAL BEARING CAPACITY OF A SPUDCAN FOOTING

The bearing capacity solution for a circular footing, given by Hansen (1970) can be simplified (for vertical loading only), and written as presented by Dean et al. (1993):

$$\mathbf{V = A_p\ (1/2\ N_\gamma\ \gamma'\ B_p)} \qquad (2.45)$$

Where B_p is the penetrated diameter, A_p is the plan contact area, γ' is the soil effective (buoyant) unit weight, and N_γ is an axi-symmetric self-weight bearing capacity factor. B_p can be written in term of penetration depth D_p as:

$$\mathbf{B_p = 2\ D_p \cot \Omega} \qquad (2.46)$$

Where Ω is the cone angle (see Fig. 8.7 a)

Substituting B_p in the bearing capacity solution, we get the following equation:

$$\mathbf{V = p\ N_\gamma\ \gamma'\ \cot^3 \Omega\ D_p^3} \qquad (2.47)$$

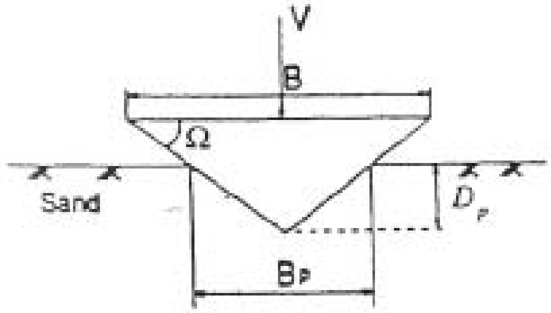

(a) Conical footing at partial penetration, p

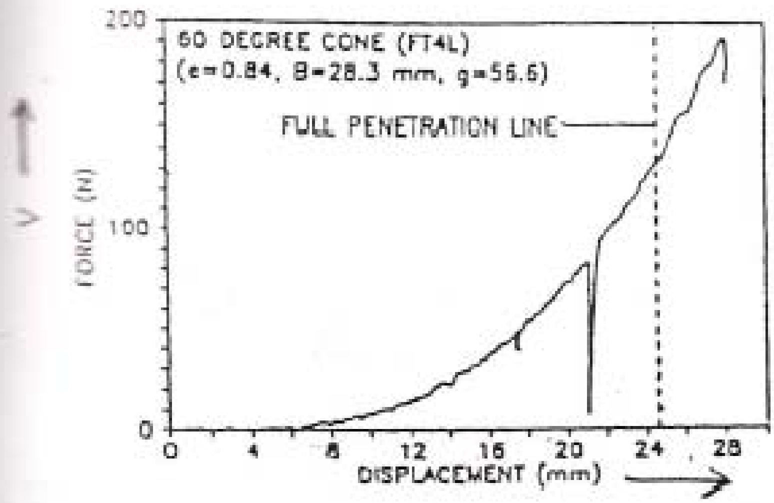

(a) Initial cubic nature of curve before full penetration

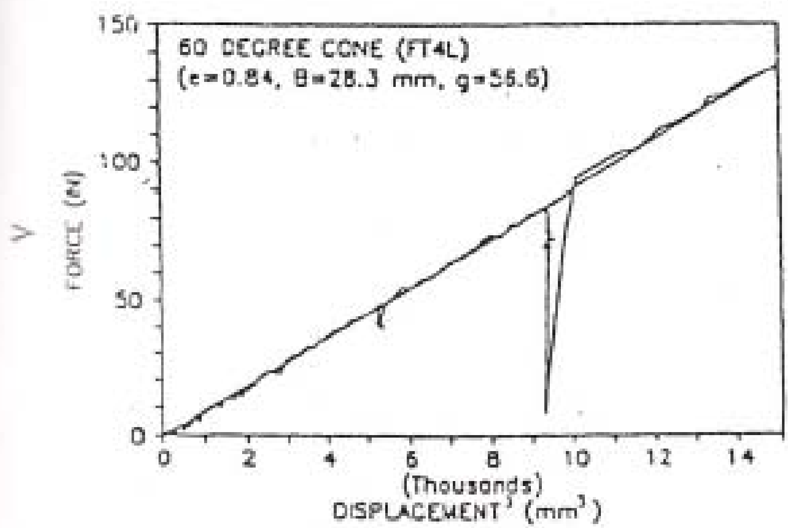

Fig. 2.20, (c) Plot of force against the cube of displacement

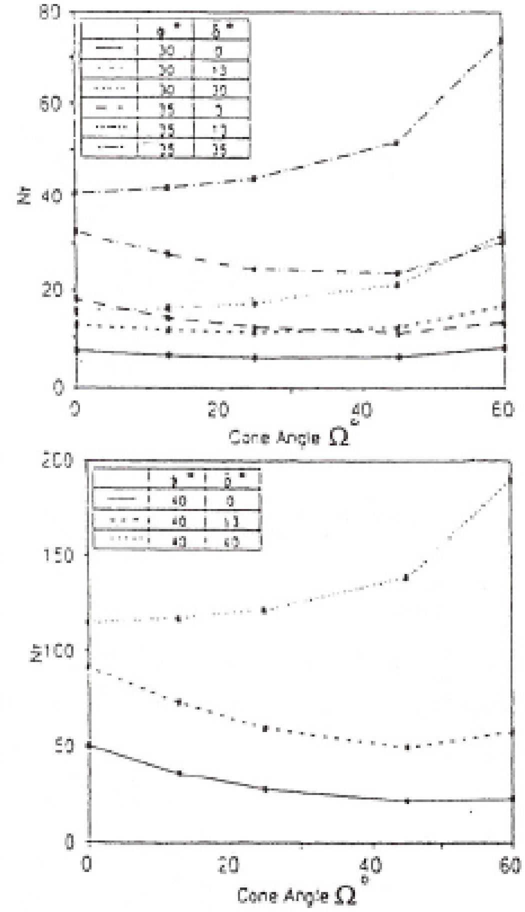

Fig 2.21 a, Theoretical axisymmetric N_γ values for cones on cohesionless soil

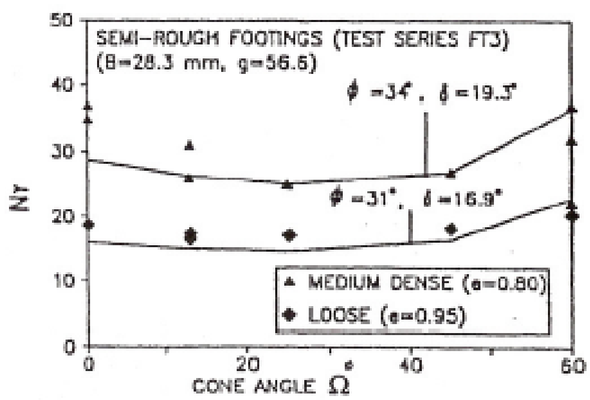

Fig 2.21 b, Effect of cone on N_γ of semi-rough footings;

Theoretical and experimental comparison.

Thus for a given angle Ω, V is directly related to the D_p^3, if N_γ is approximately constant then V and D_p^3 relationship is a straight line. Such a straight relationship is shown in figure 2.20c for a 60^o cone (Tan 1990) on fine Leighton Buzzard sand tested in the drum centrifuge at 56.6g. However, for a given depth of penetration, the value of N_γ varies with the cone angle and the variation depends on the surface roughness of the footing. The theoretical variation of N_γ with the cone angle using the method of characteristics is shone in Figure 2.21a. Figure 2.21b shows the same variation of N_γ with the cone angle calculated from the centrifuge test results using equation (2.45) and the comparison with the theoretical results. The results agree well in the region $\phi = 31^o$ and $\delta = 17^o$ for loose sand (void ratio 0.95) and $\phi = 34^o$ and $\delta = 19^o$ for medium dense send (void ratio 0.8). (In these figures ϕ is the friction angle and d represents the degree of roughness of the cone.). it can be seen from the Figures 2.21 a that for a fully rough footing (as is the case here in this chapter) the value of N_γ stays almost the same for cone angles between O^o-20^o. But for cone angles greater than 25^o there is a significant increase in the value of Ng. These results show that a conical footing with cone angle Ω = 13.46^o has a slight higher ultimate load compared to a footing with $\Omega = O^o$ (flat). But there is a need for further experimental investigation in order to prove that the load is 100% higher as we learn from Hambly (1992).

CHAPTER –3

ANALYTICAL SOLUTION FOR BEARING CAPACITY OF SPUDCAN FOOTING

Since Terzaghi's founding work, numerous experimental studies to estimate the ultimate bearing capacity of shallow foundation have been conducted. Based on these studies, it appears that Terzaghi's assumption of the failure surface in soil at ultimate load is essentially correct. However, the angle α that the sides ac and bc of the wedge (Fig. 3.1) make with the horizontal is closer to $45 + \phi/2$ and not ϕ as assumed by Terzaghi. (In actual practice, α has been found to vary from $45 - \phi/2$ for perfectly smooth base to $45 + \phi/2$ for perfectly rough base. Since footings are normally rough, α has been found closer to $45 + \phi/2$ than to ϕ).

So, I am Deriving the equations for bearing capacity factors N_c, N_q, and N_γ, by assuming the wedge angle = α. (angle that the sides ac and bc make with the horizontal surface see Fig. 3.1) The remaining assumption are same as assumed by Terzaghi (see page no. -   ).

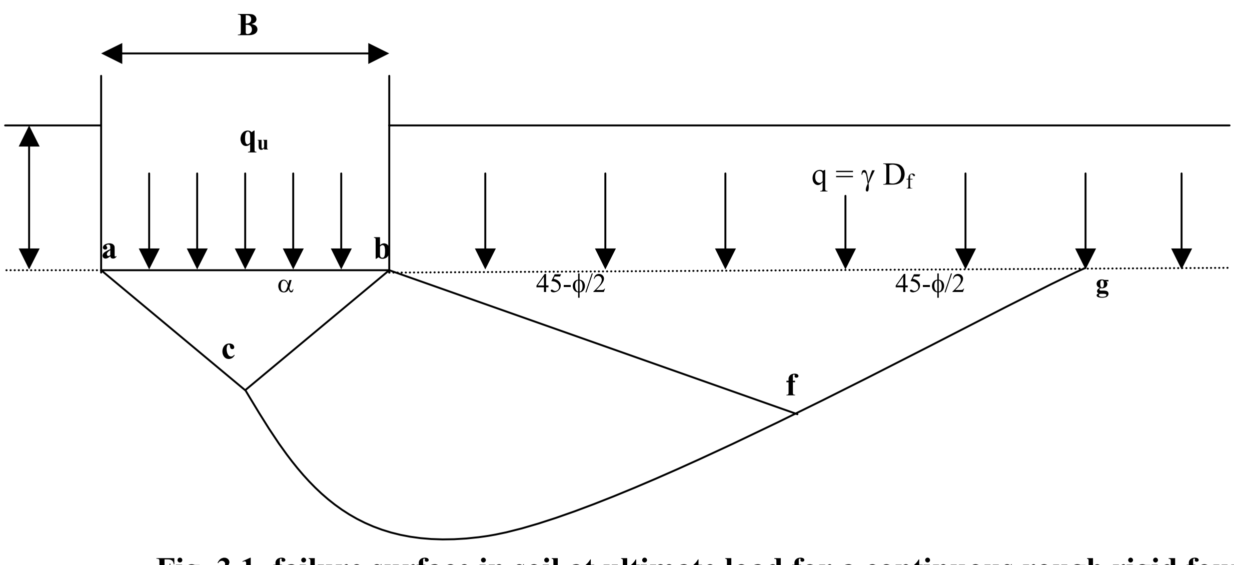

Fig. 3.1, failure surface in soil at ultimate load for a continuous rough rigid foundation as assumed by Terzaghi

The ultimate bearing capacity, q_u, of the foundation can be determined if we considered faces ac and bc of the triangle wedge abc and obtained the passive force on each face requires to cause failure. Note that the passive force P_p will be a function of the surcharge $q = \gamma D_f$. Cohesion c, unit weight γ, and angle of friction of the soil ϕ. So, referring to Fig. 3.2. The passive force P_p on the face bc per unit length of the foundation at right to the cross section is

$$P_p = P_{pq} + P_{pc} + P_{p\gamma} \qquad (3.1)$$

Where P_{pq}, P_{pc} and $P_{p\gamma}$ = passive force contributions of q, c and γ, respectively.

It is important to note that the directions of P_{pq}, P_{pc} and $P_{p\gamma}$ are vertical, since the face bc makes an angle ϕ with the horizontal, and P_{pq}, P_{pc} and $P_{p\gamma}$ must make an angle ϕ to the normal to bc. In order to obtain P_{pq}, P_{pc} and $P_{p\gamma}$, the method of superposition can be used.

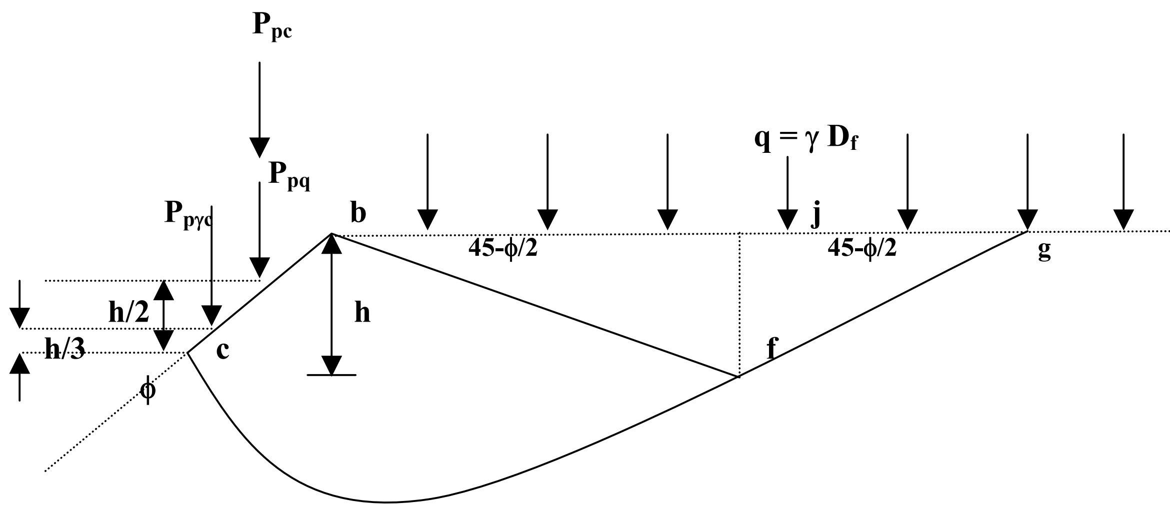

Fig. 3.2, Passive forceon the face bc of wedge abc shone in figure 3.1

3.1 RELATIONSHIP FOR P_{pq} ($\phi \neq 0, \gamma = 0, q \neq 0, c = 0$)

Considered the free body diagram of the soil wedge bcfj shown in Fig. 3.2 (also shown in Fig. 3.3). For this case the center of the log spiral, of which cf is an arc, will be at point b. the forces per unit length of the wedge bcfj due to the surcharge q only are shown in Fig.3.3a, and they are:

1. P_{pq}
2. Surcharge, q

3. The Rankine passive force, $P_{p(1)}$
4. The frictional resistance force alone the arc cf, F

The Rankine passive force, $P_{p(1)}$, can be expressed as

$$\mathbf{P_{p(1)} = q\, K_p\, H_d = q\, H_d \tan^2 (45 + \phi/2)} \qquad (3.2)$$

Where, H_d = fj

K_p = Rankine passive earth pressure coefficient = $\tan^2 (45 + \phi/2)$

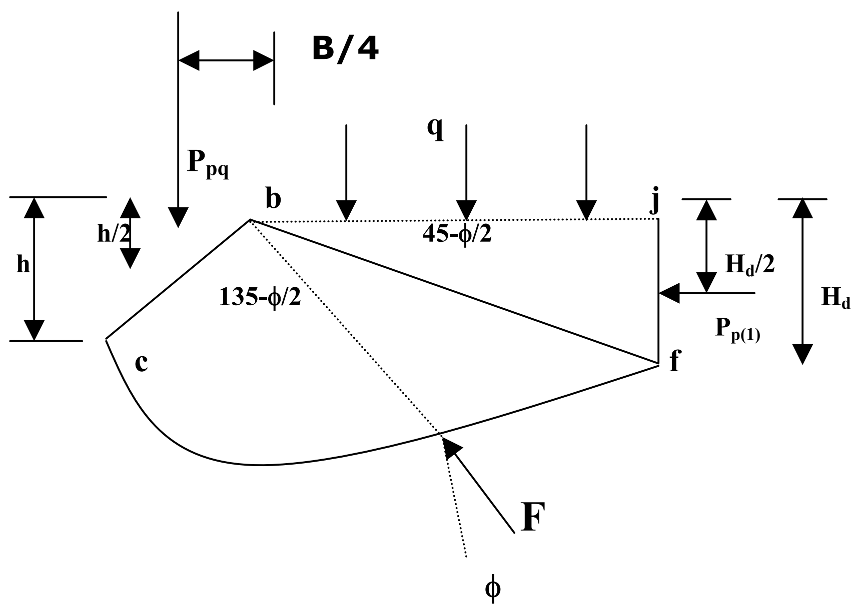

(a)

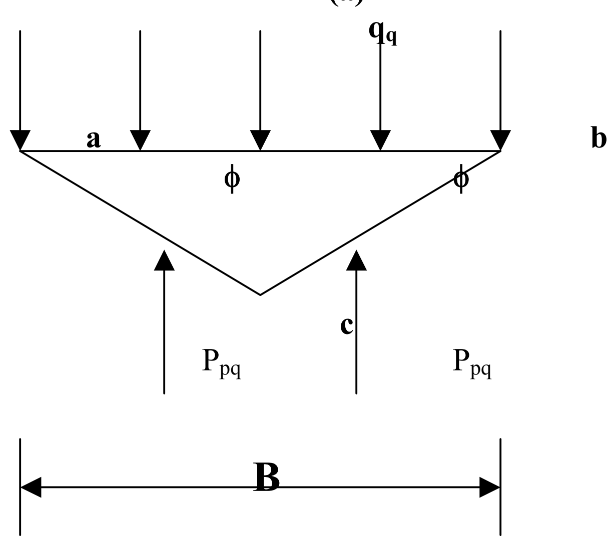

(b)

Fig. 3.3 Determination of P_{pq} ($\phi \neq 0$, $\gamma = 0$, $q \neq 0$, $c = 0$)

According to the property of a log spiral defined by the equation $r = r_o e^{\theta\tan\phi}$, the radial line at any point makes an angle ϕ with the normal. Hence, the lines of action of the friction force F will pass through b, the center of the log spiral (as shown in Fig. 3.3a). Taking the moment about point b

$$P_{pq}(B/4) = q(bj)(bj/2) + P_{p(1)} H_d/2 \tag{3.3}$$

Let

$$bc = r_o = (b/2)\sec\alpha \tag{3.4}$$

$$bf = r_1 = r_o e^{(3\pi/4 - \alpha + \phi/2)} \tag{3.5}$$

So

$$bj = r_1 \cos(45 - \phi/2) \tag{3.6}$$

And

$$H_d = r_1 \sin(45 - \phi/2) \tag{3.7}$$

Combining Eqs. (3.2), (3.3), (3.6) and (3.7)

$$P_{pq} B/4 = q r_1^2 \cos^2(45-\phi/2)/2 + q r_1^2 \sin^2(45-\phi/2)\tan^2(45+\phi/2)/2$$

Or

$$P_{pq} = 4/B\,[q r_1^2 \cos^2(45-\phi/2)] \tag{3.8}$$

Now combining Eqs. (3.4), (3.5), and (3.8)

$$P_{pq} = qB\, e^{2(3\pi/4 - \alpha + \phi/2)\tan\phi} \cos^2(45-\phi/2) / \cos^2\alpha \tag{3.9}$$

Considering the stability of the elastic wedge abc under the foundation as shown in Fig. 3.3b.

$$q_q (B \times 1) = 2 P_{pq}$$

Where, q_q = load per unit area on the foundation, or

$$q_q = 2P_{pq}/B = q\,[2 e^{2(3\pi/4 - \alpha + \phi/2)\tan\phi} \cos^2(45-\phi/2) / \cos^2\alpha] = q N_q \tag{3.10}$$

$$\mathbf{N_q = 2 e^{2(3\pi/4 - \alpha + \phi/2)\tan\phi} \cos^2(45-\phi/2)/\cos^2\alpha} \tag{3.11}$$

3.2 RELATIONSHIP FOR P_{pc} ($\phi \neq 0$, $\gamma = 0$, $q = 0$, $c \neq 0$)

Figure 3.4 shows the free body diagram for the wedge bcfj (also refer to Fig. 3.2). As in the case of P_{pq}, the center of arc of the log spiral will be located at point b. the forces on the wedge which are due to cohesion c are also shown in Fig. 3.4, and they are

1. Passive force, P_{pc}
2. Cohesive force, C = c(bc x 1)
3. Rankine passive force due to cohesion,

$$P_{p(2)} = 2c\ (K_p)1/2\ H_d = 2\ c\ H_d \tan(45 + \phi/2) \qquad (3.12)$$

4. Cohesive force per unit area along arc cf, c.

Taking the moment of all the forces about point b

$$P_{pc}\ (B/4) = P_{p(2)}\ [\ r_1 \sin(45 - \phi/2)\ /2] + M \qquad (3.13)$$

Where Mc = moment due to cohesion c along arc cf

$$= c/2 \tan\phi\ \ (r_1^2 - r_o^2) \qquad (3.14)$$

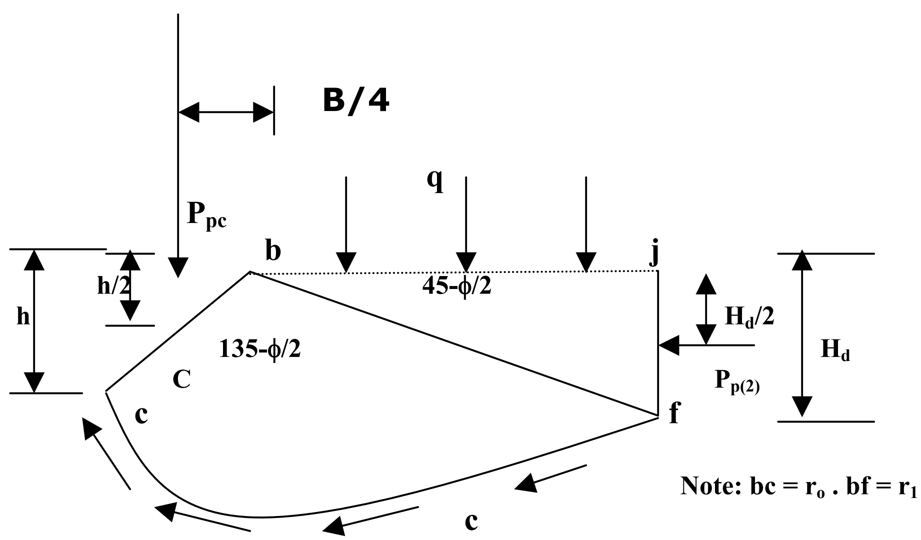

(a)

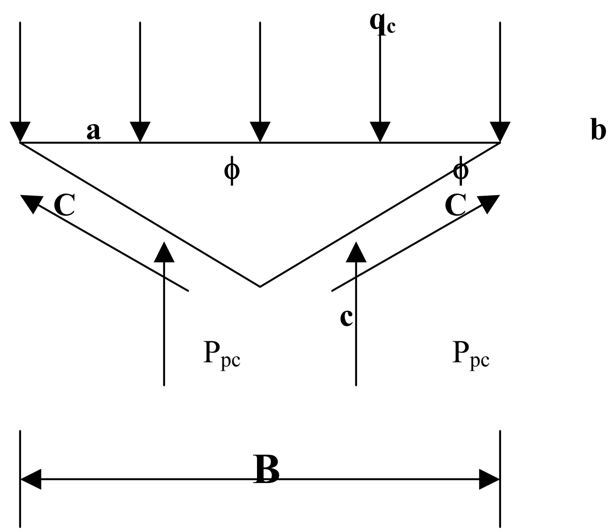

(b)

Fig. 3.4 Determination of P_{pc} ($\phi \neq 0, \gamma = 0, q = 0, c \neq 0$)

$$P_{pc}\,(B/4) = [2c\,H_d \tan(45+\phi/2)]\,[r_1 \sin(45-\phi/2)/2] + (c/2\tan\phi)(r_1^2 - r_o^2) \qquad (3.15)$$

The relationship for H_d, r_o, and r_1 in terms of B and ϕ given in Eqs. (3.7), (3.4) and (3.5), respectively. Combining Eqs. (3.4), (3.5), (3.7), and (3.15), and noting that $\sin^2(45-\phi/2) \times \tan(45+\phi/2) = ½ \cos\phi$

$$P_{pc} = Bc(\sec^2\alpha)\{[e^{2(3\pi/4-\alpha+\phi/2)\tan\phi}\ ½\cos\phi\,] + [(e^{2(3\pi/4-\alpha+\phi/2)\tan\phi} - 1)/2\tan\phi]\} \qquad (3.16)$$

Considering the equilibrium of the soil wedge abc (Fig.3.4b)

$$q_c(B \times 1) = 2\,C \sin\alpha + 2P_{pc}$$

Or

$$q_c\,B = cB \sec\alpha \sin\alpha + 2P_{pc} \qquad (3.17)$$

Where q_c = load per unit area of the foundation combining Eqs.(3.16) and (3.17)

$$q_c = c[\tan\alpha + 2\sec^2\alpha\{(e^{2(3\pi/4 - \alpha + \phi/2)\tan\phi} \tfrac{1}{2}\cos\phi \ + (e^{2(3\pi/4 - \alpha + \phi/2)\tan\phi} - 1)/2\tan\phi\}] \quad (3.18)$$

$$N_c = [\tan\alpha + 2\sec^2\alpha\{(e^{2(3\pi/4 - \alpha + \phi/2)\tan\phi} \tfrac{1}{2}\cos\phi + (e^{2(3\pi/4 - \alpha + \phi/2)\tan\phi} - 1)/2\tan\phi\} \quad (3.19)$$

3.3 RELATIONSHIP FOR $P_{p\gamma}$ ($\phi \neq 0$, $\gamma \neq 0$, $q = 0$, $c = 0$)

Figure 3.5a shows the free body diagram of wedge bcfj. Unlike the free body diagram shown in Figs. 3.3 and 3.4, the center of the log spiral of which bf is an arc is at a point O along line bf and not at b. this is because the minimum value of $P_{p\gamma}$ has to be determined by several trials. Point O is only one trail center. The forces per unit length of the wedge that need to be considered are:

1. Passive force, $P_{p\gamma}$
2. The weight of wedge bcfj, W
3. The resultant of the frictional resistance force acting along arc cf, F
4. The Rankine passive force, $P_{p(3)}$

The Rankine passive force $P_{p(3)}$ can be given the relation

$$P_{p(3)} = \tfrac{1}{2}\,\gamma\, H_d^2 \tan^2(45+\phi/2) \quad (3.20)$$

Also note the line of action of force F will pass through O. taking the moment about O

$$P_{p\gamma}\, l_p = W\, l_w + P_{p(3)}\, l_R \quad (3.21)$$

Also note that the line of action of force F will pass through O.
Taking the moment about O.

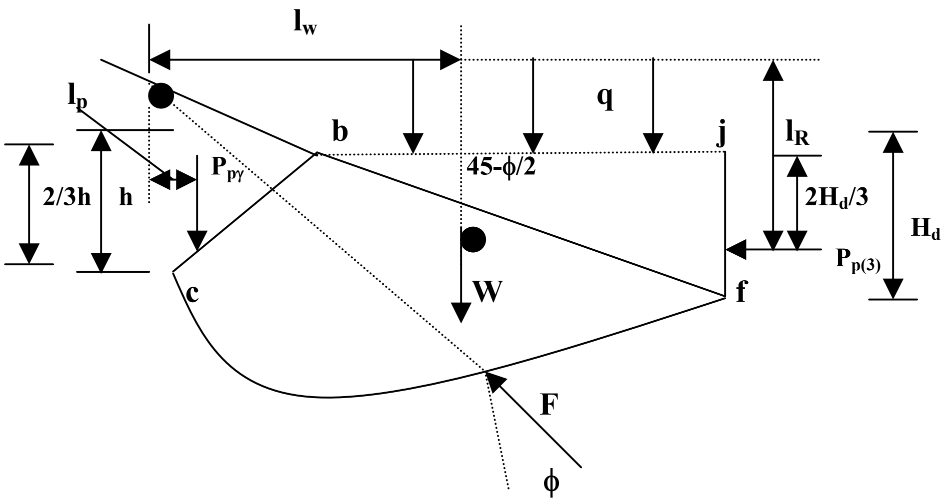

(a)

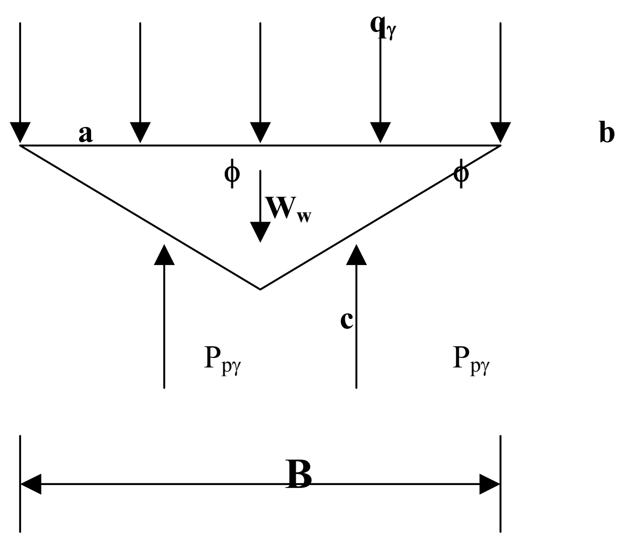

(b)

Fig. 3.5 Determination of $P_{p\gamma}$ ($\phi \neq 0, \gamma \neq 0, q = 0, c = 0$)

$$P_{p\gamma}\, l_p = W\, l_p + P_{p(3)}\, l_R$$

Or

$$P_{p\gamma} = 1/l_p \,[W\, l_w + P_{p(3)}\, l_R] \qquad (3.22)$$

If numbers of trail of this type are made by changing the location at the center of log spiral O along line bf, then the minimum value of $P_{p\gamma}$ can be determined

Considered the stability of wedge abc as shown in Fig. 3.5, we can write that

$$q_\gamma B = 2 P_{p\gamma} - W_w \qquad (3.23)$$

Where, q_γ = force per unit area of the foundation

W_w = weight of wedge abc

However,

$$W_w = B^2/4\ \gamma \tan\alpha \qquad (3.24)$$

So

$$q_\gamma = 1/B\ (\ 2 P_{p\gamma} - B^2/4\ \gamma \tan\alpha) \qquad (3.25)$$

The passive force $P_{p\gamma}$ can be expressed in the form

$$P_{p\gamma} = ½\ \gamma\ h^2 K_{p\gamma} = ½\ \gamma\ (B \tan\alpha/2)^2 K_{p\gamma} = 1/8\ \gamma\ B^2 K_{p\gamma} \tan^2\alpha \qquad (3.26)$$

Where $K_{p\gamma}$ = passive earth pressure coefficient

Substituting Eq. (2.28) into Eq. (2.27)

$$q_\gamma = 1/B\ (1/4\ \gamma\ B^2 K_{p\gamma} \tan^2\alpha - B^2/4\ g \tan\alpha)$$

$$= ½\ \gamma\ B\ (½\ K_{p\gamma} \tan^2\alpha - \tan\alpha/2) = ½\ \gamma\ B\ N_\gamma \qquad (3.27)$$

$$\mathbf{N_\gamma = (½\ K_{p\gamma} \tan^2\alpha - \tan\alpha/2)} \qquad (3.28)$$

So, the new ultimate bearing capacity factors for angle of wedge = α are

$$\boxed{\begin{aligned} &\mathbf{N_q = 2\, e^{2\,(3\pi/4 - \alpha + \phi/2)\tan\phi} \cos^2(45-\phi/2)/\cos^2\alpha} \\ &\mathbf{N_c = [\ \tan\alpha + 2\sec^2\alpha\{(\ e^{2(3\pi/4 - \alpha + \phi/2)\tan\phi}\ ½ \cos\phi} \\ &\qquad\qquad\mathbf{+ (e^{2(3\pi/4 - \alpha + \phi/2)\tan\phi} - 1)/2\tan\phi\}]} \\ &\mathbf{N_\gamma = (½\ K_{p\gamma} \tan^2\alpha - (\tan\alpha)/2)} \end{aligned}}$$

- Now the bearing capacity factors **for $\alpha = \phi$**, are same as given by Trezaghi (see page no).

- If we take $\alpha = 45 + \phi/2$ (as assumed by Meyerhof bearing capacity theory) see the difference in values of bearing capacity factors N_q, N_c and N_γ in comparison to Terzaghi's values, shown in TABLES and in FIGURES.

TABLE-1, COMPARISION OF BEARING CAPACITY FACTOR N_q

ANGLE OF INTERNAL FRICTION		TERZAGHI	MEYERHOF
ϕ	ϕ	N_q	N_q
DEGREE	RADIANS	FOR $\alpha = \phi$	FOR $\alpha = 45+\phi/2$
1	0.0175	1.10	2.19
2	0.0349	1.22	2.39
3	0.0524	1.35	2.62
4	0.0698	1.49	2.87
5	0.0873	1.64	3.14
6	0.1047	1.81	3.43
7	0.1222	2.00	3.76
8	0.1396	2.21	4.12
9	0.1571	2.44	4.51
10	0.1745	2.69	4.94
11	0.1920	2.98	5.42
12	0.2094	3.29	5.95
13	0.2269	3.63	6.53
14	0.2443	4.02	7.17
15	0.2618	4.45	7.88
16	0.2793	4.92	8.67
17	0.2967	5.45	9.54
18	0.3142	6.04	10.52
19	0.3316	6.70	11.60
20	0.3491	7.44	12.80
21	0.3665	8.26	14.14
22	0.3840	9.19	15.64
23	0.4014	10.23	17.32
24	0.4189	11.40	19.21
25	0.4363	12.72	21.32
26	0.4538	14.21	23.71
27	0.4712	15.90	26.40
28	0.4887	17.81	29.44
29	0.5061	19.98	32.89
30	0.5236	22.46	36.80
31	0.5411	25.28	41.26
32	0.5585	28.52	46.35
33	0.5760	32.23	52.18
34	0.5934	36.50	58.88
35	0.6109	41.44	66.59
36	0.6283	47.16	75.50
37	0.6458	53.80	85.84
38	0.6632	61.55	97.87
39	0.6807	70.61	111.91
40	0.6981	81.27	128.39
41	0.7156	93.85	147.79
42	0.7330	108.75	170.75
43	0.7505	126.50	198.03
44	0.7679	147.74	230.62
45	0.7854	173.29	269.75
46	0.8029	204.19	317.00
47	0.8203	241.80	374.41
48	0.8378	287.85	444.60
49	0.8552	344.64	530.99
50	0.8727	415.15	638.11

TABLE-2, COMPARISION OF BEARING CAPACITY FACTOR N_c

ANGLE OF INTERNAL FRICTION		TERZAGHI	MEYERHOF
ϕ	ϕ	N_c	N_c
DEGREE	RADIANS	FOR $\alpha = \phi$	FOR $\alpha = 45+\phi/2$
1	0.0175	5.997	9.741
2	0.0349	6.300	10.228
3	0.0524	6.624	10.746
4	0.0698	6.968	11.298
5	0.0873	7.337	11.886
6	0.1047	7.730	12.515
7	0.1222	8.151	13.186
8	0.1396	8.602	13.904
9	0.1571	9.086	14.673
10	0.1745	9.605	15.498
11	0.1920	10.163	16.383
12	0.2094	10.763	17.334
13	0.2269	11.410	18.358
14	0.2443	12.108	19.460
15	0.2618	12.861	20.650
16	0.2793	13.676	21.935
17	0.2967	14.559	23.325
18	0.3142	15.517	24.831
19	0.3316	16.558	26.465
20	0.3491	17.690	28.241
21	0.3665	18.925	30.175
22	0.3840	20.272	32.283
23	0.4014	21.746	34.586
24	0.4189	23.361	37.107
25	0.4363	25.135	39.871
26	0.4538	27.085	42.908
27	0.4712	29.236	46.252
28	0.4887	31.612	49.942
29	0.5061	34.242	54.023
30	0.5236	37.162	58.547
31	0.5411	40.411	63.575
32	0.5585	44.036	69.176
33	0.5760	48.090	75.435
34	0.5934	52.637	82.447
35	0.6109	57.754	90.326
36	0.6283	63.528	99.208
37	0.6458	70.067	109.254
38	0.6632	77.495	120.653
39	0.6807	85.966	133.637
40	0.6981	95.663	148.482
41	0.7156	106.807	165.522
42	0.7330	119.669	185.167
43	0.7505	134.580	207.915
44	0.7679	151.950	234.383
45	0.7854	172.285	265.333
46	0.8029	196.219	301.720
47	0.8203	224.549	344.741
48	0.8378	258.285	395.913
49	0.8552	298.718	457.173
50	0.8727	347.509	531.016

FIG. 3.6, COMPARISION OF BEARING CAPACITY FACTOR N_q
FOR $\alpha = \phi$ AND $\alpha = 45 + \phi/2$

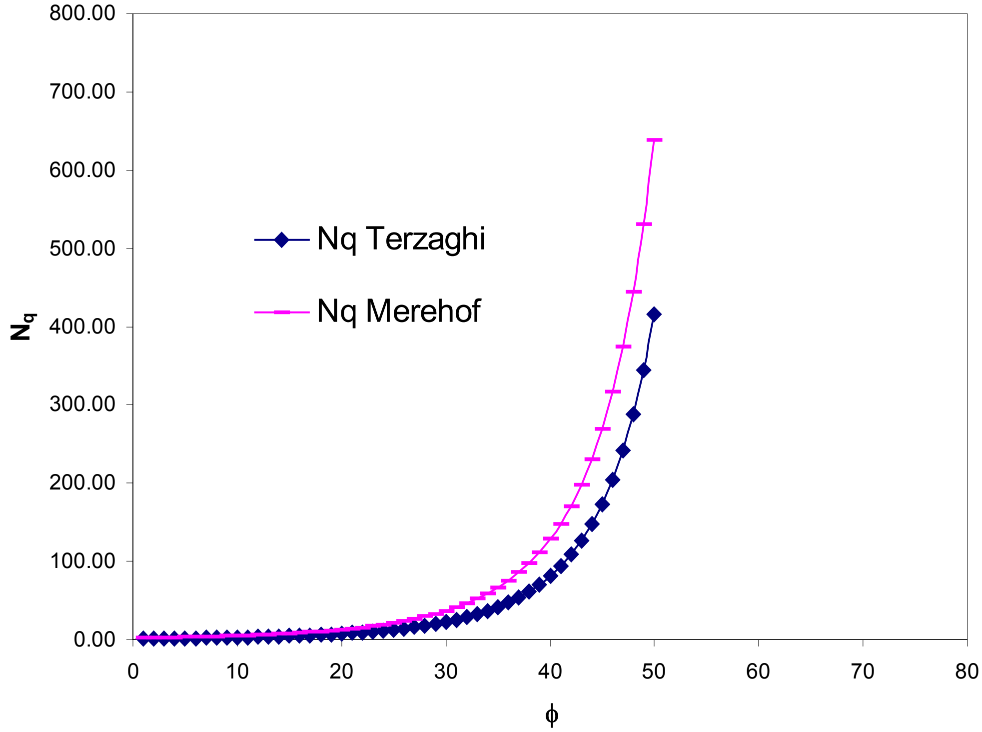

FIG. 3.7, COMPARISON OF BEARING CAPACITY FACTOR N_c
FOR $\alpha = \phi$ AND $\alpha = 45 + \phi/2$

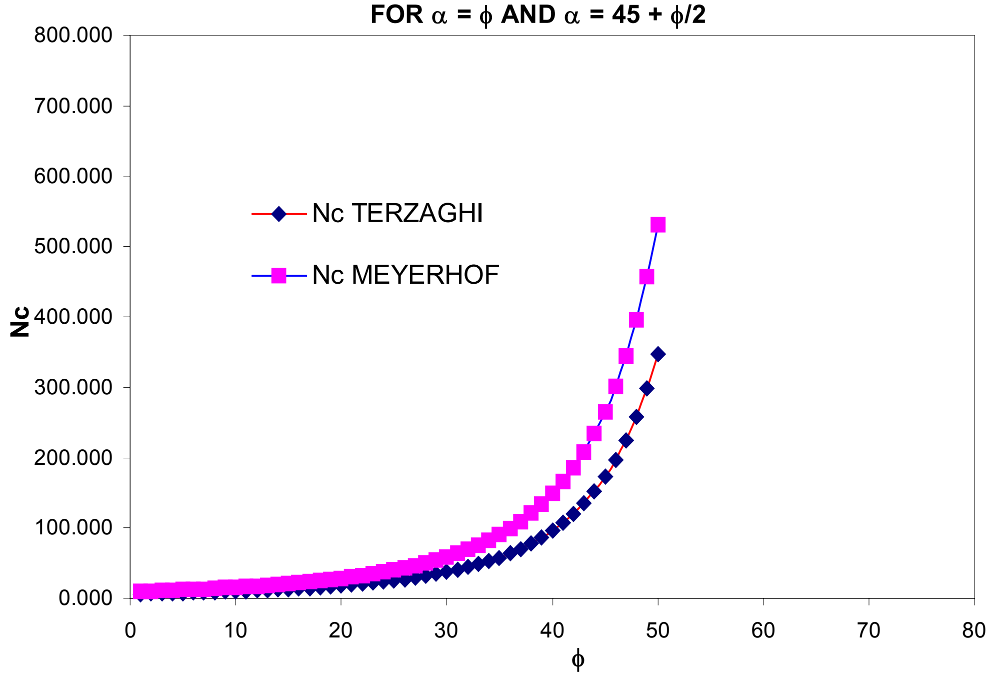

TABLE-3, COMPARISION OF BEARING CAPACITY FACTOR N_γ

ANGLE OF INTERNAL FRICTION		θ MINIMUM VALUE	TERZAGHI	θ MINIMUM VALUE	MEYERHOF
ϕ	ϕ	FOR $\alpha = \Phi$	N_γ	FOR $\alpha = 45+\Phi/2$	N_γ
DEGREE	RADIANS	DEGREE	FOR $\alpha = \Phi$	DEGREE	FOR $\alpha = 45+\Phi/2$
1	0.0175	88.833	0.014	96.950	115.162
2	0.0349	90.910	0.035	96.944	133.327
3	0.0524	92.494	0.063	96.932	154.466
4	0.0698	93.753	0.099	96.912	179.101
5	0.0873	94.782	0.144	96.882	207.857
6	0.1047	95.637	0.200	96.856	241.479
7	0.1222	96.356	0.267	96.821	280.861
8	0.1396	96.966	0.348	96.781	327.076
9	0.1571	97.486	0.444	96.736	381.415
10	0.1745	97.931	0.559	96.688	445.440
11	0.1920	98.311	0.694	96.636	521.042
12	0.2094	98.637	0.854	96.580	610.518
13	0.2269	98.916	1.041	96.522	716.668
14	0.2443	99.152	1.262	96.461	842.918
15	0.2618	99.352	1.520	96.397	993.471
16	0.2793	99.519	1.822	96.330	1173.503
17	0.2967	99.656	2.175	96.262	1389.411
18	0.3142	99.768	2.589	96.191	1649.132
19	0.3316	99.855	3.074	96.119	1962.557
20	0.3491	99.921	3.641	96.044	2342.052
21	0.3665	99.968	4.305	95.968	2803.157
22	0.3840	99.996	5.085	95.890	3365.481
23	0.4014	100.009	6.000	95.812	4053.881
24	0.4189	100.006	7.076	95.731	4900.029
25	0.4363	99.989	8.342	95.650	5944.474
26	0.4538	99.960	9.836	95.567	7239.218
27	0.4712	99.918	11.602	95.484	8852.421
28	0.4887	99.866	13.693	95.400	10871.438
29	0.5061	99.804	16.175	95.314	13411.662
30	0.5236	99.732	19.129	95.229	16624.905
31	0.5411	99.652	22.653	95.142	20712.570
32	0.5585	99.563	26.871	95.055	25943.690
33	0.5760	99.467	31.935	94.967	32680.244
34	0.5934	99.363	38.035	94.879	41412.971
35	0.6109	99.253	45.410	94.790	52812.471
36	0.6283	99.137	54.360	94.701	67802.810
37	0.6458	99.015	65.266	94.612	87668.530
38	0.6632	98.888	78.614	94.523	114211.831
39	0.6807	98.755	95.028	94.433	149985.865
40	0.6981	98.618	115.311	94.343	198644.894
41	0.7156	98.477	140.509	94.253	265476.022
42	0.7330	98.331	171.990	94.162	358216.664
43	0.7505	98.181	211.556	94.072	488327.751
44	0.7679	98.028	261.603	93.982	673004.157
45	0.7854	97.872	325.342	93.891	938395.634
46	0.8029	97.712	407.113	93.801	1324847.070
47	0.8203	97.550	512.836	93.711	1895564.156
48	0.8378	97.385	650.673	93.620	2751193.652
49	0.8552	97.218	831.990	93.530	4054810.739
50	0.8727	97.048	1072.797	93.440	6075589.081

FIG.3.8, VARIATION OF TERZAGHI N_γ WITH ϕ , FOR $\alpha = \phi$

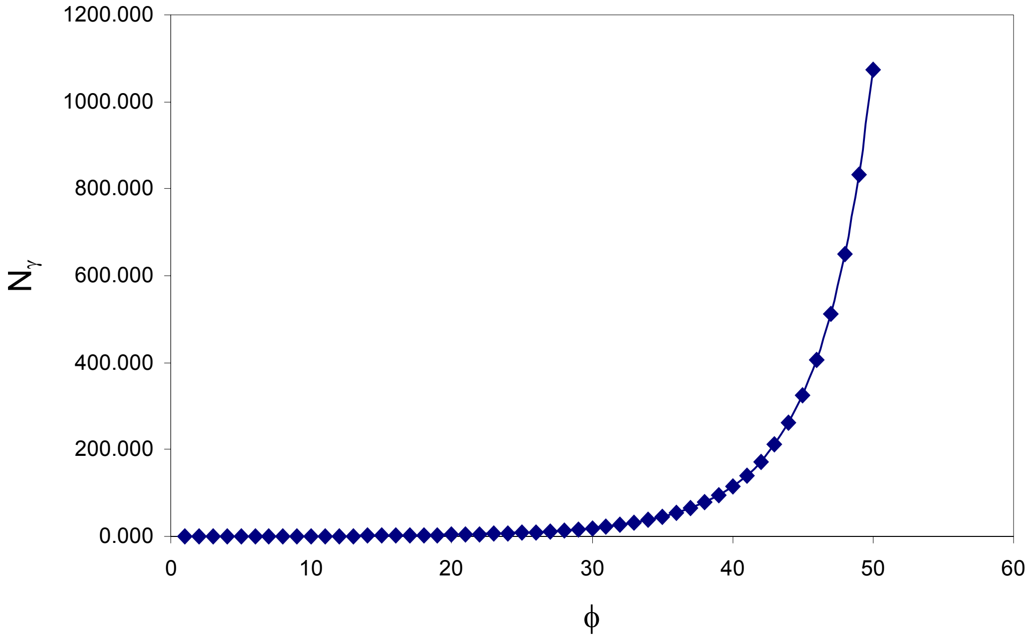

FIG. 3.9, VARIATION OF N_γ WITH ϕ, FOR $\alpha = 45 + \phi/2$

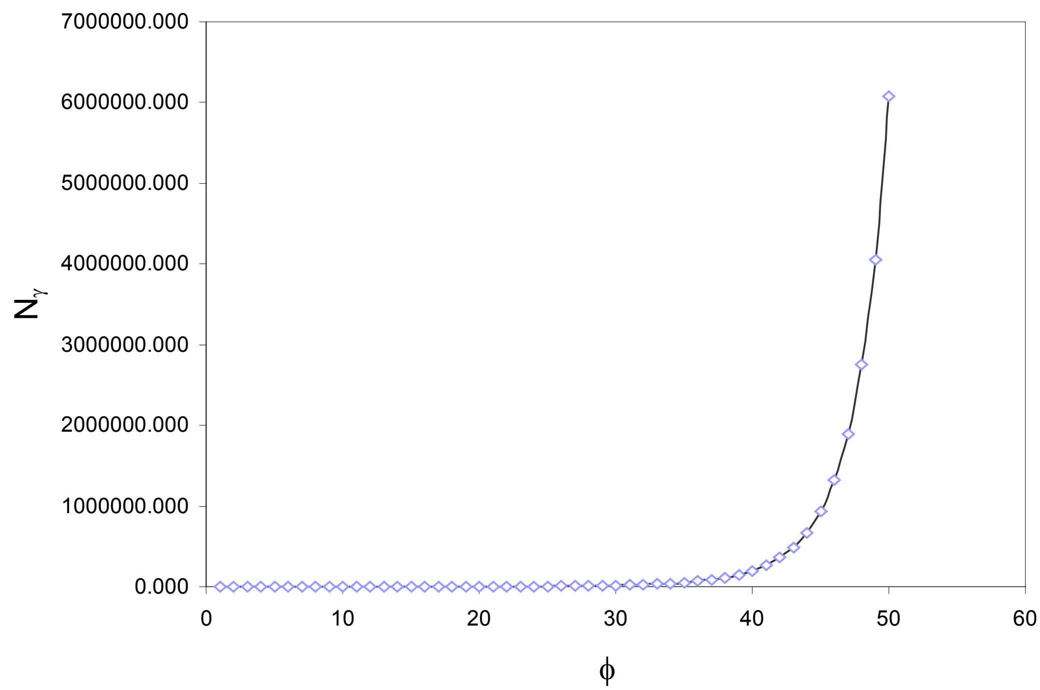

FIG. 3.10, VARIATION OF TERZAGHI'S N_γ WITH MINIMUM ANGLE OF LOG SPIRAL θ

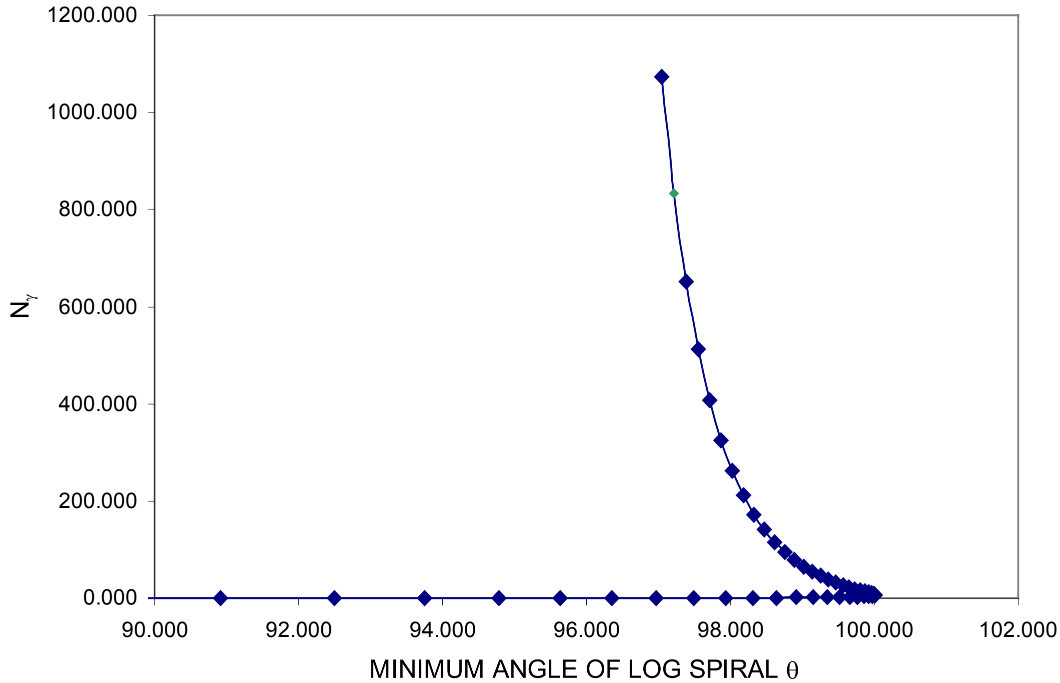

FIG. 3.11, VARIATION OF N_γ FOR MINMUM ANGLE OF LOG SPIRAL θ, IF $\alpha = 45 + \phi/2$

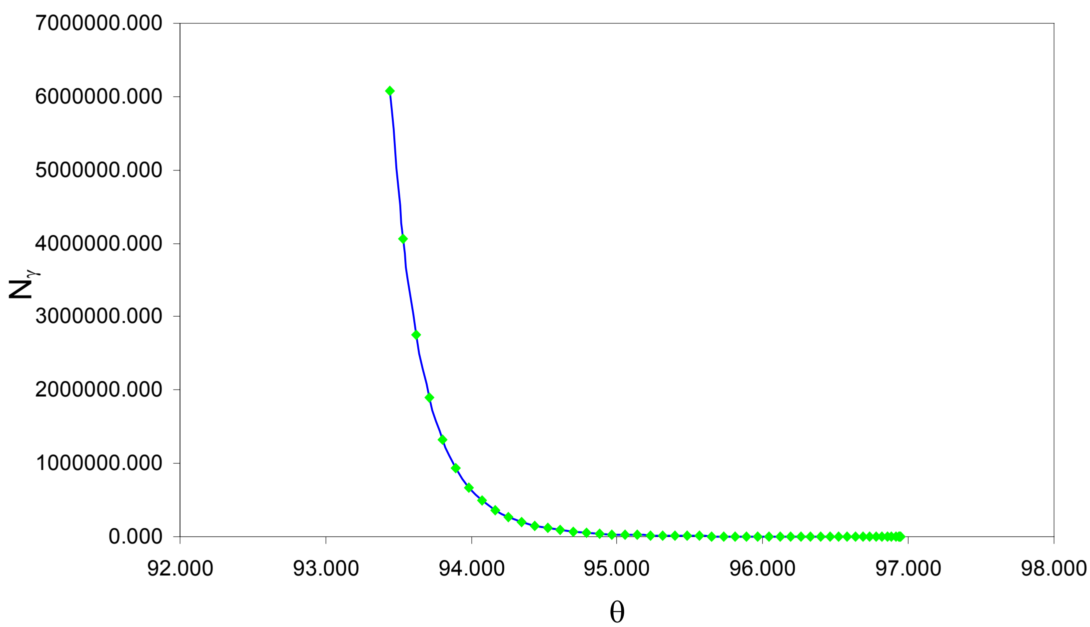

- Now applying the Terzaghi's modified bearing capacity factors formulas (Eq. 3.11, 3.19, and 3.28) for calculating the value of N_q, N_C, and N_γ for "SPUDCAN footing".

- SPUDCAN footing is type of conical shaped footing with protruding tip at the center (see Fig.3.12). It is use in the Mobile jackup units of a floatable platform (use in offshore structures). For details see Literature review page no.-

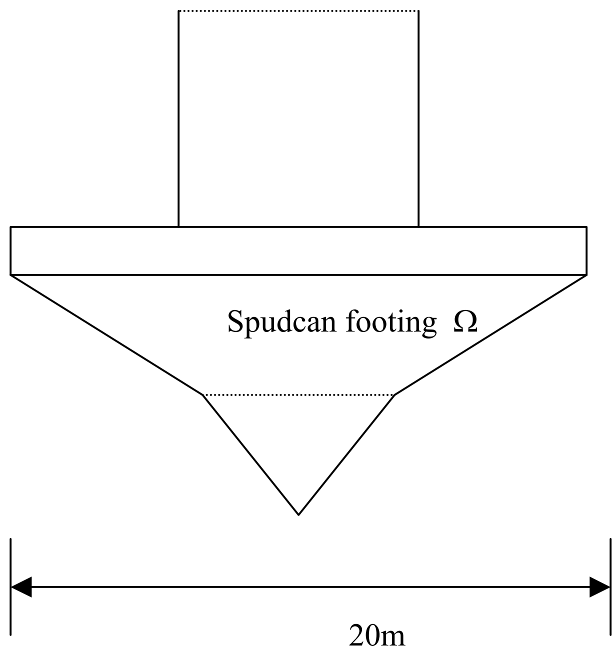

Fig. 3.12

- In the SPUDCAN footings, their embedded circular area in plane is used for the bearing capacity calculations. The SPUDCAN footing is treated as equivalent cone enclosing the same volume.

In my study the series of cone angles $\Omega = 0^o$ (Flat), 5^o, 10^o, and 15^o is use for calculating the bearing capacity factors N_q, N_c, and N_γ.

Also two approaches is used

1. The wedge angle, $\alpha = \Omega + \phi$.
2. And, $\alpha = \Omega + [45+\phi/2]$. See Fig. 3.13

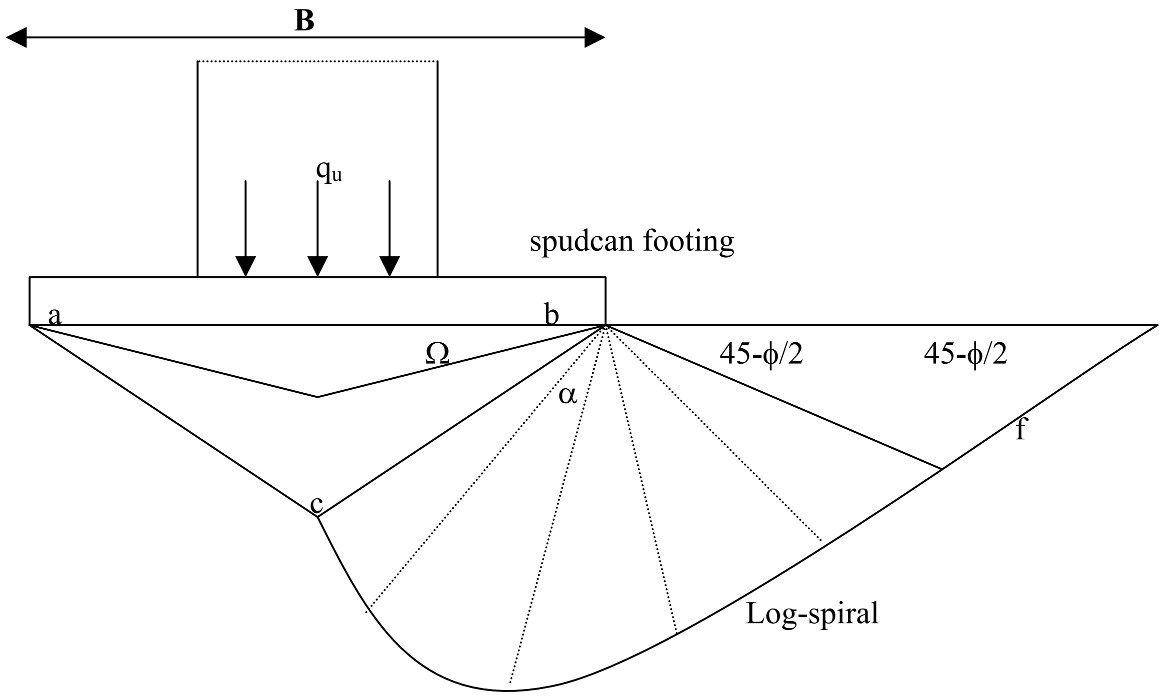

Fig. 3.13 Failure surface in soil at ultimate load for spudcan footing as assumed in the proposed analysis

All the values of bearing capacity factors N_q, N_c, and N_γ are calculated in the Tables for different cone angles, $\Omega = 5^o$, 10^o, and 15^o and there variation are shown in the Figures.

TABLE-3.4, COMPARISION OF BEARING CAPACITY FACTOR N_q FOR SPUDCAN FOOTING FOR $\alpha = \Omega + \phi$ AND $\Omega = 5^o$, 10^o, AND 15^o.

ANGLE OF INTERNAL FRICTION		TERZAGHI	$\Omega=5^o$	$\Omega=10^o$	$\Omega=15^o$
ϕ	ϕ	N_q	N_q	N_q	N_q
DEGREE	RADIANS	IF $\alpha = \phi$	IF $\alpha = \Omega + \phi$	IF $\alpha = \Omega + \phi$	IF $\alpha = \Omega + \phi$
1	0.0175	1.10	1.11	1.14	1.18
2	0.0349	1.22	1.23	1.26	1.31
3	0.0524	1.35	1.36	1.39	1.45
4	0.0698	1.49	1.50	1.53	1.60
5	0.0873	1.64	1.65	1.69	1.76
6	0.1047	1.81	1.83	1.87	1.95
7	0.1222	2.00	2.02	2.06	2.15
8	0.1396	2.21	2.23	2.28	2.38
9	0.1571	2.44	2.46	2.52	2.62
10	0.1745	2.69	2.72	2.78	2.90
11	0.1920	2.98	3.00	3.07	3.21
12	0.2094	3.29	3.31	3.40	3.54
13	0.2269	3.63	3.66	3.76	3.92
14	0.2443	4.02	4.05	4.16	4.34
15	0.2618	4.45	4.48	4.60	4.81
16	0.2793	4.92	4.96	5.09	5.33
17	0.2967	5.45	5.50	5.64	5.91
18	0.3142	6.04	6.09	6.26	6.55
19	0.3316	6.70	6.76	6.94	7.28
20	0.3491	7.44	7.50	7.71	8.09
21	0.3665	8.26	8.34	8.57	9.00
22	0.3840	9.19	9.27	9.54	10.03
23	0.4014	10.23	10.33	10.63	11.18
24	0.4189	11.40	11.51	11.85	12.48
25	0.4363	12.72	12.84	13.23	13.95
26	0.4538	14.21	14.35	14.79	15.61
27	0.4712	15.90	16.05	16.56	17.50
28	0.4887	17.81	17.99	18.57	19.65
29	0.5061	19.98	20.19	20.86	22.10
30	0.5236	22.46	22.69	23.46	24.90
31	0.5411	25.28	25.56	26.44	28.10
32	0.5585	28.52	28.83	29.86	31.79
33	0.5760	32.23	32.60	33.79	36.04
34	0.5934	36.50	36.93	38.32	40.95
35	0.6109	41.44	41.93	43.55	46.64
36	0.6283	47.16	47.73	49.63	53.27
37	0.6458	53.80	54.48	56.71	61.01
38	0.6632	61.55	62.34	64.98	70.09
39	0.6807	70.61	71.56	74.69	80.78
40	0.6981	81.27	82.39	86.12	93.42
41	0.7156	93.85	95.18	99.64	108.44
42	0.7330	108.75	110.35	115.72	126.36
43	0.7505	126.50	128.42	134.91	147.87
44	0.7679	147.74	150.06	157.95	173.81
45	0.7854	173.29	176.12	185.76	205.30
46	0.8029	204.19	207.66	219.52	243.76
47	0.8203	241.80	246.07	260.76	291.04
48	0.8378	287.85	293.15	311.47	349.59
49	0.8552	344.64	351.25	374.26	422.64
50	0.8727	415.15	423.47	452.61	514.56

TABLE-3.5, COMPARISION OF BEARING CAPACITY FACTOR N_C FOR SPUDCAN FOOTING FOR $\alpha = \Omega + \phi$ AND $\Omega = 5^o$, 10^o, AND 15^o.

ANGLE OF INTERNAL FRICTION		TERZAGHI	Ω=5°	Ω =10°	Ω =15°
ϕ	ϕ	Nc	Nc	Nc	Nc
DEGREE	RADIANS	IF $\alpha = \phi$	IF $\alpha = \Omega + \phi$	IF $\alpha = \Omega + \phi$	IF $\alpha = \Omega + \phi$
1	0.0175	5.997	5.954	5.999	6.133
2	0.0349	6.300	6.260	6.311	6.457
3	0.0524	6.624	6.585	6.644	6.803
4	0.0698	6.968	6.932	6.999	7.172
5	0.0873	7.337	7.303	7.378	7.567
6	0.1047	7.730	7.699	7.784	7.989
7	0.1222	8.151	8.123	8.218	8.441
8	0.1396	8.602	8.578	8.683	8.927
9	0.1571	9.086	9.065	9.182	9.448
10	0.1745	9.605	9.588	9.718	10.008
11	0.1920	10.163	10.150	10.295	10.611
12	0.2094	10.763	10.754	10.915	11.261
13	0.2269	11.410	11.406	11.585	11.963
14	0.2443	12.108	12.109	12.307	12.721
15	0.2618	12.861	12.869	13.088	13.542
16	0.2793	13.676	13.691	13.933	14.431
17	0.2967	14.559	14.582	14.850	15.396
18	0.3142	15.517	15.548	15.845	16.445
19	0.3316	16.558	16.598	16.927	17.588
20	0.3491	17.690	17.740	18.106	18.834
21	0.3665	18.925	18.986	19.392	20.196
22	0.3840	20.272	20.347	20.797	21.687
23	0.4014	21.746	21.835	22.336	23.321
24	0.4189	23.361	23.467	24.025	25.118
25	0.4363	25.135	25.259	25.881	27.096
26	0.4538	27.085	27.230	27.925	29.279
27	0.4712	29.236	29.405	30.182	31.693
28	0.4887	31.612	31.808	32.678	34.370
29	0.5061	34.242	34.469	35.447	37.344
30	0.5236	37.162	37.425	38.524	40.657
31	0.5411	40.411	40.714	41.954	44.359
32	0.5585	44.036	44.386	45.786	48.505
33	0.5760	48.090	48.494	50.080	53.163
34	0.5934	52.637	53.104	54.905	58.413
35	0.6109	57.754	58.293	60.345	64.348
36	0.6283	63.528	64.152	66.497	71.082
37	0.6458	70.067	70.790	73.477	78.748
38	0.6632	77.495	78.335	81.427	87.508
39	0.6807	85.966	86.944	90.513	97.560
40	0.6981	95.663	96.804	100.941	109.142
41	0.7156	106.807	108.143	112.957	122.547
42	0.7330	119.669	121.238	126.866	138.133
43	0.7505	134.580	136.430	143.040	156.349
44	0.7679	151.950	154.139	161.942	177.750
45	0.7854	172.285	174.887	184.148	203.035
46	0.8029	196.219	199.327	210.381	233.091
47	0.8203	224.549	228.281	241.556	269.048
48	0.8378	258.285	262.792	278.839	312.362
49	0.8552	298.718	304.194	323.727	364.924
50	0.8727	347.509	354.209	378.165	429.216

FIG. 3.14, Comparision of N_q for diffrent Spudcan footing angles(5^o, 10^o, & 15^o) FOR $\alpha = \Omega + \phi$

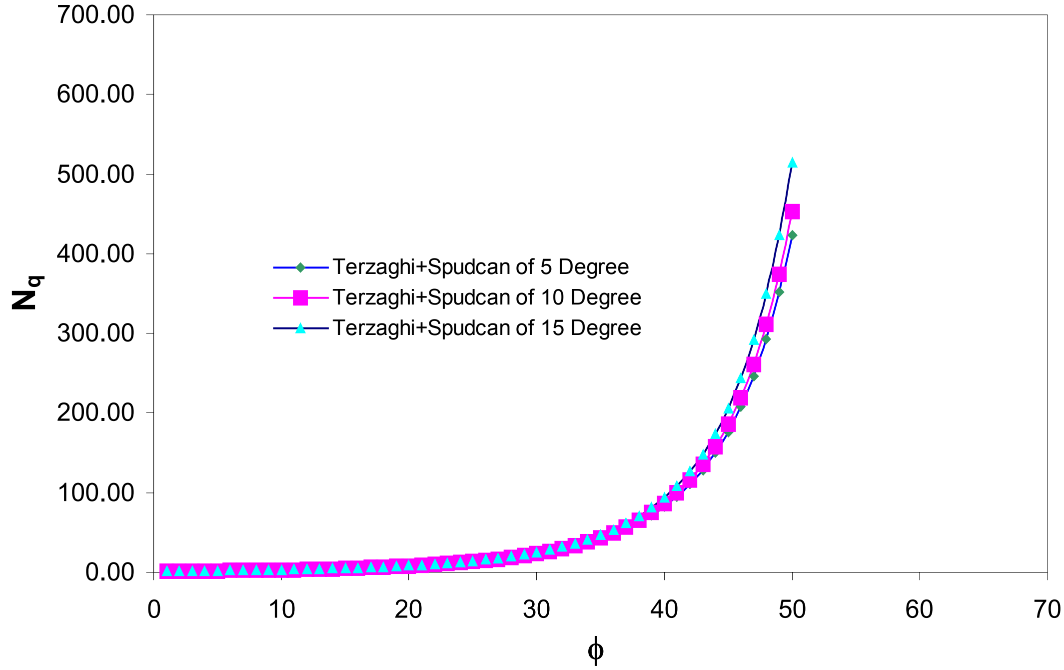

FIG. 3.15, COMPARISION OF Nc FOR DIFFERENT SPUDCAN FOOTING ANGLES (5^o, 10^o, & 15^o) FOR $\alpha = \Omega + \phi$

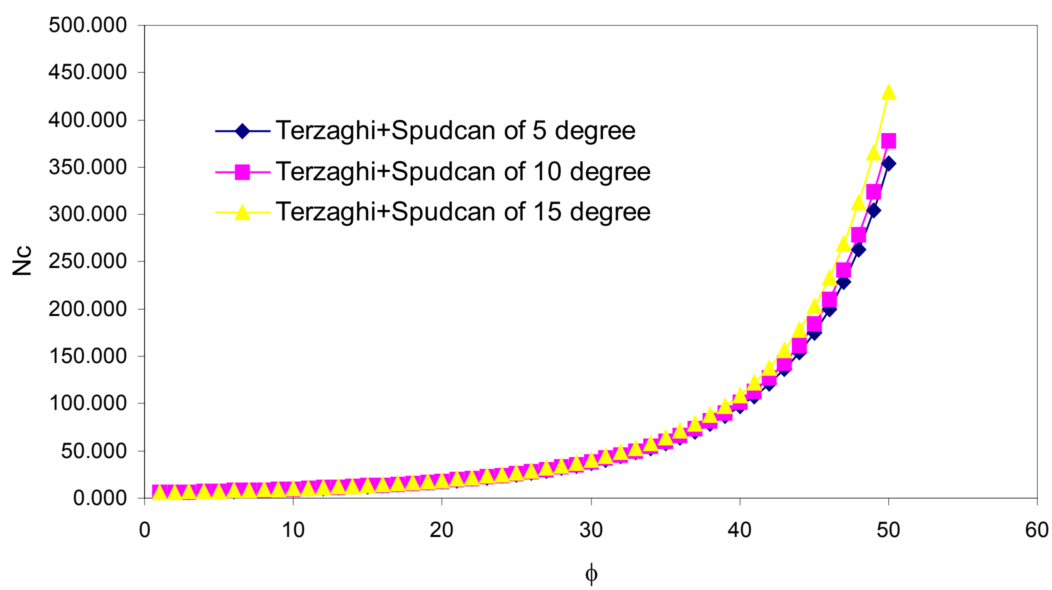

TABLE- 3.6, COMPARISION OF BEARING CAPACITY FACTOR N_γ FOR SPUDCAN FOOTING FOR $\alpha = \Omega + \phi$ AND $\Omega = 5^o$, 10^o, AND 15^o.

ϕ	Ω	$\alpha = \Omega + \phi$	θ	N_γ
1	5	6.000	93.486	0.076
5	5	10.000	97.572	0.358
10	5	15.000	99.015	1.161
15	5	20.000	99.487	2.985
20	5	25.000	99.455	7.115
25	5	30.000	99.089	16.750
30	5	35.000	98.526	40.543
35	5	40.000	97.823	104.559
40	5	45.000	96.162	298.868
50	5	55.000	95.856	2548.325
1	10	11.000	85.919	0.244
5	10	15.000	94.849	0.831
10	10	20.000	97.822	2.375
15	10	25.000	98.864	5.953
20	10	30.000	99.100	14.453
25	10	35.000	98.895	35.754
30	10	40.000	98.419	93.779
35	10	45.000	97.765	271.817
40	10	50.000	96.995	917.546
50	10	60.000	95.259	9856.548
1	15	16.000	91.903	0.699
5	15	20.000	96.168	1.815
10	15	25.000	98.076	4.868
15	15	30.000	98.680	12.267
20	15	35.000	98.664	31.111
25	15	40.000	98.292	83.136
30	15	45.000	97.699	244.436
35	15	50.000	96.962	836.397
40	15	55.000	96.134	3586.521
50	15	65.000	94.347	12456.363

FIG. 3.16, COMPARISION OF Ng FOR DIFFERENT SPUDCAN FOOTING ANGLES(5^o, 10^o, 15^o) FOR $\alpha = \Omega + \phi$

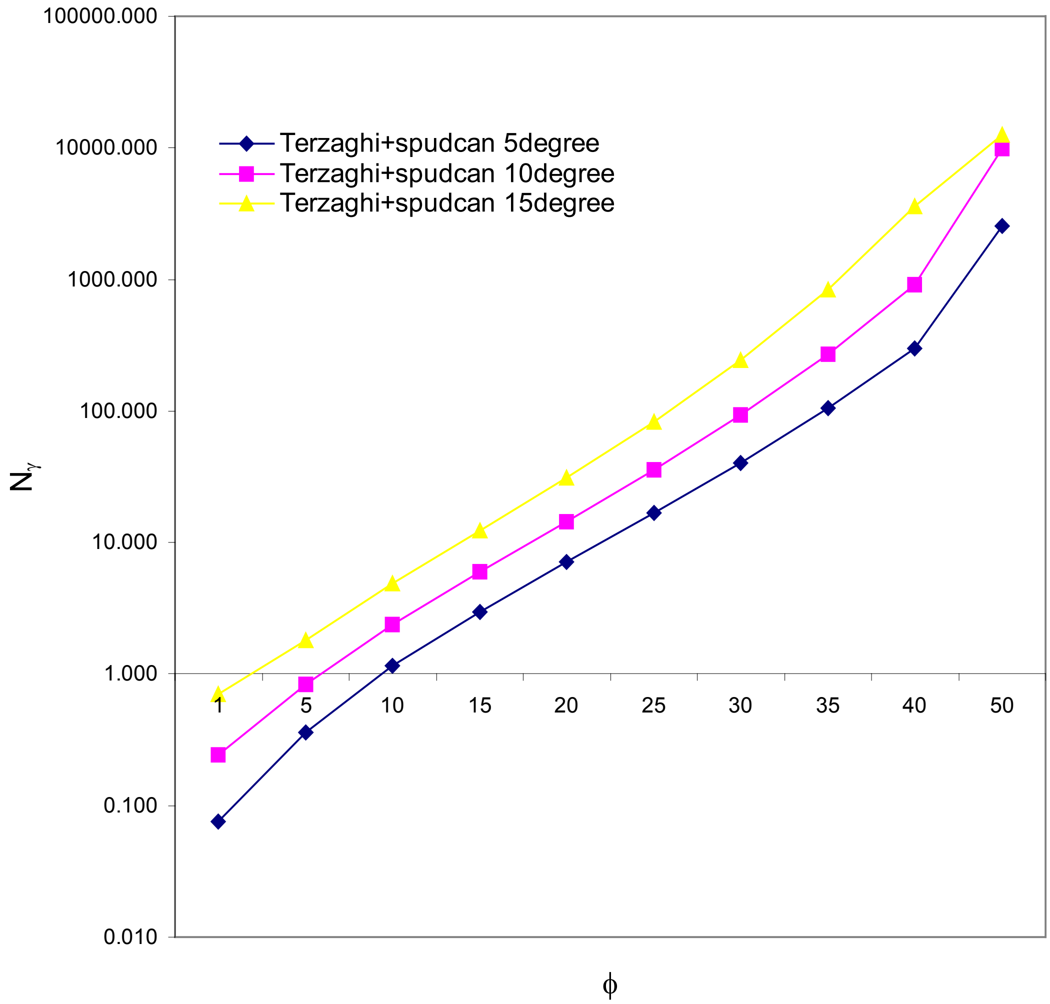

TABLE- 3.7, COMPARISION OF BEARING CAPACITY FACTOR N_q FOR SPUDCAN FOOTING FOR $\alpha = \Omega + 45 + \phi/2$ AND $\Omega = 5^o, 10^o, 15^o$

ANGLE OF INTERNAL FRICTION		TERZAGHI	$\Omega = 5^o$	$\Omega = 10^o$	$\Omega = 15^o$
ϕ	ϕ	Nq	N_q	N_q	N_q
DEGREE	RADIANS	IF $\alpha = \phi$	IF $\alpha = \Omega+45+\phi/2$	IF $\alpha = \Omega+45+\phi/2$	IF $\alpha = \Omega+45+\phi/2$
1	0.0175	1.10	2.65	3.33	4.39
2	0.0349	1.22	2.90	3.65	4.82
3	0.0524	1.35	3.17	4.00	5.30
4	0.0698	1.49	3.47	4.38	5.83
5	0.0873	1.64	3.80	4.81	6.41
6	0.1047	1.81	4.17	5.28	7.06
7	0.1222	2.00	4.56	5.79	7.77
8	0.1396	2.21	5.00	6.36	8.56
9	0.1571	2.44	5.49	6.99	9.45
10	0.1745	2.69	6.02	7.68	10.43
11	0.1920	2.98	6.61	8.45	11.52
12	0.2094	3.29	7.26	9.30	12.74
13	0.2269	3.63	7.98	10.25	14.10
14	0.2443	4.02	8.77	11.30	15.62
15	0.2618	4.45	9.66	12.48	17.34
16	0.2793	4.92	10.64	13.78	19.26
17	0.2967	5.45	11.73	15.24	21.42
18	0.3142	6.04	12.94	16.88	23.86
19	0.3316	6.70	14.29	18.71	26.62
20	0.3491	7.44	15.81	20.76	29.75
21	0.3665	8.26	17.50	23.07	33.30
22	0.3840	9.19	19.39	25.68	37.35
23	0.4014	10.23	21.52	28.62	41.97
24	0.4189	11.40	23.92	31.95	47.26
25	0.4363	12.72	26.62	35.72	53.33
26	0.4538	14.21	29.67	40.02	60.33
27	0.4712	15.90	33.12	44.91	68.42
28	0.4887	17.81	37.04	50.51	77.81
29	0.5061	19.98	41.49	56.92	88.74
30	0.5236	22.46	46.58	64.30	101.52
31	0.5411	25.28	52.39	72.80	116.52
32	0.5585	28.52	59.05	82.64	134.21
33	0.5760	32.23	66.72	94.07	155.17
34	0.5934	36.50	75.56	107.39	180.15
35	0.6109	41.44	85.80	122.97	210.06
36	0.6283	47.16	97.69	141.27	246.09
37	0.6458	53.80	111.55	162.86	289.79
38	0.6632	61.55	127.77	188.45	343.13
39	0.6807	70.61	146.83	218.93	408.74
40	0.6981	81.27	169.33	255.41	490.10
41	0.7156	93.85	195.99	299.32	591.86
42	0.7330	108.75	227.74	352.48	720.39
43	0.7505	126.50	265.76	417.24	884.45
44	0.7679	147.74	311.52	496.68	1096.33
45	0.7854	173.29	366.91	594.79	1373.55
46	0.8029	204.19	434.36	716.92	1741.61
47	0.8203	241.80	517.05	870.20	2238.36
48	0.8378	287.85	619.11	1064.30	2921.52
49	0.8552	344.64	746.01	1312.45	3881.55
50	0.8727	415.15	905.06	1633.03	5265.14

TABLE- 3.8, COMPARISION OF BEARING CAPACITY FACTOR N_C FOR SPUDCAN FOOTING FOR $\alpha = \Omega + 45 + \phi/2$ AND $\Omega = 5^o, 10^o, 15^o$

ANGLE OF INTERNAL FRICTION		TERZAGHIS	$\Omega=5^o$	$\Omega=10^o$	$\Omega=15^o$
ϕ	ϕ	N_c	N_c	N_c	N_c
DEGREE	RADIANS	IF $\alpha = \phi$	IF $\alpha = \Omega+45+\phi/2$	IF $\alpha = \Omega+45+\phi/2$	IF $\alpha = \Omega+45+\phi/2$
1	0.0175	5.997	11.342	13.647	17.131
2	0.0349	6.300	11.927	14.386	18.127
3	0.0524	6.624	12.551	15.177	19.198
4	0.0698	6.968	13.218	16.024	20.351
5	0.0873	7.337	13.930	16.933	21.595
6	0.1047	7.730	14.691	17.908	22.938
7	0.1222	8.151	15.507	18.956	24.390
8	0.1396	8.602	16.381	20.084	25.963
9	0.1571	9.086	17.320	21.299	27.668
10	0.1745	9.605	18.328	22.611	29.521
11	0.1920	10.163	19.414	24.027	31.536
12	0.2094	10.763	20.583	25.560	33.733
13	0.2269	11.410	21.844	27.221	36.131
14	0.2443	12.108	23.206	29.024	38.753
15	0.2618	12.861	24.679	30.982	41.627
16	0.2793	13.676	26.276	33.115	44.783
17	0.2967	14.559	28.007	35.440	48.254
18	0.3142	15.517	29.889	37.980	52.082
19	0.3316	16.558	31.936	40.759	56.312
20	0.3491	17.690	34.169	43.806	60.997
21	0.3665	18.925	36.607	47.153	66.200
22	0.3840	20.272	39.274	50.838	71.992
23	0.4014	21.746	42.198	54.903	78.458
24	0.4189	23.361	45.409	59.397	85.697
25	0.4363	25.135	48.942	64.377	93.826
26	0.4538	27.085	52.839	69.909	102.983
27	0.4712	29.236	57.146	76.070	113.332
28	0.4887	31.612	61.918	82.950	125.070
29	0.5061	34.242	67.218	90.654	138.433
30	0.5236	37.162	73.118	99.305	153.707
31	0.5411	40.411	79.704	109.051	171.237
32	0.5585	44.036	87.075	120.065	191.447
33	0.5760	48.090	95.351	132.553	214.857
34	0.5934	52.637	104.670	146.765	242.112
35	0.6109	57.754	115.195	162.998	274.017
36	0.6283	63.528	127.125	181.614	311.581
37	0.6458	70.067	140.693	203.051	356.088
38	0.6632	77.495	156.181	227.848	409.176
39	0.6807	85.966	173.930	256.666	472.965
40	0.6981	95.663	194.354	290.323	550.222
41	0.7156	106.807	217.958	329.840	644.603
42	0.7330	119.669	245.362	376.500	761.003
43	0.7505	134.580	277.331	431.927	906.062
44	0.7679	151.950	314.819	498.191	1088.934
45	0.7854	172.285	359.019	577.958	1322.454
46	0.8029	196.219	411.433	674.691	1624.975
47	0.8203	224.549	473.973	792.933	2023.316
48	0.8378	258.285	549.085	938.712	2557.655
49	0.8552	298.718	639.933	1120.113	3289.942
50	0.8727	347.509	750.639	1348.121	4318.943

FIG. 3.17, COMPARISION OF Nq FOR DIFFERENT SPUDCAN FOOTING ANGLE (5^o, 10^o, AND 15^o) FOR $\alpha = \Omega + 45+\phi/2$

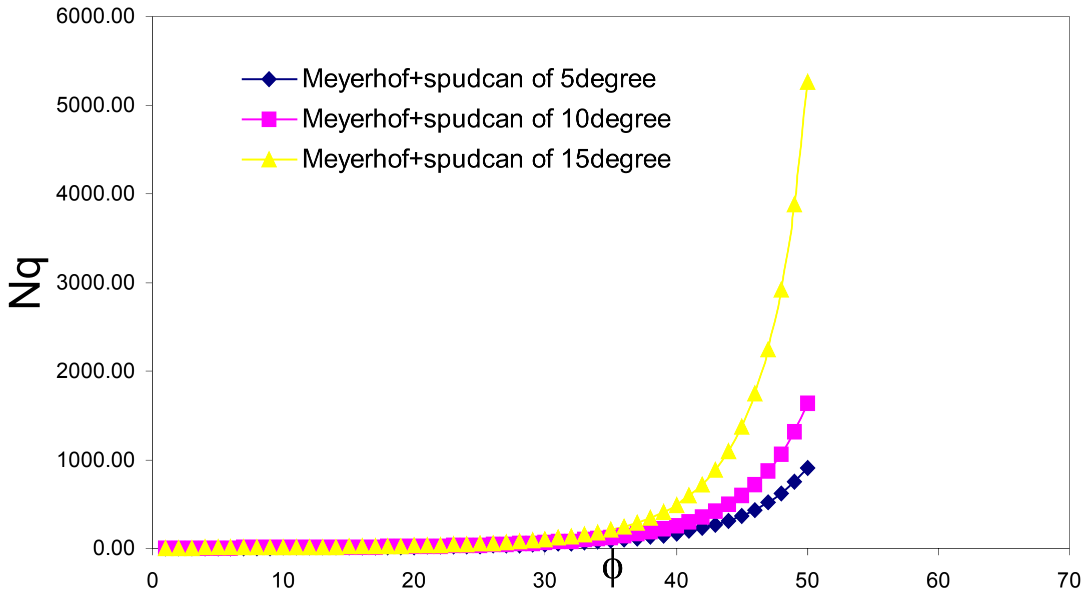

FIG. 3.18, COMPARISION OF Nc FOR DIFFERENT SPUDCAN FOOTING ANGLES (5^o, 10^o, AND 15^o) FOR $\alpha = \Omega+45+\phi/2$

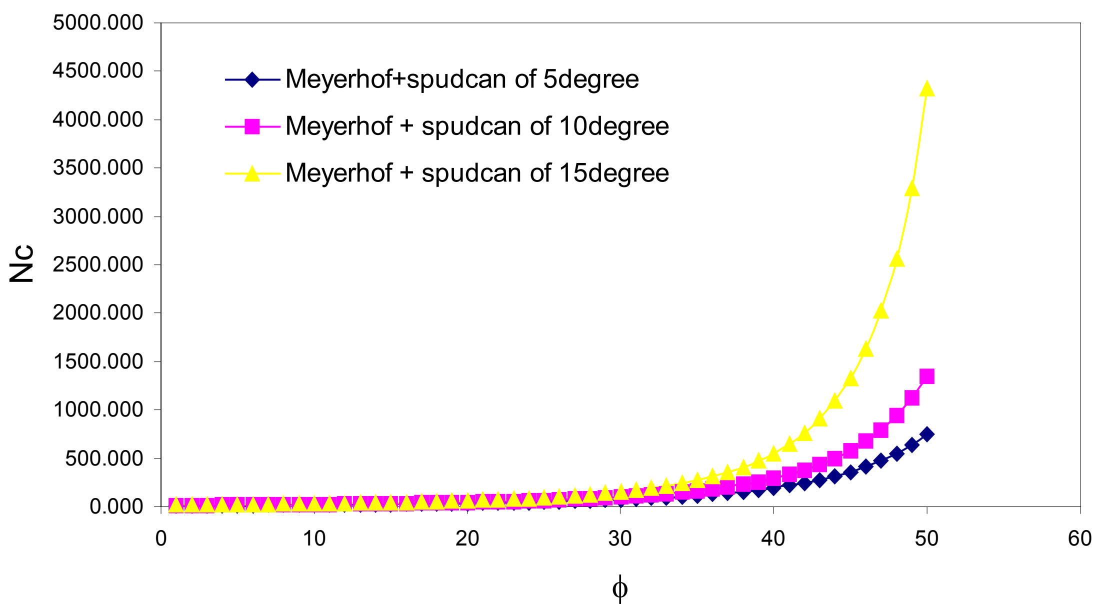

TABLE- 3.9, COMPARISION OF BEARING CAPACITY FACTOR N_γ FOR SPUDCAN FOOTING FOR $\alpha = \Omega + 45 + \phi/2$ AND $\Omega = 5^o$, 10^o, AND 15^o.

ϕ	Ω	$\alpha = \Omega + 45 + \phi/2$	θ	N_γ
1	5	50.500	96.460	371.240
5	5	52.500	96.279	727.028
10	5	55.000	95.973	1765.905
12	5	56.000	95.833	2565.796
15	5	57.500	95.608	4604.157
20	5	60.000	95.205	13196.229
25	5	62.500	94.778	42882.508
30	5	65.000	94.337	50845.244
40	5	70.000	93.439	63258.334
45	5	72.500	92.992	72458.107
50	5	75.000	92.549	84582.025

1	10	55.500	95.814	1525.784
5	10	57.500	95.551	3388.915
10	10	60.000	95.173	9592.506
15	10	62.500	94.761	24580.265
20	10	65.000	94.328	48584.356
25	10	67.500	93.885	62466.128
30	10	70.000	93.438	78480.652
40	10	75.000	92.549	88155.699
50	10	80.000	91.992	93254.111

1	15	60.500	95.053	9074.841
5	15	62.500	94.737	19256.365
10	15	65.000	94.316	29248.316
15	15	67.500	93.879	46586.215
20	15	70.000	93.435	55879.100
25	15	72.500	92.991	65482.322
30	15	75.000	92.549	86265.215
40	15	80.000	92.115	98125.125
50	15	85.000	91.987	112485.321

FIG. 3.19, COMPARISION OF N_γ FOR DIFFERENT SPUDCAN FOOTING ANGLES(5^o, 10^o, AND 15^o) FOR $\alpha = 45+\phi/2$

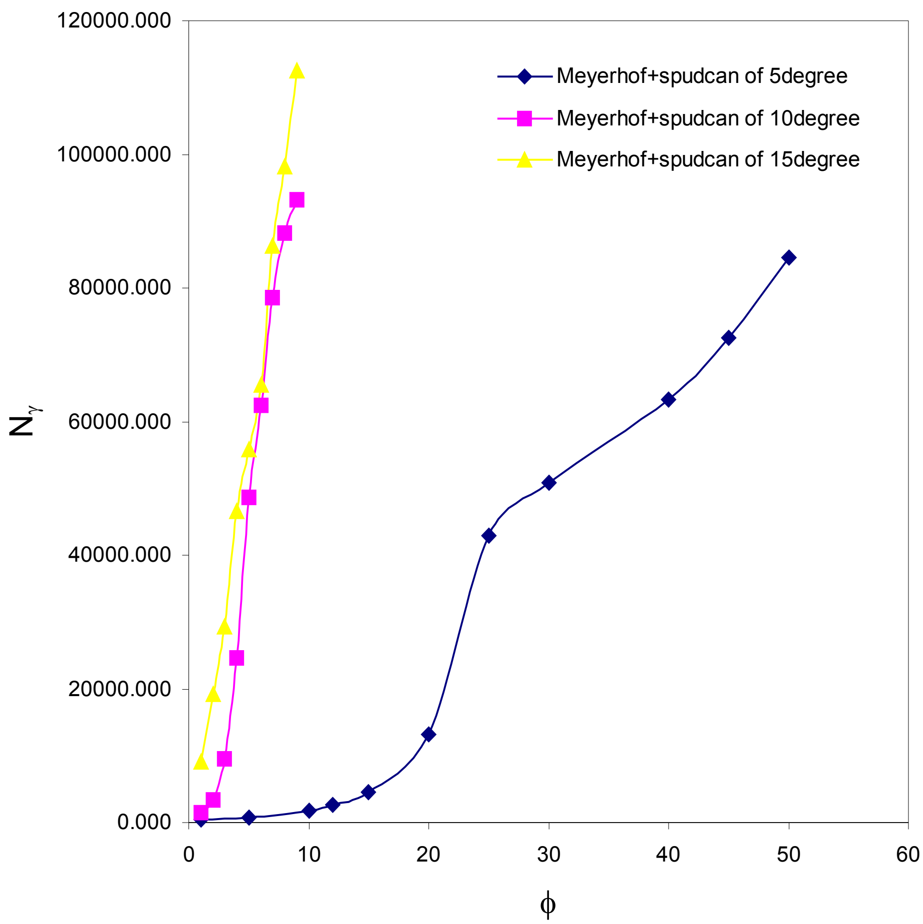

CHAPTER –4

ANALYTICAL SOLUTION FOR BEARING CAPACITY OF SKIRTED FOOTING

4.1 INTRODUCTION

This chapter presents the results of Analytical solutions for the influence of soil confinement on the behavior of circular footing resting on granular soil. Skirts with different heights and diameters were used to confine the sand. The ultimate bearing capacity of circular footing supported on confining sand bed was studied. The studied parameter includes the skirt height and skirt diameter. Initially, the response of a nonconfined case (bearing capacity by using Terzaghi's formulation) was determined and then compared with that of confined soil. The results were than analyzed to study the effect of each parameter. The results indicate that the bearing capacity of circular footing can be appreciably increased by soil confinement. It was concluded that such reinforcement (skirts) resist lateral displacement of soil underneath the footing leading to a significant improvement in the response of the footing. For small skirt diameters, the skirt-soil footing behaves as one unit (deep foundation), while this pattern of behavior was no longer observed with large skirt diameters. The recommended skirt heights, depth and diameter that give the maximum bearing capacity improvement are presented and discussed.

4.2 MODELING DETAILS

The geometry of the soil, model footing, and confining cylindrical skirt are shown in the Fig. (4.1). The confining cylindrical skirt is assumed to be made of the steel shell with different diameters and heights. The used diameters are 100, 107, 133, 160 and 200 centimeter and heights of 50, 100, 150, 250 and 300 centimeters. The interior and exterior surfaces of the cylindrical skirt are assumed to be very smooth and rough (by considering the angle of wall friction) for studying both the cases for calculating bearing capacity. The thickness of the cylindrical skirt wall is assumed to be 1 centimeter. The model footing is circular with diameter of 100 centimeter.

The analytical solution is carrying out to study the effect of soil confinement on bearing capacity of foundation by varying height and diameters of cylindrical skirts as shown in Table 4.1.

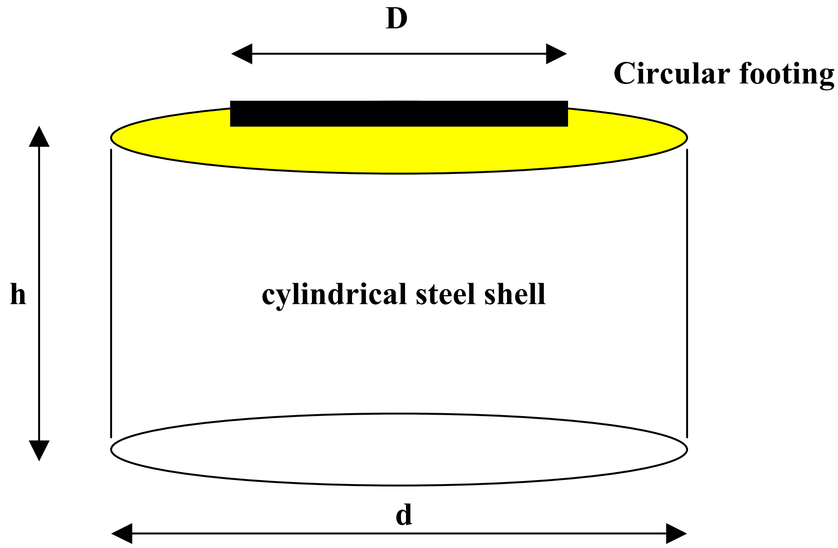

fig. 4.1

TABLE 4.1

	Constant parameters	variables parameter
1.	d/D = 1.00	h/D = 0.5, 1.00, 1.50, 2.00, 2.50, 3.00
2.	d/D = 1.07	h/D = 0.5, 1.00, 1.50, 2.00, 2.50, 3.00
3.	d/D = 1.33	h/D = 0.5, 1.00, 1.50, 2.00, 2.50, 3.00
4.	d/D = 1.60	h/D = 0.5, 1.00, 1.50, 2.00, 2.50, 3.00
5.	d/D = 2.00	h/D = 0.5, 1.00, 1.50, 2.00, 2.50, 3.00

4.3 PROPERTIES OF THE MATERIAL

COHESIONLESS SOIL (SAND)

- Medium to coarse having
- Unit weight (γ) = 18 N/m^3
- Void ratio = 0.35 to 0.45
- Angle of internal friction(ϕ) = 42, 38, and 34 degree
- Angle of wall friction (δ) = 0, 22, and 25 degree

THIN CYLINDRICAL STEEL SHELL

- Thickness, t = 1 cm
- Height, h = 0.5, 1.0, 1.5, 2.0, 2.5, and 3.0 meter

- Diameter, d = 1.00, 1.07, 1.33, 1.60, and 2.00 meter
- Permissible tensile stress for the steel shell = 100 N/mm^2 = 100000 Kpa

4.4 PROPOSED ANALYSIS & FORMULATION

In calculation of bearing capacity of skirted foundation two approaches are PROPOSED

First, the cylindrical skirts of different diameter and heights as shown in Table-3.1 above is used for calculating the bearing capacity (see Fig. 4.2). It is called **NORMAL APPROACH.**

Second, as per Terzaghi's theory of bearing capacity (as explained in literature review) the path of the log-spiral has taken as the boundary for the height of the cylindrical shell. Means at every change of diameter the height is also varies with path of log-spiral. If we provide the height beyond the line of log-spiral this will acts as factor of safety for calculating bearing capacity (see Fig.4.3). It is called **TERZAGH'S APPROACH.**

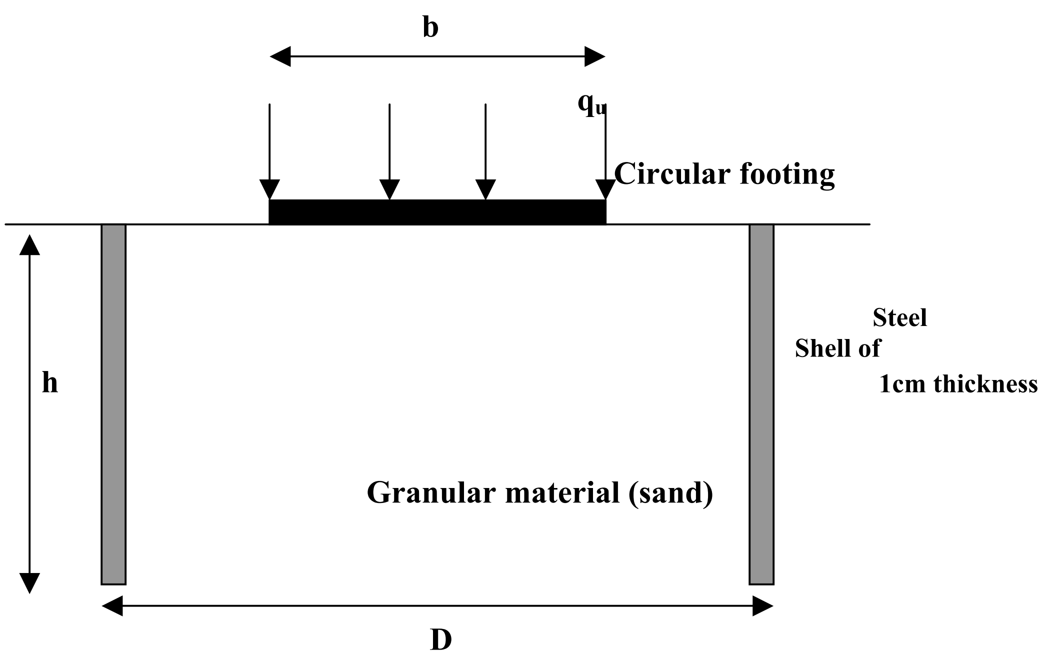

Fig. 4.2, This figure shows Normal approach. The h & d varies as shown in Table-4.1, used for calculating bearing capacity of footing

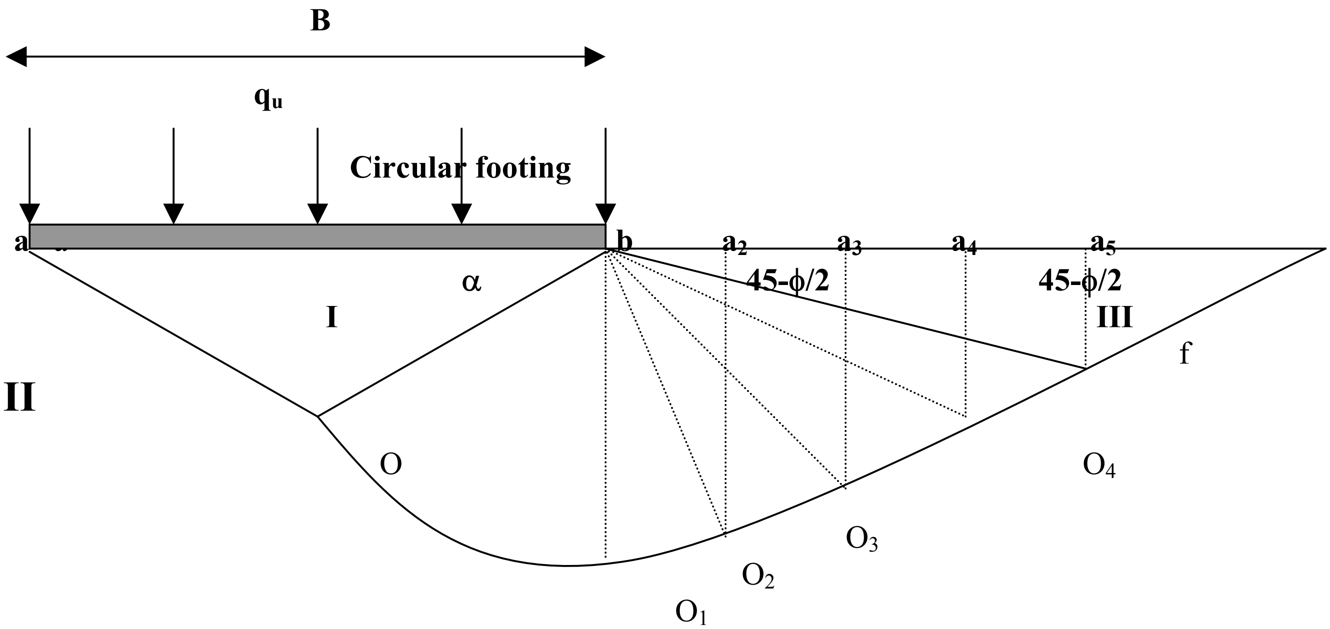

Fig. 4.3 This figure shows Terzaghi's approach, the height of the shell varies from bO_1 to a_5f as per the path of the Log-spiral. If the height is provide beyond the Path of log-spiral it will acts as the factor of safety.

The analysis here is done for the cylindrical shell of very smooth surface (δ =0) (exterior and interior both) and also for rough surface ($\delta \neq 0$).

- For very smooth surface of cylindrical shell the angle of wall friction (δ) = 0, as assumed by Rankine in his theory of earth pressure for calculating the Active and Passive (K_a & K_p) earth pressure. So, I will call the smooth surface cylindrical shell as **RANKINE WALL.**
- And for the rough surface of cylindrical shell the angle of wall friction (δ) $\neq$ 0, for that the Coulomb has given the formulas for calculating the active and passive earth pressure for cohesionless soil (K_a & K_p) in his wedge theory. so, I will call the rough surface cylindrical shell as **COULOMB WALL**.

4.4.1 CACULATION OF K_a AND K_p

- **K_a & K_p FOR RANKINE WALL (δ = 0)**

$K_a = \tan^2 (45-\phi/2)$
$K_p = \tan^2 (45+\phi/2)$

- **K_a & K_p FOR COULOMB WALL ($\delta \neq 0$)**

$$K_a = \frac{\sin^2(\alpha+\phi)}{\sin^2\alpha \sin(\alpha-\delta)\left\{1+\sqrt{\dfrac{\sin(\phi+\delta)\sin(\phi-\beta)}{\sin(\alpha-\delta)\sin(\alpha+\beta)}}\right\}^2}$$

$$K_p = \frac{\sin^2(\alpha-\phi)}{\sin^2\alpha \sin(\alpha+\delta)\left\{1 - \sqrt{\frac{\sin(\phi+\delta)\sin(\phi+\beta)}{\sin(\alpha+\delta)\sin(\alpha+\beta)}}\right\}^2}$$

Where,
ϕ = angle of internal friction of wall.
δ = angle of wall friction.
β = angle of inclination of the soil above the ground surface, in our case it is zero degree.
α = angle of inclination of wall, in our case it is 90 degree.
All the values of K_a and K_p are given in Table- 4.2, for different values of ϕ and δ.

TABLE – 4.2

ϕ	**K_a For** $\delta = 0^o$	**K_a For** $\delta = 22^o$	**K_a For** $\delta = 25^o$	**K_p For** $\delta = 0^o$	**K_p For** $\delta = 22^o$	**K_p For** $\delta = 25^o$
42	0.198	0.183	0.183	5.044	15.776	19.758
38	0.238	0.217	0.217	4.204	11.466	13.901
34	0.238	0.254	0.254	3.537	8.641	10.193

4.4.2 FORMULATION FOR RANKINE AND COULOMB WALL

- Active earth pressure, $\mathbf{P_a = ½ K_a \gamma h^2}$
- Passive earth pressure, $\mathbf{P_p = ½ K_p \gamma h^2}$
- Circumferential tensile stress (or hoop stress),

$$\boldsymbol{f = p.d /2.}$$

So, $\quad \mathbf{p = \boldsymbol{f}.2.t /d}$

Where , p = internal pressure.
D = diameter of shell.
T = thickness of shell.

4.4.2.1 RANKINE WALL ($\delta = 0$)

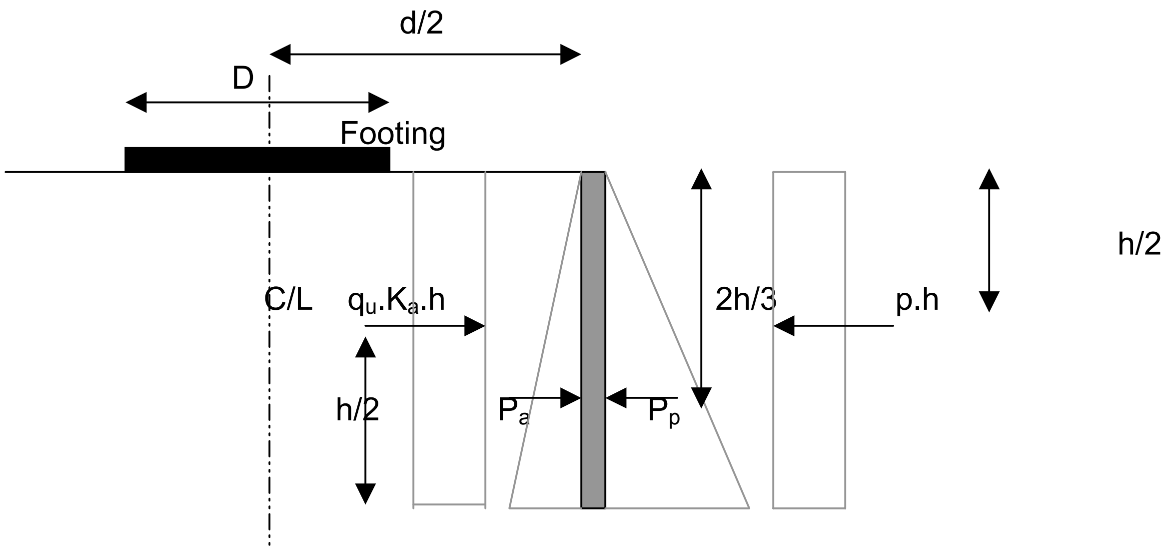

Fig. 4.4

Taking moment of all the forces about the center line of the footing

$q_u.K_a.h.h/2 + \frac{1}{2} K_a.\gamma.h^2.2/3\ .h = (f.2.t.h/d)\ .\ (h/2) + \frac{1}{2} K_{p.}\gamma h^2).(2/3\ .h)$

So from this we get

$$\boxed{\mathbf{q_u = 2.f.t/d.K_a + 2/3\ \gamma.h(K_p - K_a)/K_a}}$$

4.4.2.2 COULOMB WALL ($\delta \neq 0$)

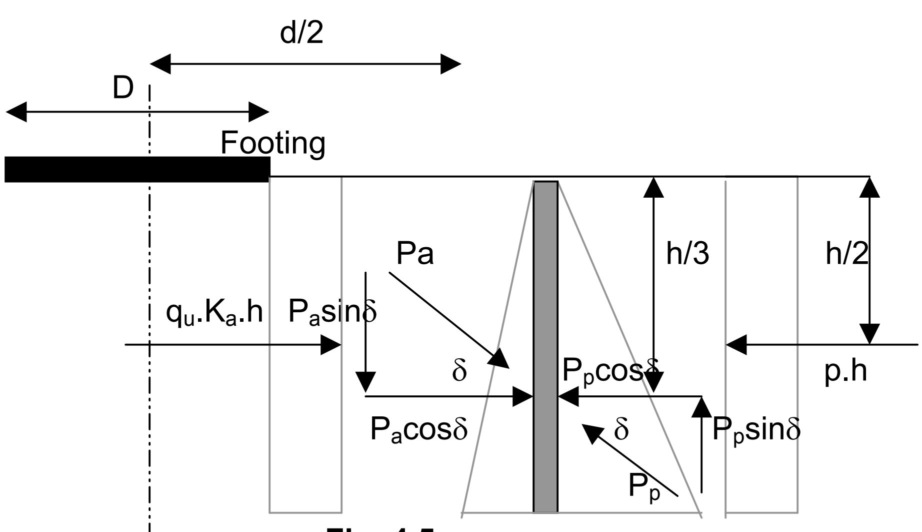

Fig. 4.5

Taking moment of all the forces about the center line of the footing

$$(f.2.t.h/d)\,(h/2) + 1/2\, K_p.\gamma.h^2.\cos\delta(2/3.h) + 1/2\, K_a.\gamma.h^2.\sin\delta.d/2$$
$$= ½\, K_a.\gamma.h^2.\cos\delta(2/3.h) + ½\, K_p.\gamma.h^2.\sin\delta.d/2 + q_u.K_a.h.h/2$$

$$\boxed{\begin{aligned} \mathbf{q_u} &= (2.f.t/d.K_a) + (2.\gamma.K_p/K_a)\mathrm{x}(\cos\delta.h/3 - \sin\delta.d/4) \\ &\quad + 2.\gamma\,(\sin\delta.d/4 - \cos\delta.h/3) \end{aligned}}$$

4.4.2.3 BEARING CAPACITY OF THE FOOTING WITHOUT CONFINEMENT

The ultimate bearing capacity of the footing can be calculated by the formula:

$$\mathbf{q_u = ½\, \gamma\, D\, \zeta_\gamma\, N_\gamma}$$

Where,

Unit weight of soil, γ = 18.00 KN/m^3

Bearing capacity factor $\mathbf{N_\gamma}$ for different ϕ as given by Kumbhojkar are, N_γ = 171.99 for $\phi = 42^o$, N_γ = 78.61 for $\phi = 38^o$, and N_γ = 38.04 for $\phi = 34^o$.

Diameter of the footing = 1m

Shape factor ζ_γ = 0.6 as given by Terzaghi for circular footing.

$\mathbf{q_u}$ = 928.75 KN/m^3 for N_γ = 171.99 & $\phi = 42^o$

$\mathbf{q_u}$ = 424.50 KN/m^3 for N_γ = 78.610 & $\phi = 38^o$

$\mathbf{q_u}$ = 205.42 KN/m^3 for N_γ = 38.040 & $\phi = 34^o$

4.4.2.4 BEARING CAPACITY RATIO

The bearing capacity improvement due to the soil confinement is represented using a nondimensional factor, called the bearing capacity ratio (BCR). This is defined as the ratio of the footing ultimate load with soil confinement (Q_u) to the footing ultimate load without confinement (q_u).

$$\mathbf{BCR = Q_u / q_u}$$

4.5 EFFECT OF THE SOIL PRESSURE ON THE CYLLINDRICAL SHELL

One of the proposed parameter to be investigated was the thickness of the shell wall to study the effect of the shell rigidity on the footing shell system behavior and also to study the hoop tension in the shell sue to the pressure under the footing. The horizontal pressure acting on the side wall of the shell is equal to the vertical pressure multiplied by the coefficient of lateral earth pressure. It can be seen that the maximum estimated horizontal earth pressure on the side walls of the shell are very small in comparison to the allowable hydraulic pressure, another point is that the given allowable value is the net inside pressure while the shell in the model is subjected to both internal and external pressure.

4.6 RESULTS AND DISCUSSION

4.6.1 EFFECT OF CYLINDRICAL SHELL DIAMETER

In order to investigate the effect of shell diameter on the footing behavior, different diameter of cylindrical shell 100, 107, 133, 160, and 200 cm were used.

Tables and Figures show the variation of BCR with normalized cylindrical shell diameter (d/D) for different shell heights (h/D) with a constant footing diameter (D) of 1 meter. A significant increase of bearing capacity of model footing supported on confined sand has observed, but also found that the BCR decreases with an increase in the d/D ratio.

The coming figures show (for tables see APPINDEX) for different Proposed Approaches as explained in above articles 4.4. E.g. Normal approach and Terzaghi's approach, also for the Rankine wall and

Coulomb wall for different value of ϕ (34o, 38^o, and 42^o) and angle of wall friction ($\delta = 0^o$, 22^o, and 25^o).

The significant increase in the bearing capacity of the footing can be explained as follows, when the footing is loaded, such confinement resist the lateral displacement of soil piratical underneath the footing and confines the soil leading to a significant decrease in the vertical settlement and hence improving the bearing capacity. For small cylindrical shell diameters, as the pressure is increased, the plastic state is developed initially around the edges of the footing and then spreads initially around the edges of the footing and then spread downward and outward. The mobilized vertical friction between the sand and the inside wall of the cylinder increases with the increase of the active earth pressure until the point when the system (the cylinder, sand and footing) starts behave as one unit. The behavior is similar to that observed in deep foundations (piles and caissons) in which the bearing load increases due to the shear resistance of shell surface. This illustrate the increase of the bearing load with the increase of the shell diameter and shell height, based on tests performed with shell made with very smooth surfaces, it can be concluded that increased surface roughness results in greater bearing load improvement.

Normal approach for Rankine wall

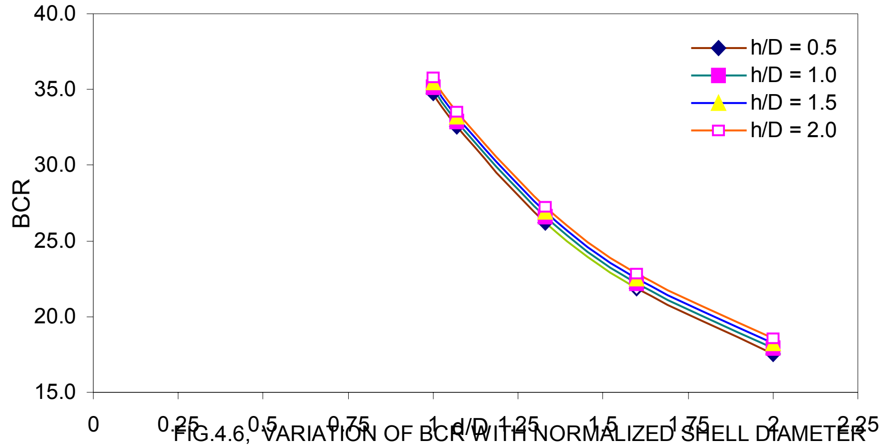

FIG.4.6, VARIATION OF BCR WITH NORMALIZED SHELL DIAMETER (d/D) FOR DIFFRENT SHELL HEIGHT & for Rankine wall(ϕ =34^{o} & δ =0^{o})

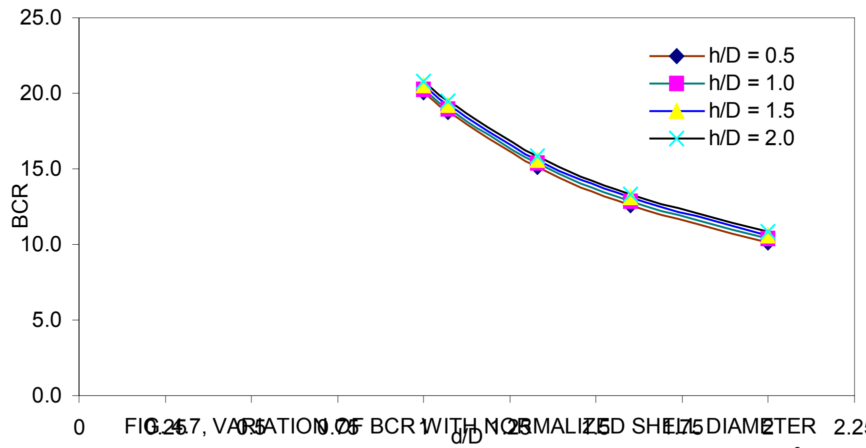

FIG.4.7, VARIATION OF BCR WITH NORMALIZED SHELL DIAMETER (d/D) FOR DIFFRENT SHELL HEIGHT &FOR RANKINE WALL(ϕ = 38^{o} & δ =0^{o})

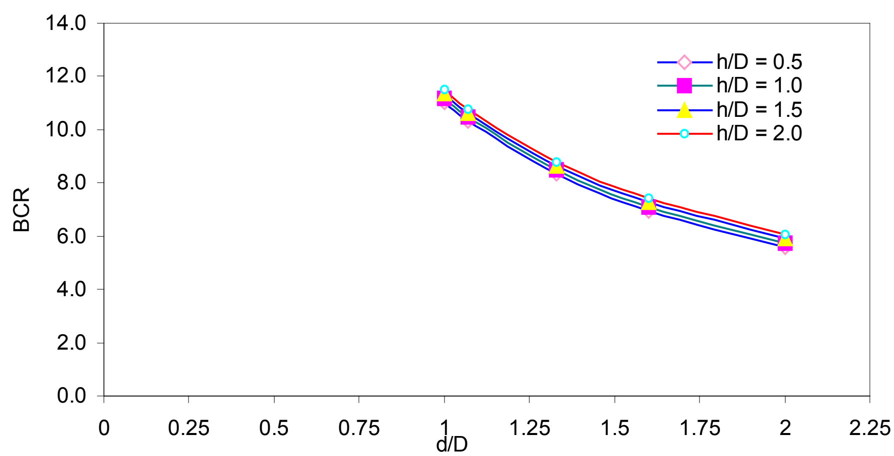

FIG. 4.8 VARIATION OF BCR WITH NORMALIZED SHELL DIAMETER (d/D) FOR DIFFRENT SHELL HEIGHT & FOR RANKINE WALL(ϕ = 42^{o} & δ =0^{o})

Normal approach for Coulomb wall

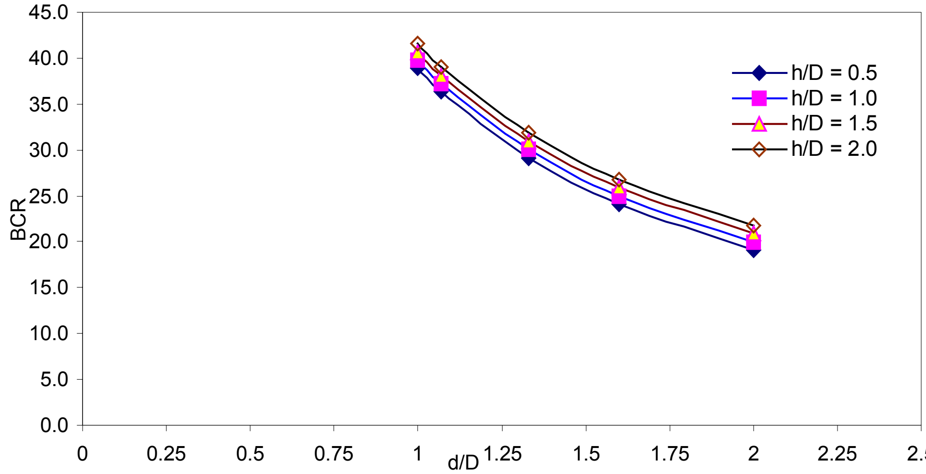

FIG. 4.9, VARIATION OF BCR WITH NORMALIZED SHELL DIAMETER (d/D) FOR DIFFRENT SHELL HEIGHT & FOR COULOMB WALL (ϕ = 34^o & δ =22^o)

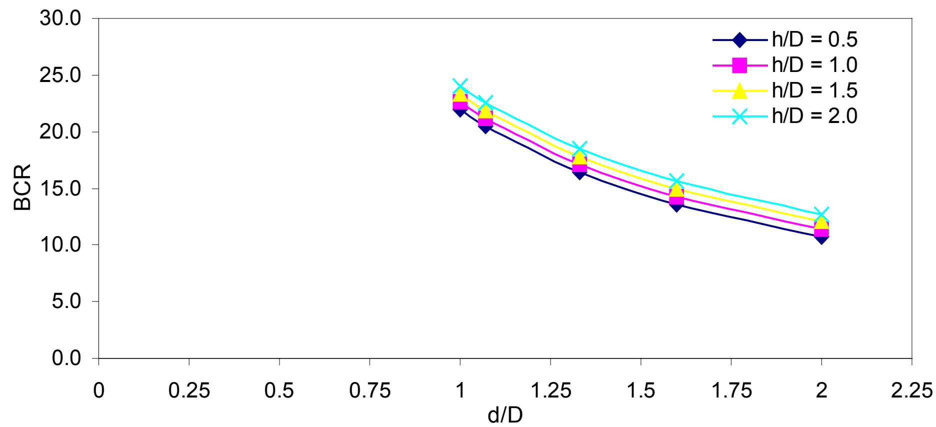

FIG.4.10, The variation of BCR with normalized shell diameter (d/D) for different shell heights, for Coulomb wall(ϕ = 38^o and δ = 22^o)

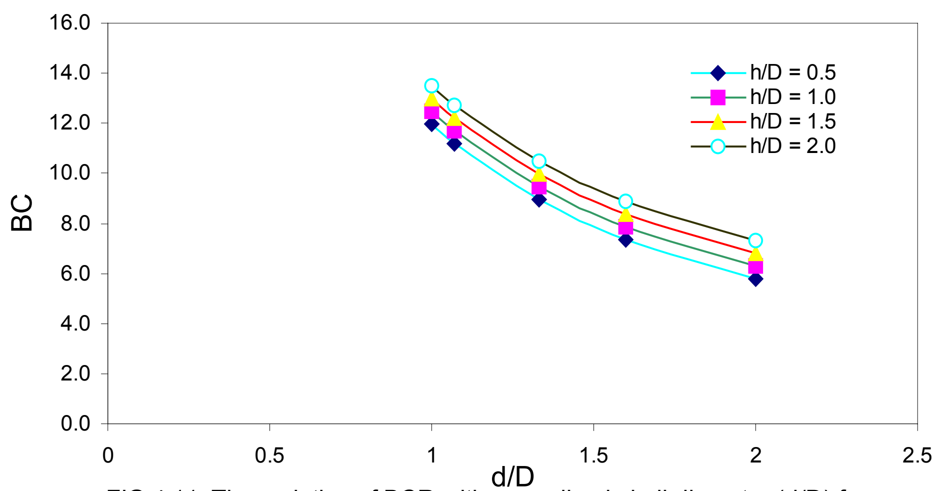

FIG.4.11, The variation of BCR with normalized shell diameter (d/D) for different shell heights & for Coulomb wall (ϕ = 42^o & δ = 22^o)

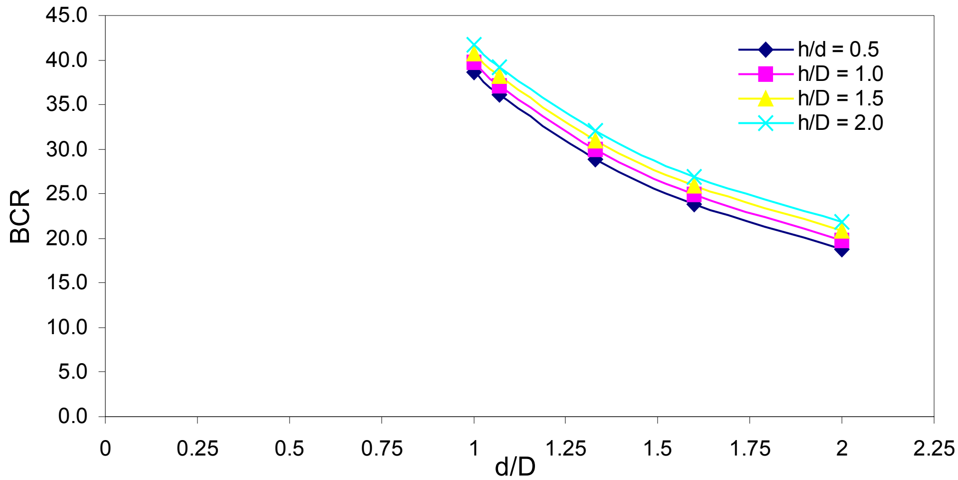

Fig.4.12, The variation of BCR with normalized shell diameter (d/D) for different shell heights & for Coulomb wall ($\phi = 34^{o}$ & $\delta = 25^{o}$)

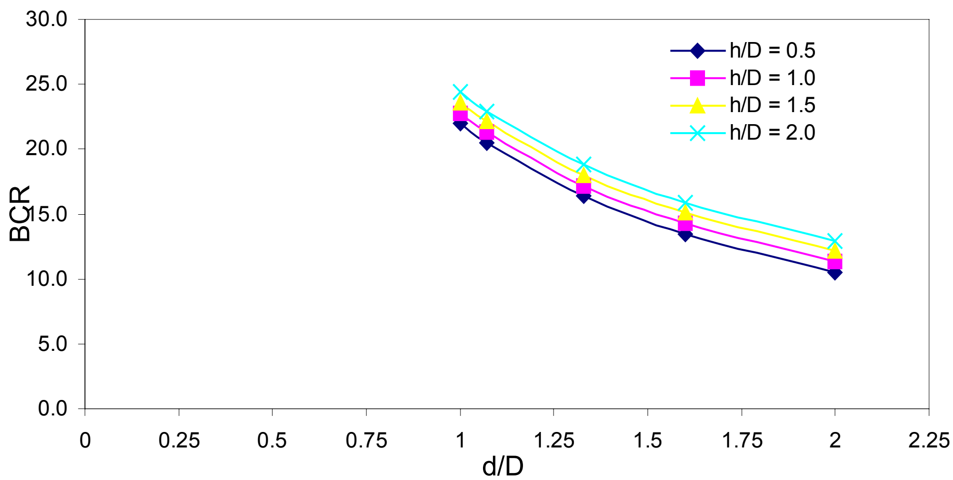

Fig.4.13, The variation of BCR with normalized shell diameter (d/D) for different shell heights & for Coulomb wall ($\phi = 38^{o}$ & $\delta = 25^{o}$)

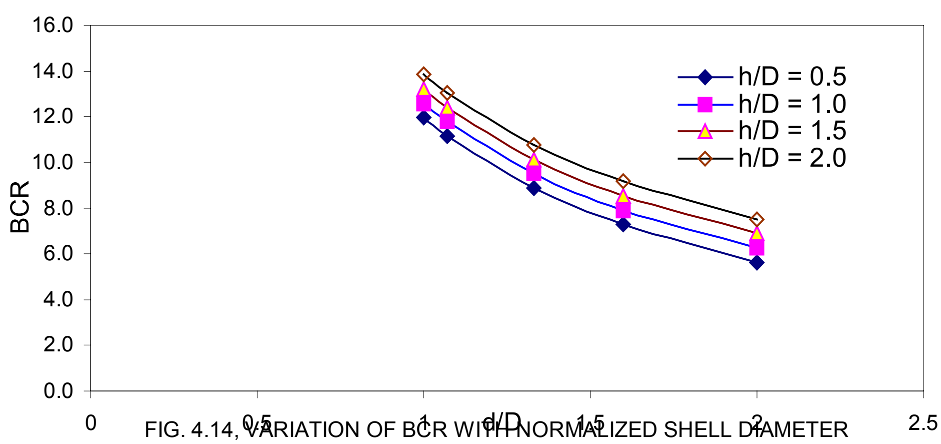

FIG. 4.14, VARIATION OF BCR WITH NORMALIZED SHELL DIAMETER (d/D) FOR DIFFRENT SHELL HEIGHT& FOR COLOUMB WALL($\phi = 42^{o}$ & $\delta = 25^{o}$)

Terzaghi's approach for Rankine wall

Fig. 4.15, Variation of BCR with normalized shell diameter (d/D) for different shell heights (h/D)(For ϕ = 42°, 38°, and 34°)

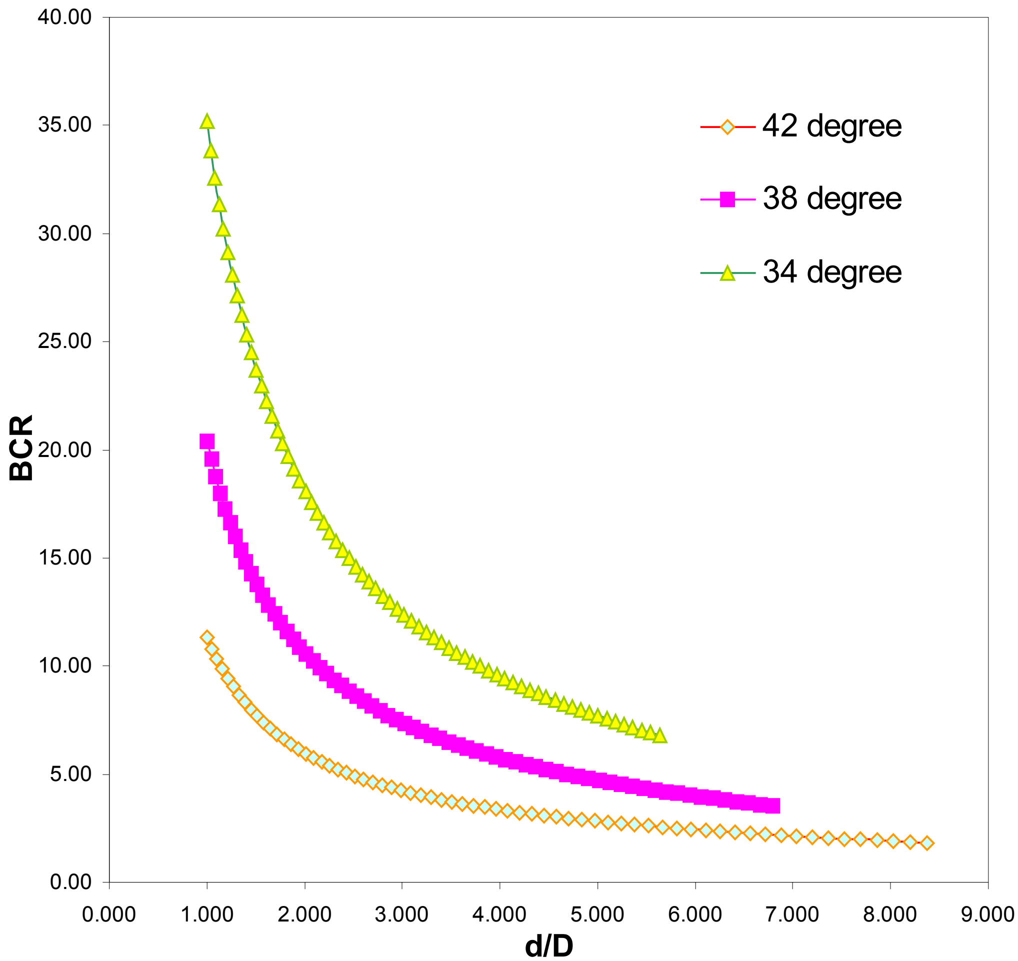

Terzaghi's approach for Coulomb's wall

Fig. 4.16, Variation of BCR with normalized shell diameter (d/D) for different height (h/D). (ϕ = 42°, 38°, 34° and δ = 22°)

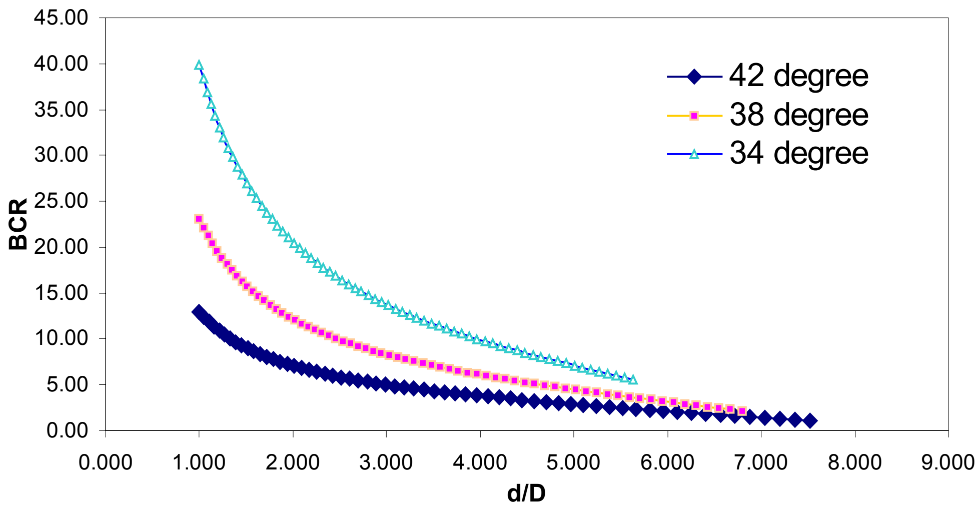

Fig. 4.17, Variation of BCR with normalized shell diameter (d/D) for different height (h/D), (ϕ = 42°, 38°, 34°, and δ = 25°)

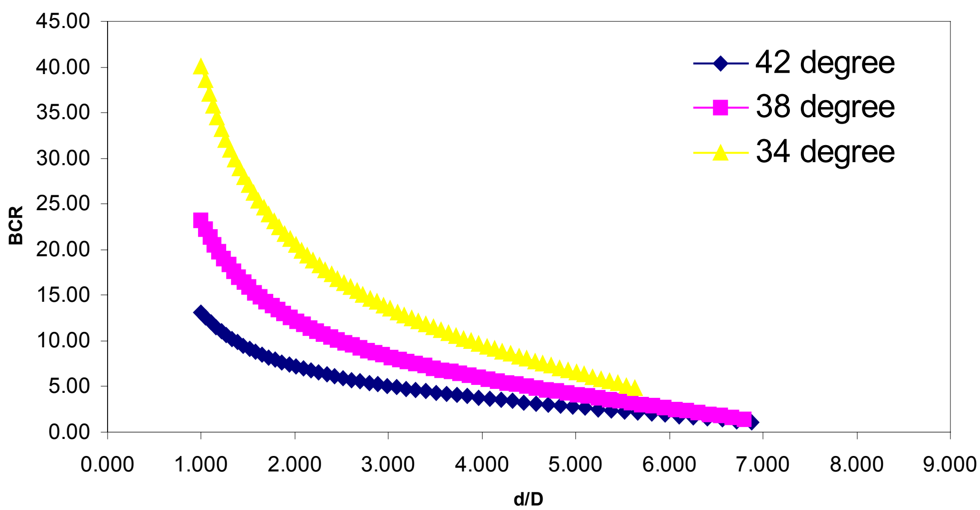

4.6.2 EFFECT OF CYLINDRICAL SHELL HEIGHT

In order to investigate the effect of shell height on the footing response, analysis has been done by using six different heights for each shell diameters. The variation of BCR with normalized shell height (h/D) is shown in the Table (see appendix) and figures for Normal approach and Terzaghi approach for different angles of internal friction of soil (ϕ = 42, 38, and 34 degree) and angle d wall friction (δ = 0, 22, and 25 degree).

For different normalized shell diameter) d/D). The figures show the same pattern of behavior for the different shell diameter, increase in shell height result in an improvement in BCR. This increase in shell height results in the enlargement in the surface area of the cylindrical shell-model footing leading to the higher bearing capacity load.

Normal approach for Rankine wall

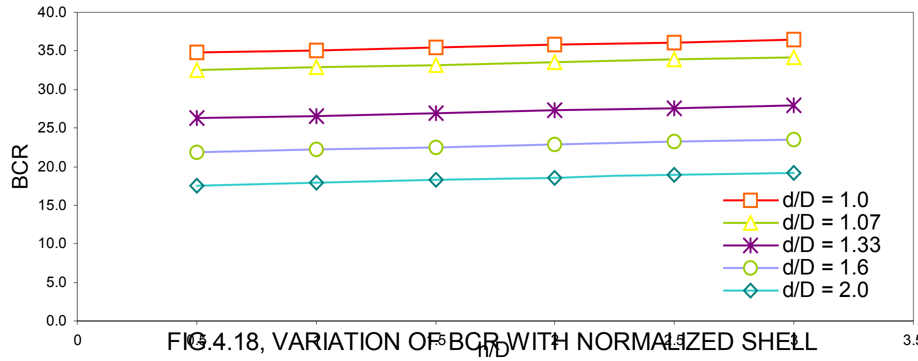

FIG.4.18, VARIATION OF BCR WITH NORMALIZED SHELL HEIGHT (h/D) FOR DIFFRENT SHELL DIAMETER(d), ($\phi = 34^o$ and $\delta = 0^o$)

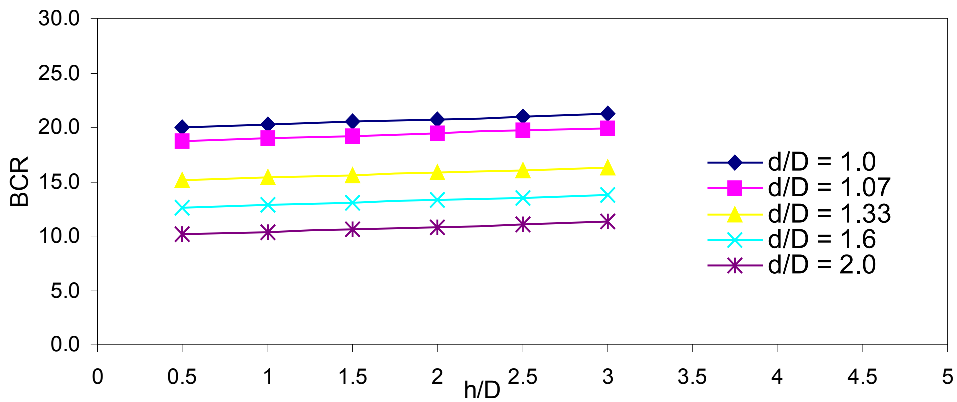

Fig.4.19, The variation of BCR with normalized shell height (h/D) for different shell diameter,(FOR $\phi = 38^o$ and $\delta = 0^o$)

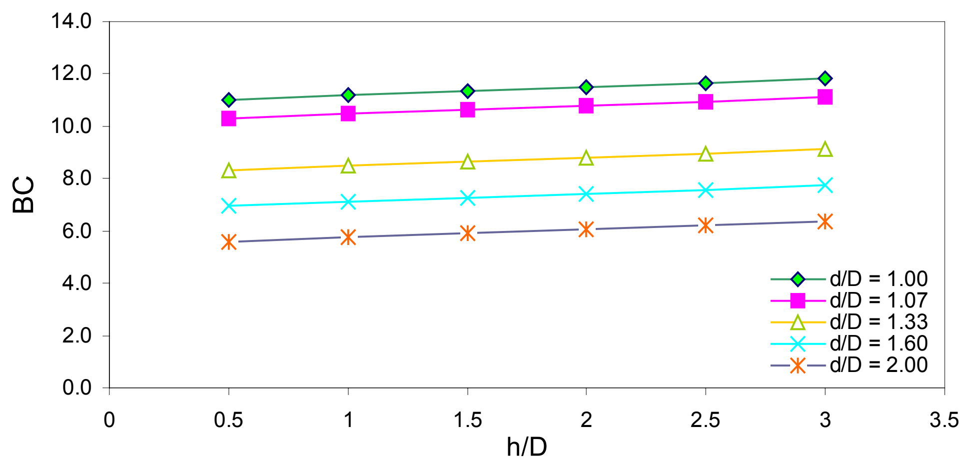

Fig. 4.20, The variation of BCR with normalized shell height (h/D) for different shell diameterl (FOR $\phi = 42^o$ and $\delta = 0^o$)

Normal approach for Coulomb wall

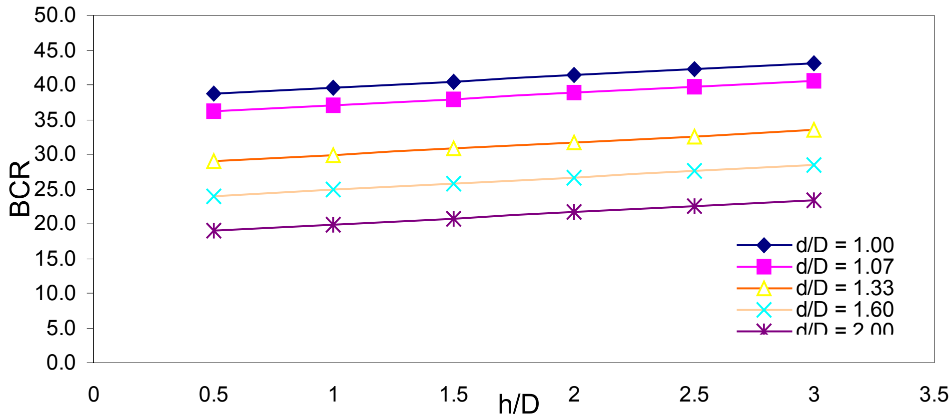

Fig. 4.21, The variation of BCR with normalized shell height (h/D) for different shell diameter (FOR $\phi = 34^{o}$ and $\delta = 22^{o}$)

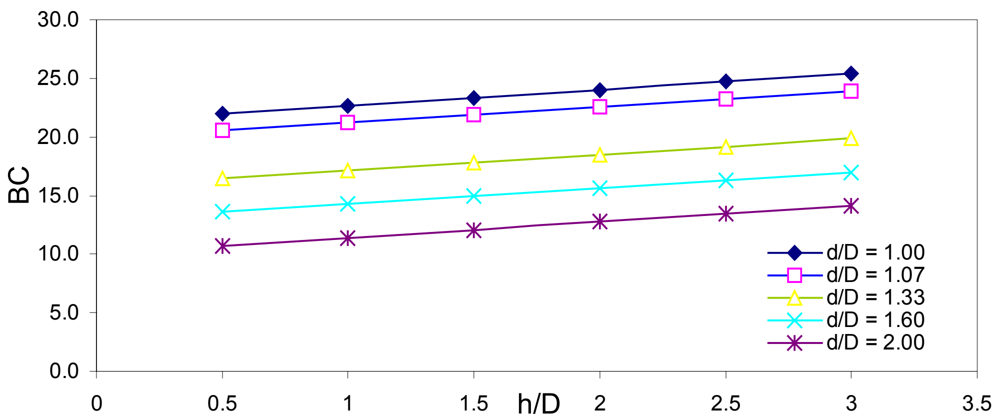

Fig. 4.22, The variation of BCR with normalized shell height (h/D) for different shell diameter (FOR $\phi = 38^{o}$ and $\delta = 22^{o}$)

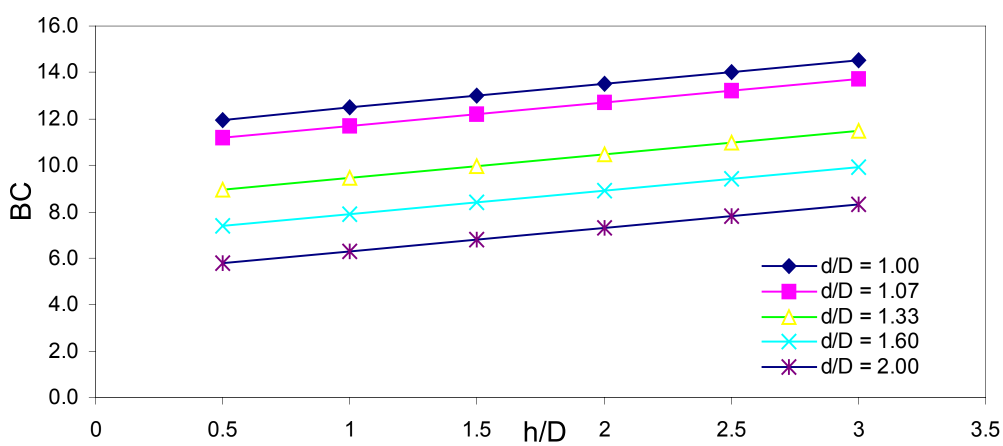

Fig. 4.23, The variation of BCR with normalized shell height (h/D) for different shell diameter ($\phi = 42^{o}$ and $\delta = 22^{o}$)

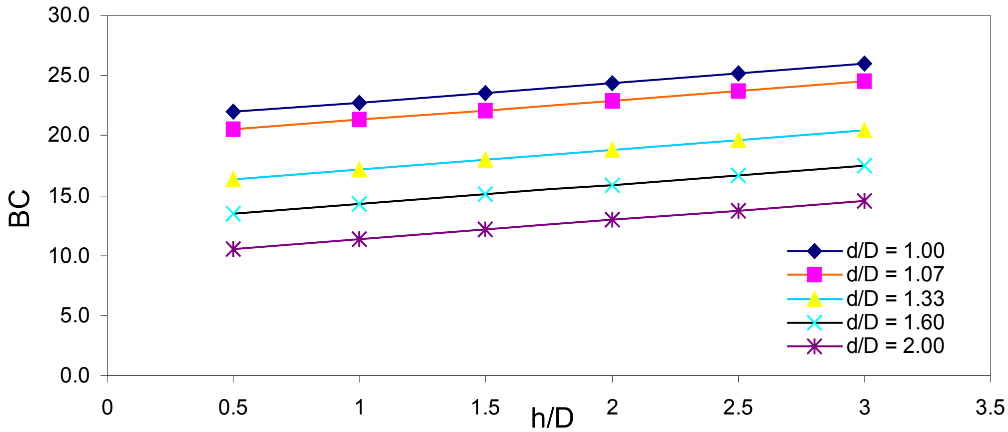

Fig. 4.24, The variation of BCR with normalized shell height (h/D) for different shell diameter(FOR $\phi = 38^{o}$ and $\delta = 25^{o}$)

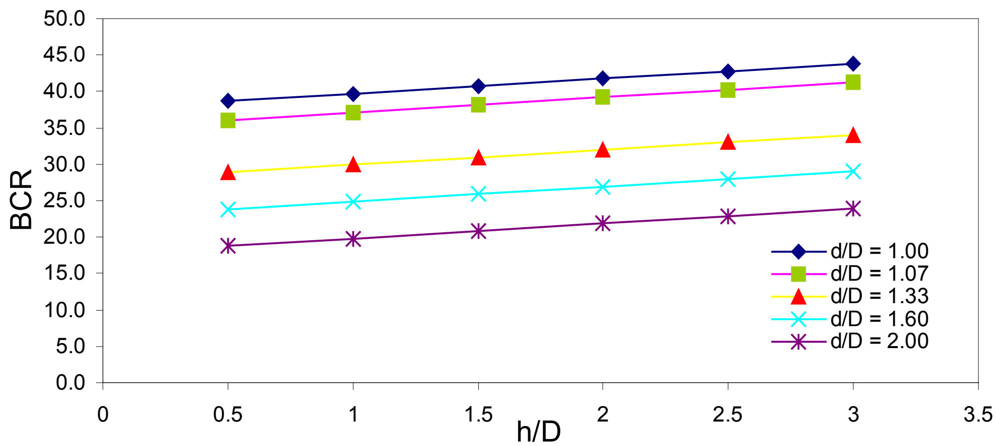

Fig. 4.25, The variation of BCR with normalized shell height (h/D) for different shell diameter (FOR $\phi = 34^{o}$ and $\delta = 25^{o}$)

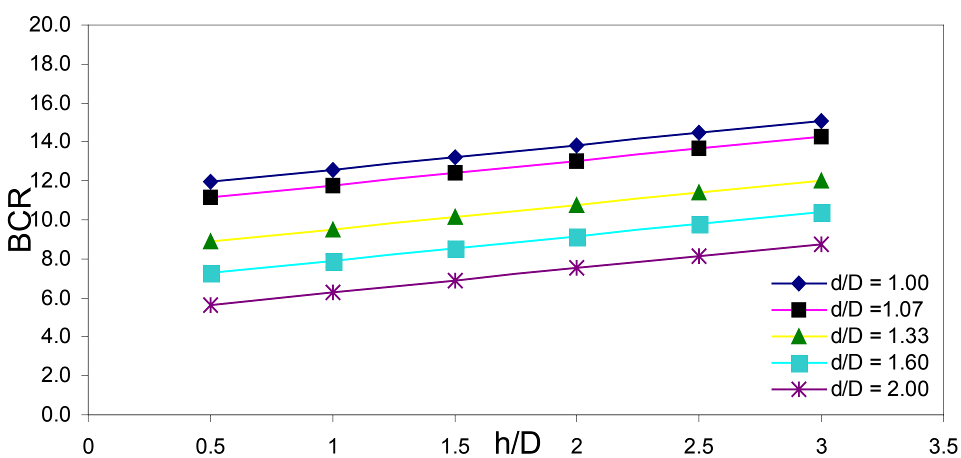

Fig. 4.26, The variation of BCR with normalized shell height (h/D) for different shell diameter (FOR $\phi = 42^{o}$ and $\delta = 25^{o}$)

Terzaghi approach for Rankine wall

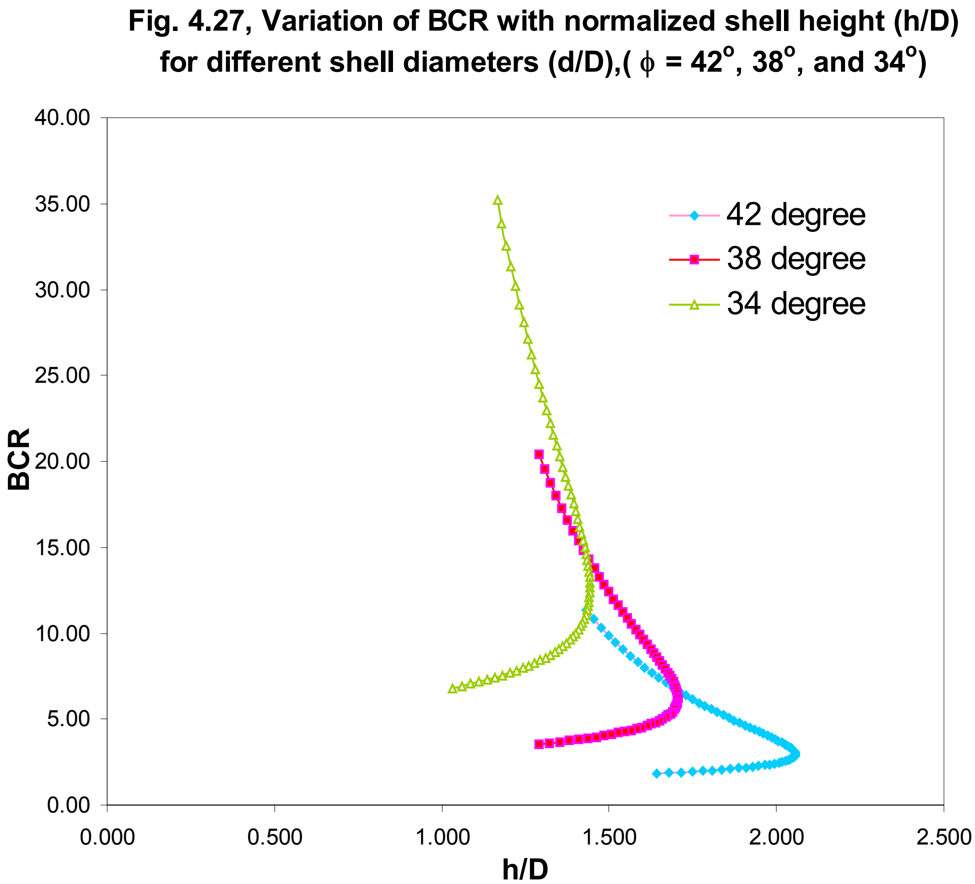

Terzaghi approach for Coulomb wall

Fig. 4.28, Variation of BCR with Normalized shell height (h/D) for different shell diameter (d/D), ($\phi = 42^o, 38^o, 34^o$ and $\delta = 22^o$)

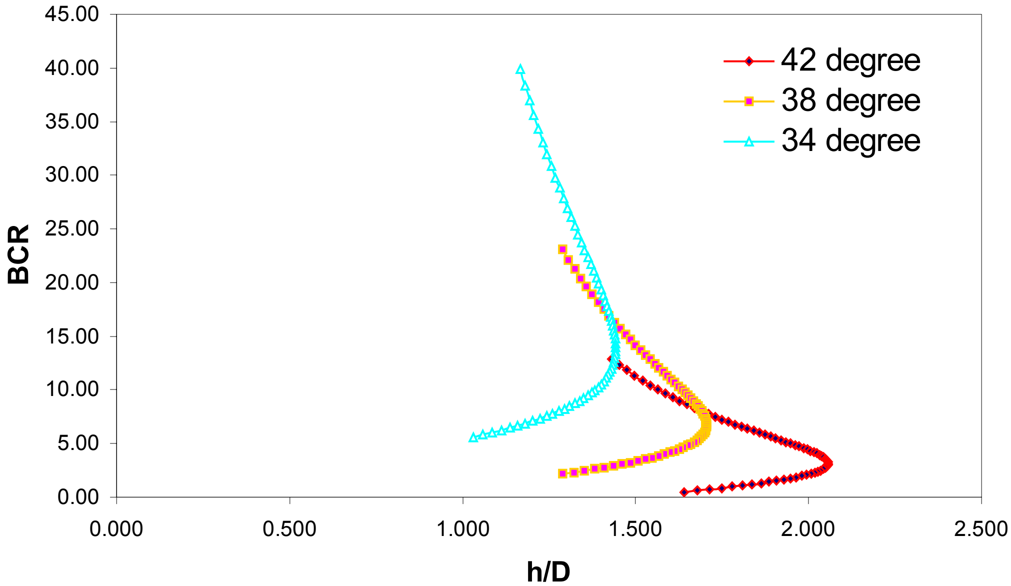

CHAPTER-5

CONCLUSIONS AND SCOPE OF FURTHER STUDY

5.1 CONCLUSIONS

The objective of this thesis is to study the effect of special type of footings on improvement of bearing capacity of shallow foundations using the extension of Terzaghi (1943) and Kumbhojkar (1993) approach.

The **first case** was considered for a spudcan footing supported on soil.
Since the spudcan footing uses a cone at the base, the log-spiral tends to grow downward and outward to increase the bearing capacity factor N_c, N_q, and N_γ , this represents the angle of a spudcan (Ω) has got a significant effect that can be observed for the values of bearing capacity at $\phi = 30^{o.}$ The N_c, N_q, and N_γ for spudcan footing with cone angle (Ω) of 15^o are 40.6, 24.9, and 244.4, compared to Terzaghi's values of 37.1, 22.4, and 19.1 respectively.

In **second case** the circular footing supported on dry sand and surrounded from all sides by skirts (cylindrical steel shell) with very smooth and rough surfaces ($\delta \geq 0$). Based on the analytical solutions the following conclusions can be drawn for skirted footing.

1. Soil confinement has a significant effect on improving the behavior of circular footing supported on granular soil. The ultimate bearing capacity was 43 times as compared to unconfined case. Therefore it can be concluded that the sheet piles used to brace cuts have a significant effect on improving the bearing capacity of soils under raft foundation.
2. Based on the analytical results, soil confinement could be considered as a method to improve the bearing capacity of isolated footing bearing on sand. Steel shells of different heights,

diameters, and thickness could be easily manufactured and placed and the individual footing leading to a significant improvement in there response.

3. In case where structures are very sensitive to settlement, soil confinement can used to obtain the same allowable bearing capacity at much lower settlement.
4. The BCR is highly depends on the d/D ratio (shell diameter/footing diameter ratio) the optimum ratio is about one, beyond which the improvement decreases as the ratio increases.
5. The two following approaches are used Normal approach and Terzaghi approach with Rankine's wall and Coulomb's wall ($\delta = 22^o$ & 25^o). It was observed that maximum BCR in all cases are decreases as the angle of internal friction increases from 34^o to 42^o. Also the BCR is decreases as the d/D (shell diameter/ footing diameter ratio) increases and BCR increases as the h/D (shell height/footing diameter) increases.
6. Increase the height of the cylindrical shell results in increasing the surface area of the shell-model footing, which transfers loads to deep depths and lead to improving the BCR.
7. At the time of design of the foundation by calculating the upcoming loads the thickness and height of the cylindrical shell can be economically decided.
8. The permissible value of circumferential tensile stress (or hoop stress) has considered $100 N/mm^2$. If it is increases the thickness of the shell is reduces.
9. In Terzaghi's approach the height of the shell varies as the path of the log-spiral varies if the height provides beyond the path of log-spiral it will acts as the factor of safety for unpredictable settlement and loading.
10. As I considered steel as the material of cylindrical shell, it can be replaced by some other material, which is corrosion resistance and economical, compared to steel, like polyvinyl chloride cylinders.

5.2 SCOPE OF FURTHER STUDY

Behavior of other footings, square and rectangular along with the influence of the roughness and the stiffness of shell material were not studied. Therefore it is recommended that further work is investigates the effect of these parameter for both dry and wet sand conditions.

Studying the effect of soil confinement on the behavior of footing bearing on weak type of soil such as loose sand and soft clay is also the scope of further study.

This analytical solution can be further extent for studying it by using Finite Element Modeling so that it can incorporates all the variability of the soil, shell and footing material properties which otherwise becomes difficult.

REFRENCES

[1]. Bowles, J. E. (1968). Foundation analysis and design. McGraw-Hill, New York, N.Y.

[2]. Das, B. M. (1987). Theoretical foundation engineering. Elsevier Book Publishing Co., New York, N.Y.

[3]. Das, B. M. (1990). Principles of geotechnical engineering. 2nd Ed., PWS-KENT Publishing Co., Boston, Mass.

[4]. Meyerhof, G. G. (1951). " The ultimate bearing capacity of foundations." Geotechnique, 2, 201-331.

[5]. Terzaghi, K. (1943). Theoretical soil mecanics. 5th Ed., John Wily and Sons Inc., New York, N.Y.

[6]. Vesic, A. S. (1973). " Analysis of ultimate loads of shallow foundations." J. Soil Mech. Found. Div., ASCE, 99(1), 45-73.

[7]. Kumbhojkar, A. S. (1993). " Numerical evaluation of Terzaghi's N_γ." J. Geotech. Eng., 119(3), 598-607.

[8]. Baki, A. A., and Beil, L. A. (1970). "Bearing capacity of foundation on sand." J. Soil Mech. Found. Div., Am. Soc. Civ. Eng., 96(2), 545-559.

[9]. Chen, W. F. (1975). Limit analysis and soil plasticity, Elesvier Scientific, London.

[10]. Dewaikar, D. M., and Mohapatro, B. G. (2003). "Computation of Bearing Capacity Factor N_γ – Terzaghi's Mechanism." International J. of Geomechanics. Vol-3, No.1.

[11]. Frydman, S., and Burd, H. J. (1997). "Numerical studies of bearing capacity factor N_γ." J. Geotech. Geoenviron. Eng., 123(1), 20-29.

[12]. Hansen, J. B. (1970). "A revision and extended formula for bearing capacity ." Bull. No. 28, Danish Geotechnical Institute, Copenhagen, Denmark.

[13]. Ingra, S. T., and Baecher, G. B. (1983). "Uncertanity in bearing capacity of sands." J. Geotech. Eng., 109(7), 899-914.

[14]. Meyerhof, G. G. (1963). "Some recent research on the bearing capacity of foundations." Can. Geotech. J., 1(1), 16-26.

[15]. Mohapatro, B. G. (2001). "Some studies on bearing capacity of shallow foundations." PhD thesis. IIT Bombay, India.

[16]. Soubra, A. H. (1999). "Upperbound solutions for bearing capacity of foundations," J. Geotech. Geoenviron. Eng., 125(1), 59-68.

[17].Zadroga, B. (1994). “Bearing capacity of shallow foundations on noncohesive soils.” J. Geotech. Eng., 120(11), 1991.

[18]. Binquet, J., and Lee, K. L. (1975). “Bearing capacity tests on reinforced earth slabs.” *J. Geotech. Eng. Div.* 101(12), 1241–1255.

[19]. Das, B. M., and Omar, M. T. (1994). “The effects of foundation width on model tests for the bearing capacity of sand with geogrid reinforcement.” *Geotech. Geologic. Eng.*, 12, 133–141.

[20]. Das, B. M., Puri, V. K., Omar, M. T., and Evgin, E. (1996). “Bearing capacity of strip foundation on geogrid reinforced sand-scale effects in model tests.” *Proc., 6th Int. Conf. on Offshore and Polar Engineering*, Vol. I, 527–530.

[21]. De Beer, E. E. (1970). “Expermential determination of the shape factor and the bearing capacity factors of sand.” *Geotechnique*, 20, 387–411.

[22]. Fragaszy, R. J., and Lawton, E. (1984). “Bearing capacity of reinforced sand subgrades.” *J. Geotech. Eng.*, 110(10), 1500–1507.

[23]. Guido, V. A., Chang, D. K., and Sweeney, M. A. (1986). “Comparison of geogrid and geotextile reinforced earth slabs.” *Can. Geotech. J.*, 23, 435–440.

[24]. Mandal, J. M., and Manjunath, V. R. (1995). “Bearing capacity of strip footing resting on reinforced sand subgrades.” *Constr. Build. Mater.*, 9(1), 35–38.

[25]. Omar, M. T., Das, B. M., Puri, V. K., and Yen, S. C. (1993a). “Ultimate bearing capacity of shallow foundations on sand with geogrid reinforcement.” *Can. Geotech. J.*, 30, 545–549.

[26]. Rajagopal, K., Krishanaswamy, N., and Latha, G. (1999). “Behaviour of sand confined with single and multiple geocells.” *Geotext. Geomembr.*, 17, 171–184.

[27]. Steenfelt, J. S. (1977), “Scale effect on bearing capacity factor (N_γ).” *Proc., 9th Int. Conf. on Soil Mechanics and Foundation Engineering*, Vol. 1, 749–752.

[28]. Sawwaf, M. El., and Nazer, A. (2005). “Behavior of Circular Footing Resting on Confined Granular Soil.” J. of Geotechnical and Geoenvironmental Engineering, Vol. 131, No. 3.

[29]. Prandtl, L.:Uber die harte plastischer korper (in German). Nachr, Kgl. GesWiss Gottingen Math. Phys. K.O.I. Berlin, 74–85 (1920)

[30]. Reissner, H.: “Zum erddrulk problem”, (in German). Proc. Ist Int. Conf. App. Mech., Delft, The Netherlands, 295–311 (1924)

[31]. Feda, J.: “Research on bearing capacity of loose soil”. Proc. 5th Int. Conf. Soil Mech. Found. Eng., Paris, Vol. **1**: 635–642 (1961)

[32]. Meyerhof, G.G.: “Shallow foundations”. J. Soil Mech. Found. Div., ASCE, Vol. 91: SM2, 21–31 (1965)

[33]. de Beer, E.E.: " The scale effect in the transposition of the results of deep sounding tests on the ultimate bearing capacity of piles and cassion foundations". Geotechnique, 8(1): 39–75 (1963)

[34]. de Beer, E.E.: "Bearing capacity and settlement of shallow foundations on sand". Proc. Symposium on Bearing Capacity and Settlement of Foundations, Duke University, Durham, N.C., 15–33 (1965)

[35]. Perkins, S.W., and Madson, C.R.: "Bearing capacity of shallow foundations on sand:A relative density approach". J. Geotech. And Geoenv. Eng., ASCE, Vol. 126(6): 521–529 (2000)

[36]. Das, B. M. (1999). Shallow Foundations, Bearing capacity and settlement. PWS-KENT Publishing Co., Boston, Mass.

[37]. Das, B. M. (1999). Principles of foundation engineering. 4^{nd} Ed., PWS-KENT Publishing Co., Boston, Mass.

[38]. Vesic, A. S., Bearing capacity of deep foundations in sand. Highway Res. Rec. 39, National Reserch Council, Washington, D.C., 112, 1963.

[39]. Caquot, A., and Kerisel, J., Sue le terme de surface dans le calcul des foundations en milieupilverulent, in Proc., III Int. Conf. Soil Mech. Found. Eng., Zurich Switzerland, 1, 1953,336.

[40]. Lundgren, H., and Mortensen, K., Determination by the theory of plasticity of the bearing capacity of continuous footing on sand, in Proc., III Int. Conf. Mech. Foundation. Eng., Zurich, Switzerland, 1, 1953,409.

[41]. Ko, H. Y. and Davidson, L. W., Bearing capacity of fooying in plane strain, J. soil Mech. Found. Div., ASCE, 99(1), 1, 1973.

[42]. Balla, A., Bearing capacity of foundations, J. soil Mech. Found. Div., ASCE 88(5), 13, 1962.

[43]. Stuart, J. G., Interference between foundations with special reference to surface footing on sand, Geotechnique, 12(1), 15, 1962

[44]. Das, B. M., and Labri-cherif, S., Bearing capacity of two closely spaced shallow foundations on sand, Soil and foundations, 23(1), 1, 1983

[45]. Dubrova, G. A., Interaction of soil and structures, Rechnoy Transport Moscow, 1973.

[46]. Purkayastha, R. D., and Char, R. A. N., Stability analysis for eccentrically loaded footing, J. Grotech. Eng. Div., ASCE, 103(6), 647, 1977.

[47]. Craig, W. H., and Chua, K. (1990). Deep penetration of spudcan foundation on sand and clay. Geotechnique, Vol.40, No. 4, 541-556.

[48]. Houlsby, G.T., and Martin, C.M. (2003). Undrained bearing capacity factor for conical footing on clay. Geotechnique, Vol.53, No.5, 513-520

[49]. Martin, C.M., and Houlsby, G.T. (2000). Combined loading of spudcan foundations on clay: laboratory test, Geotechnique, Vol.50, No. 4, 325-338.

[50]. Doherty, J. P., Deek, A. J. "*Elastic response of circular footing embedded in a non-homogenous half-space"*. Geotechnique 2003

[51]. Hously, G. T. & Cassidy, M. J. (2002). "*A plasity model for the behaviour of footing on sand under combined loading"*. Geotechnique 52, No. 2, 117-129

APPENDIX

Table-1, The variation of BCR with normalized shell diameter (d/D) for different shell heights, for Rankine wall and $\phi = 34^o$.

h/D	K_p	K_a	K_p-K_a	d	Q_u	BCR
						Q_u/q_u
0.5	3.537	0.283	3.254	1	7143.33	34.8
0.5	3.537	0.283	3.254	1.07	6680.53	32.5
0.5	3.537	0.283	3.254	1.33	5388.06	26.2
0.5	3.537	0.283	3.254	1.6	4490.48	21.9
0.5	3.537	0.283	3.254	2	3606.20	17.6
1	3.537	0.283	3.254	1	7212.40	35.1
1	3.537	0.283	3.254	1.07	6749.60	32.9
1	3.537	0.283	3.254	1.33	5457.13	26.6
1	3.537	0.283	3.254	1.6	4559.55	22.2
1	3.537	0.283	3.254	2	3675.27	17.9
1.5	3.537	0.283	3.254	1	7281.47	35.4
1.5	3.537	0.283	3.254	1.07	6818.67	33.2
1.5	3.537	0.283	3.254	1.33	5526.20	26.9
1.5	3.537	0.283	3.254	1.6	4628.62	22.5
1.5	3.537	0.283	3.254	2	3744.34	18.2
2	3.537	0.283	3.254	1	7350.54	35.8
2	3.537	0.283	3.254	1.07	6887.73	33.5
2	3.537	0.283	3.254	1.33	5595.27	27.2
2	3.537	0.283	3.254	1.6	4697.69	22.9
2	3.537	0.283	3.254	2	3813.40	18.6

Table-2, The variation of BCR with normalized shell diameter (d/D) for different shell heights, for Rankine wall and $\phi = 38^o$.

h/D	K_p	K_a	K_p-K_a	d/D	Q_u	BCR
						Q_u/q_u
0.5	4.204	0.238	3.966	1	8507.52	20.0
0.5	4.204	0.238	3.966	1.07	7957.50	18.7
0.5	4.204	0.238	3.966	1.33	6421.45	15.1
0.5	4.204	0.238	3.966	1.6	5354.71	12.6
0.5	4.204	0.238	3.966	2	4303.77	10.1
1	4.204	0.238	3.966	1	8607.55	20.3
1	4.204	0.238	3.966	1.07	8057.53	19.0
1	4.204	0.238	3.966	1.33	6521.48	15.4
1	4.204	0.238	3.966	1.6	5454.74	12.8
1	4.204	0.238	3.966	2	4403.80	10.4
1.5	4.204	0.238	3.966	1	8707.58	20.5
1.5	4.204	0.238	3.966	1.07	8157.56	19.2
1.5	4.204	0.238	3.966	1.33	6621.51	15.6
1.5	4.204	0.238	3.966	1.6	5554.77	13.1
1.5	4.204	0.238	3.966	2	4503.83	10.6
2	4.204	0.238	3.966	1	8807.61	20.7
2	4.204	0.238	3.966	1.07	8257.58	19.5
2	4.204	0.238	3.966	1.33	6721.54	15.8
2	4.204	0.238	3.966	1.6	5654.80	13.3

Table-3, The variation of BCR with normalized shell diameter (d/D) for different shell heights, for Rankine wall and $\phi = 42^o$.

h/D	K_p	K_a	K_p-K_a	D/D	Q_u	BCR
						Q_u/q_u
0.5	5.045	0.198	4.846	1	10236.06	11.0
0.5	5.045	0.198	4.846	1.07	9576.00	10.3
0.5	5.045	0.198	4.846	1.33	7732.68	8.3
0.5	5.045	0.198	4.846	1.6	6452.54	6.9
0.5	5.045	0.198	4.846	2	5191.37	5.6
1	5.045	0.198	4.846	1	10382.75	11.2
1	5.045	0.198	4.846	1.07	9722.70	10.5
1	5.045	0.198	4.846	1.33	7879.37	8.5
1	5.045	0.198	4.846	1.6	6599.24	7.1
1	5.045	0.198	4.846	2	5338.07	5.7
1.5	5.045	0.198	4.846	1	10529.44	11.3
1.5	5.045	0.198	4.846	1.07	9869.39	10.6
1.5	5.045	0.198	4.846	1.33	8026.07	8.6
1.5	5.045	0.198	4.846	1.6	6745.93	7.3
1.5	5.045	0.198	4.846	2	5484.76	5.9
2	5.045	0.198	4.846	1	10676.13	11.5
2	5.045	0.198	4.846	1.07	10016.08	10.8
2	5.045	0.198	4.846	1.33	8172.76	8.8
2	5.045	0.198	4.846	1.6	6892.62	7.4
2	5.045	0.198	4.846	2	5631.45	6.1

Table-4, The variation of BCR with normalized shell diameter (d/D) for different shell heights, for Coulomb wall and $\phi = 34^o$ and $\delta = 22^o$.

h/D	K_a	K_p	K_p-K_a	δ	d/D	Q_u	BCR
							Q_u/q_u
0.5	0.254	8.641	8.387	0.384	1	7946.38	38.9
0.5	0.254	8.641	8.387	0.384	1.07	7423.47	36.3
0.5	0.254	8.641	8.387	0.384	1.33	5955.94	29.1
0.5	0.254	8.641	8.387	0.384	1.6	4926.83	24.1
0.5	0.254	8.641	8.387	0.384	2	3898.05	19.1
1	0.254	8.641	8.387	0.384	1	8130.08	39.8
1	0.254	8.641	8.387	0.384	1.07	7607.16	37.2
1	0.254	8.641	8.387	0.384	1.33	6139.63	30.0
1	0.254	8.641	8.387	0.384	1.6	5110.52	25.0
1	0.254	8.641	8.387	0.384	2	4081.74	20.0
1.5	0.254	8.641	8.387	0.384	1	8313.77	40.7
1.5	0.254	8.641	8.387	0.384	1.07	7790.85	38.1
1.5	0.254	8.641	8.387	0.384	1.33	6323.33	30.9
1.5	0.254	8.641	8.387	0.384	1.6	5294.22	25.9
1.5	0.254	8.641	8.387	0.384	2	4265.43	20.9
2	0.254	8.641	8.387	0.384	1	8497.46	41.6
2	0.254	8.641	8.387	0.384	1.07	7974.54	39.0
2	0.254	8.641	8.387	0.384	1.33	6507.02	31.8
2	0.254	8.641	8.387	0.384	1.6	5477.91	26.8
2	0.254	8.641	8.387	0.384	2	4449.13	21.8

Table-5, The variation of BCR with normalized shell diameter (d/D) for different shell heights, for Coulomb wall and ϕ = 38^o and δ = 22^o.

h/D	K_a	K_p	K_p-K_a	δ	d/D	Q_u	BCR
							Q_u/q_u
0.5	0.217	11.466	11.249	0.384	1	9330.20	22.0
0.5	0.217	11.466	11.249	0.384	1.07	8715.01	20.5
0.5	0.217	11.466	11.249	0.384	1.33	6985.70	16.5
0.5	0.217	11.466	11.249	0.384	1.6	5769.12	13.6
0.5	0.217	11.466	11.249	0.384	2	4547.13	10.7
1	0.217	11.466	11.249	0.384	1	9618.59	22.7
1	0.217	11.466	11.249	0.384	1.07	9003.40	21.2
1	0.217	11.466	11.249	0.384	1.33	7274.09	17.1
1	0.217	11.466	11.249	0.384	1.6	6057.50	14.3
1	0.217	11.466	11.249	0.384	2	4835.52	11.4
1.5	0.217	11.466	11.249	0.384	1	9906.97	23.3
1.5	0.217	11.466	11.249	0.384	1.07	9291.78	21.9
1.5	0.217	11.466	11.249	0.384	1.33	7562.47	17.8
1.5	0.217	11.466	11.249	0.384	1.6	6345.89	14.9
1.5	0.217	11.466	11.249	0.384	2	5123.90	12.1
2	0.217	11.466	11.249	0.384	1	10195.35	24.0
2	0.217	11.466	11.249	0.384	1.07	9580.17	22.6
2	0.217	11.466	11.249	0.384	1.33	7850.86	18.5
2	0.217	11.466	11.249	0.384	1.6	6634.27	15.6
2	0.217	11.466	11.249	0.384	2	5412.29	12.7

Table-6, The variation of BCR with normalized shell diameter (d/D) for different shell heights, for Coulomb wall and ϕ = 42^o and δ = 22^o.

h/D	K_a	K_p	K_p-K_a	δ	d/D	Q_u	BCR
							Q_u/q_u
0.5	0.183	15.726	15.543	0.384	1	11115.11	12.0
0.5	0.183	15.726	15.543	0.384	1.07	10380.08	11.2
0.5	0.183	15.726	15.543	0.384	1.33	8308.91	8.9
0.5	0.183	15.726	15.543	0.384	1.6	6844.94	7.4
0.5	0.183	15.726	15.543	0.384	2	5364.27	5.8
1	0.183	15.726	15.543	0.384	1	11587.61	12.5
1	0.183	15.726	15.543	0.384	1.07	10852.58	11.7
1	0.183	15.726	15.543	0.384	1.33	8781.41	9.5
1	0.183	15.726	15.543	0.384	1.6	7317.43	7.9
1	0.183	15.726	15.543	0.384	2	5836.77	6.3
1.5	0.183	15.726	15.543	0.384	1	12060.11	13.0
1.5	0.183	15.726	15.543	0.384	1.07	11325.08	12.2
1.5	0.183	15.726	15.543	0.384	1.33	9253.91	10.0
1.5	0.183	15.726	15.543	0.384	1.6	7789.93	8.4
1.5	0.183	15.726	15.543	0.384	2	6309.27	6.8
2	0.183	15.726	15.543	0.384	1	12532.60	13.5
2	0.183	15.726	15.543	0.384	1.07	11797.58	12.7
2	0.183	15.726	15.543	0.384	1.33	9726.41	10.5
2	0.183	15.726	15.543	0.384	1.6	8262.43	8.9
2	0.183	15.726	15.543	0.384	2	6781.77	7.3

Table-7, The variation of BCR with normalized shell diameter (d/D) for different shell heights, for Coulomb wall and $\phi = 34^o$ and $\delta = 25^o$.

h/D	K_a	K_p	K_p-K_a	δ	D	Q_u	BCR
							Q_u/q_u
0.5	0.254	10.193	9.939	0.436	1	7937.97	38.6
0.5	0.254	10.193	9.939	0.436	1.07	7412.42	36.1
0.5	0.254	10.193	9.939	0.436	1.33	5935.15	28.9
0.5	0.254	10.193	9.939	0.436	1.6	4895.91	23.8
0.5	0.254	10.193	9.939	0.436	2	3852.12	18.8
1	0.254	10.193	9.939	0.436	1	8150.75	39.7
1	0.254	10.193	9.939	0.436	1.07	7625.21	37.1
1	0.254	10.193	9.939	0.436	1.33	6147.93	29.9
1	0.254	10.193	9.939	0.436	1.6	5108.69	24.9
1	0.254	10.193	9.939	0.436	2	4064.91	19.8
1.5	0.254	10.193	9.939	0.436	1	8363.53	40.7
1.5	0.254	10.193	9.939	0.436	1.07	7837.99	38.2
1.5	0.254	10.193	9.939	0.436	1.33	6360.71	31.0
1.5	0.254	10.193	9.939	0.436	1.6	5321.47	25.9
1.5	0.254	10.193	9.939	0.436	2	4277.69	20.8
2	0.254	10.193	9.939	0.436	1	8576.31	41.8
2	0.254	10.193	9.939	0.436	1.07	8050.77	39.2
2	0.254	10.193	9.939	0.436	1.33	6573.49	32.0
2	0.254	10.193	9.939	0.436	1.6	5534.26	26.9
2	0.254	10.193	9.939	0.436	2	4490.47	21.9

Table-8, The variation of BCR with normalized shell diameter (d/D) for different shell heights, for Coulomb wall and $\phi = 38^o$ and $\delta = 25^o$.

h/D	K_a	K_p	K_p-K_a	δ	D	Q_u	BCR
							Q_u/q_u
0.5	0.217	13.901	13.684	0.436	1	9319.65	22.0
0.5	0.217	13.901	13.684	0.436	1.07	8699.90	20.5
0.5	0.217	13.901	13.684	0.436	1.33	6953.67	16.4
0.5	0.217	13.901	13.684	0.436	1.6	5719.51	13.5
0.5	0.217	13.901	13.684	0.436	2	4471.50	10.5
1	0.217	13.901	13.684	0.436	1	9662.56	22.8
1	0.217	13.901	13.684	0.436	1.07	9042.81	21.3
1	0.217	13.901	13.684	0.436	1.33	7296.58	17.2
1	0.217	13.901	13.684	0.436	1.6	6062.43	14.3
1	0.217	13.901	13.684	0.436	2	4814.41	11.3
1.5	0.217	13.901	13.684	0.436	1	10005.47	23.6
1.5	0.217	13.901	13.684	0.436	1.07	9385.72	22.1
1.5	0.217	13.901	13.684	0.436	1.33	7639.49	18.0
1.5	0.217	13.901	13.684	0.436	1.6	6405.34	15.1
1.5	0.217	13.901	13.684	0.436	2	5157.32	12.1
2	0.217	13.901	13.684	0.436	1	10348.38	24.4
2	0.217	13.901	13.684	0.436	1.07	9728.63	22.9
2	0.217	13.901	13.684	0.436	1.33	7982.40	18.8
2	0.217	13.901	13.684	0.436	1.6	6748.25	15.9
2	0.217	13.901	13.684	0.436	2	5500.23	13.0

Table-9, The variation of BCR with normalized shell diameter (d/D) for different shell heights, for Coulomb wall and $\phi = 42^o$ and $\delta = 25^o$.

h/D	K_a	K_p	K_p-K_a	δ	D	Q_u	BCR
							Q_u/q_u
0.5	0.183	19.758	19.575	0.436	1	11103.78	12.0
0.5	0.183	19.758	19.575	0.436	1.07	10360.32	11.2
0.5	0.183	19.758	19.575	0.436	1.33	8257.82	8.9
0.5	0.183	19.758	19.575	0.436	1.6	6761.30	7.3
0.5	0.183	19.758	19.575	0.436	2	5232.44	5.6
1	0.183	19.758	19.575	0.436	1	11685.45	12.6
1	0.183	19.758	19.575	0.436	1.07	10941.99	11.8
1	0.183	19.758	19.575	0.436	1.33	8839.49	9.5
1	0.183	19.758	19.575	0.436	1.6	7342.97	7.9
1	0.183	19.758	19.575	0.436	2	5814.11	6.3
1.5	0.183	19.758	19.575	0.436	1	12267.12	13.2
1.5	0.183	19.758	19.575	0.436	1.07	11523.66	12.4
1.5	0.183	19.758	19.575	0.436	1.33	9421.16	10.1
1.5	0.183	19.758	19.575	0.436	1.6	7924.64	8.5
1.5	0.183	19.758	19.575	0.436	2	6395.78	6.9
2	0.183	19.758	19.575	0.436	1	12848.79	13.8
2	0.183	19.758	19.575	0.436	1.07	12105.33	13.0
2	0.183	19.758	19.575	0.436	1.33	10002.83	10.8
2	0.183	19.758	19.575	0.436	1.6	8506.32	9.2
2	0.183	19.758	19.575	0.436	2	6977.45	7.5

Table-10, The variation of BCR with normalized shell height (h/D) for different shell diameter, for Rankine wall (FOR $\phi = 34^o$ and $\delta = 0^o$)

h/D	Kp	Ka	Kp-Ka	d/D	Qu	BCR
						Q_u/q_u
0.5	3.537	0.283	3.254	1	7143.33	34.8
1	3.537	0.283	3.254	1	7212.40	35.1
1.5	3.537	0.283	3.254	1	7281.47	35.4
2	3.537	0.283	3.254	1	7350.54	35.8
2.5	3.537	0.283	3.254	1	7419.60	36.1
3	3.537	0.283	3.254	1	7488.67	36.5
0.5	3.537	0.283	3.254	1.07	6680.53	32.5
1	3.537	0.283	3.254	1.07	6749.60	32.9
1.5	3.537	0.283	3.254	1.07	6818.67	33.2
2	3.537	0.283	3.254	1.07	6887.73	33.5
2.5	3.537	0.283	3.254	1.07	6956.80	33.9
3	3.537	0.283	3.254	1.07	7025.87	34.2
0.5	3.537	0.283	3.254	1.33	5388.06	26.2
1	3.537	0.283	3.254	1.33	5457.13	26.6
1.5	3.537	0.283	3.254	1.33	5526.20	26.9
2	3.537	0.283	3.254	1.33	5595.27	27.2
2.5	3.537	0.283	3.254	1.33	5664.33	27.6
3	3.537	0.283	3.254	1.33	5733.40	27.9
0.5	3.537	0.283	3.254	1.6	4490.48	21.9
1	3.537	0.283	3.254	1.6	4559.55	22.2
1.5	3.537	0.283	3.254	1.6	4628.62	22.5
2	3.537	0.283	3.254	1.6	4697.69	22.9
2.5	3.537	0.283	3.254	1.6	4766.75	23.2
3	3.537	0.283	3.254	1.6	4835.82	23.5
0.5	3.537	0.283	3.254	2	3606.20	17.6
1	3.537	0.283	3.254	2	3675.27	17.9
1.5	3.537	0.283	3.254	2	3744.34	18.2
2	3.537	0.283	3.254	2	3813.40	18.6
2.5	3.537	0.283	3.254	2	3882.47	18.9
3	3.537	0.283	3.254	2	3951.54	19.2

Table-4.11, The variation of BCR with normalized shell height (h/D) for different shell diameter, for Rankine wall (FOR $\phi = 38^o$ and $\delta = 0^o$)

h/D	K_p	K_a	K_p-K_a	d	Q_u	BCR
						Q_u/q_u
0.5	4.204	0.238	3.966	1	8507.52	20.0
1	4.204	0.238	3.966	1	8607.55	20.3
1.5	4.204	0.238	3.966	1	8707.58	20.5
2	4.204	0.238	3.966	1	8807.61	20.7
2.5	4.204	0.238	3.966	1	8907.64	21.0
3	4.204	0.238	3.966	1	9007.66	21.2
0.5	4.204	0.238	3.966	1.07	7957.50	18.7
1	4.204	0.238	3.966	1.07	8057.53	19.0
1.5	4.204	0.238	3.966	1.07	8157.56	19.2
2	4.204	0.238	3.966	1.07	8257.58	19.5
2.5	4.204	0.238	3.966	1.07	8357.61	19.7
3	4.204	0.238	3.966	1.07	8457.64	19.9
0.5	4.204	0.238	3.966	1.33	6421.45	15.1
1	4.204	0.238	3.966	1.33	6521.48	15.4
1.5	4.204	0.238	3.966	1.33	6621.51	15.6
2	4.204	0.238	3.966	1.33	6721.54	15.8
2.5	4.204	0.238	3.966	1.33	6821.57	16.1
3	4.204	0.238	3.966	1.33	6921.60	16.3
0.5	4.204	0.238	3.966	1.6	5354.71	12.6
1	4.204	0.238	3.966	1.6	5454.74	12.8
1.5	4.204	0.238	3.966	1.6	5554.77	13.1
2	4.204	0.238	3.966	1.6	5654.80	13.3
2.5	4.204	0.238	3.966	1.6	5754.83	13.6
3	4.204	0.238	3.966	1.6	5854.86	13.8
0.5	4.204	0.238	3.966	2	4303.77	10.1
1	4.204	0.238	3.966	2	4403.80	10.4
1.5	4.204	0.238	3.966	2	4503.83	10.6
2	4.204	0.238	3.966	2	4603.86	10.8
2.5	4.204	0.238	3.966	2	4703.89	11.1
3	4.204	0.238	3.966	2	4803.92	11.3

Table-12, The variation of BCR with normalized shell height (h/D) for different shell diameter, for Rankine wall (FOR $\phi = 42^o$ and $\delta = 0^o$)

h/D	K_p	K_a	K_p-K_a	d	Q_u	BCR
						Q_u/q_u
0.5	5.045	0.198	4.846	1	10236.06	11.0
1	5.045	0.198	4.846	1	10382.75	11.2
1.5	5.045	0.198	4.846	1	10529.44	11.3
2	5.045	0.198	4.846	1	10676.13	11.5
2.5	5.045	0.198	4.846	1	10822.83	11.7
3	5.045	0.198	4.846	1	10969.52	11.8
0.5	5.045	0.198	4.846	1.07	9576.00	10.3
1	5.045	0.198	4.846	1.07	9722.70	10.5
1.5	5.045	0.198	4.846	1.07	9869.39	10.6
2	5.045	0.198	4.846	1.07	10016.08	10.8
2.5	5.045	0.198	4.846	1.07	10162.77	10.9
3	5.045	0.198	4.846	1.07	10309.47	11.1
0.5	5.045	0.198	4.846	1.33	7732.68	8.3
1	5.045	0.198	4.846	1.33	7879.37	8.5
1.5	5.045	0.198	4.846	1.33	8026.07	8.6
2	5.045	0.198	4.846	1.33	8172.76	8.8
2.5	5.045	0.198	4.846	1.33	8319.45	9.0
3	5.045	0.198	4.846	1.33	8466.14	9.1
0.5	5.045	0.198	4.846	1.6	6452.54	6.9
1	5.045	0.198	4.846	1.6	6599.24	7.1
1.5	5.045	0.198	4.846	1.6	6745.93	7.3
2	5.045	0.198	4.846	1.6	6892.62	7.4
2.5	5.045	0.198	4.846	1.6	7039.32	7.6
3	5.045	0.198	4.846	1.6	7186.01	7.7
0.5	5.045	0.198	4.846	2	5191.37	5.6
1	5.045	0.198	4.846	2	5338.07	5.7
1.5	5.045	0.198	4.846	2	5484.76	5.9
2	5.045	0.198	4.846	2	5631.45	6.1
2.5	5.045	0.198	4.846	2	5778.15	6.2
3	5.045	0.198	4.846	2	5924.84	6.4

Table-13, The variation of BCR with normalized shell height (h/D) for different shell diameter, for Coulomb wall (FOR $\phi = 34^o$ and $\delta = 22^o$)

h/D	K_a	K_p	K_p-K_a	δ	d	Q_u	BCR
							Q_u/q_u
0.5	0.254	8.641	8.387	0.384	1	7946.38	38.7
1	0.254	8.641	8.387	0.384	1	8130.08	39.6
1.5	0.254	8.641	8.387	0.384	1	8313.77	40.5
2	0.254	8.641	8.387	0.384	1	8497.46	41.4
2.5	0.254	8.641	8.387	0.384	1	8681.15	42.3
3	0.254	8.641	8.387	0.384	1	8864.84	43.2
0.5	0.254	8.641	8.387	0.384	1.07	7423.47	36.1
1	0.254	8.641	8.387	0.384	1.07	7607.16	37.0
1.5	0.254	8.641	8.387	0.384	1.07	7790.85	37.9
2	0.254	8.641	8.387	0.384	1.07	7974.54	38.8
2.5	0.254	8.641	8.387	0.384	1.07	8158.24	39.7
3	0.254	8.641	8.387	0.384	1.07	8341.93	40.6
0.5	0.254	8.641	8.387	0.384	1.33	5955.94	29.0
1	0.254	8.641	8.387	0.384	1.33	6139.63	29.9
1.5	0.254	8.641	8.387	0.384	1.33	6323.33	30.8
2	0.254	8.641	8.387	0.384	1.33	6507.02	31.7
2.5	0.254	8.641	8.387	0.384	1.33	6690.71	32.6
3	0.254	8.641	8.387	0.384	1.33	6874.40	33.5
0.5	0.254	8.641	8.387	0.384	1.6	4926.83	24.0
1	0.254	8.641	8.387	0.384	1.6	5110.52	24.9
1.5	0.254	8.641	8.387	0.384	1.6	5294.22	25.8
2	0.254	8.641	8.387	0.384	1.6	5477.91	26.7
2.5	0.254	8.641	8.387	0.384	1.6	5661.60	27.6
3	0.254	8.641	8.387	0.384	1.6	5845.29	28.5
0.5	0.254	8.641	8.387	0.384	2	3898.05	19.0
1	0.254	8.641	8.387	0.384	2	4081.74	19.9
1.5	0.254	8.641	8.387	0.384	2	4265.43	20.8
2	0.254	8.641	8.387	0.384	2	4449.13	21.7
2.5	0.254	8.641	8.387	0.384	2	4632.82	22.6
3	0.254	8.641	8.387	0.384	2	4816.51	23.4

Table-14, The variation of BCR with normalized shell height (h/D) for different shell diameter, for Coulomb wall (FOR $\phi = 38^o$ and $\delta = 22^o$)

h/D	K_a	K_p	K_p-K_a	δ	d	Q_u	BCR
							Q_u/q_u
0.5	0.217	11.466	11.249	0.384	1	9330.20	22.0
1	0.217	11.466	11.249	0.384	1	9618.59	22.7
1.5	0.217	11.466	11.249	0.384	1	9906.97	23.3
2	0.217	11.466	11.249	0.384	1	10195.35	24.0
2.5	0.217	11.466	11.249	0.384	1	10483.74	24.7
3	0.217	11.466	11.249	0.384	1	10772.12	25.4
0.5	0.217	11.466	11.249	0.384	1.07	8715.01	20.5
1	0.217	11.466	11.249	0.384	1.07	9003.40	21.2
1.5	0.217	11.466	11.249	0.384	1.07	9291.78	21.9
2	0.217	11.466	11.249	0.384	1.07	9580.17	22.6
2.5	0.217	11.466	11.249	0.384	1.07	9868.55	23.2
3	0.217	11.466	11.249	0.384	1.07	10156.93	23.9
0.5	0.217	11.466	11.249	0.384	1.33	6985.70	16.5
1	0.217	11.466	11.249	0.384	1.33	7274.09	17.1
1.5	0.217	11.466	11.249	0.384	1.33	7562.47	17.8
2	0.217	11.466	11.249	0.384	1.33	7850.86	18.5
2.5	0.217	11.466	11.249	0.384	1.33	8139.24	19.2
3	0.217	11.466	11.249	0.384	1.33	8427.62	19.9
0.5	0.217	11.466	11.249	0.384	1.6	5769.12	13.6
1	0.217	11.466	11.249	0.384	1.6	6057.50	14.3
1.5	0.217	11.466	11.249	0.384	1.6	6345.89	14.9
2	0.217	11.466	11.249	0.384	1.6	6634.27	15.6
2.5	0.217	11.466	11.249	0.384	1.6	6922.65	16.3
3	0.217	11.466	11.249	0.384	1.6	7211.04	17.0
0.5	0.217	11.466	11.249	0.384	2	4547.13	10.7
1	0.217	11.466	11.249	0.384	2	4835.52	11.4
1.5	0.217	11.466	11.249	0.384	2	5123.90	12.1
2	0.217	11.466	11.249	0.384	2	5412.29	12.7
2.5	0.217	11.466	11.249	0.384	2	5700.67	13.4
3	0.217	11.466	11.249	0.384	2	5989.06	14.1

Table-15, The variation of BCR with normalized shell height (h/D) for different shell diameter, for Coulomb wall (FOR $\phi = 42^o$ and $\delta = 22^o$)

h/D	K_a	K_p	K_p-K_a	δ	d	Q_u	BCR
							Q_u/q_u
0.5	0.183	15.726	15.543	0.384	1	11115.11	12.0
1	0.183	15.726	15.543	0.384	1	11587.61	12.5
1.5	0.183	15.726	15.543	0.384	1	12060.11	13.0
2	0.183	15.726	15.543	0.384	1	12532.60	13.5
2.5	0.183	15.726	15.543	0.384	1	13005.10	14.0
3	0.183	15.726	15.543	0.384	1	13477.60	14.5
0.5	0.183	15.726	15.543	0.384	1.07	10380.08	11.2
1	0.183	15.726	15.543	0.384	1.07	10852.58	11.7
1.5	0.183	15.726	15.543	0.384	1.07	11325.08	12.2
2	0.183	15.726	15.543	0.384	1.07	11797.58	12.7
2.5	0.183	15.726	15.543	0.384	1.07	12270.08	13.2
3	0.183	15.726	15.543	0.384	1.07	12742.58	13.7
0.5	0.183	15.726	15.543	0.384	1.33	8308.91	8.9
1	0.183	15.726	15.543	0.384	1.33	8781.41	9.5
1.5	0.183	15.726	15.543	0.384	1.33	9253.91	10.0
2	0.183	15.726	15.543	0.384	1.33	9726.41	10.5
2.5	0.183	15.726	15.543	0.384	1.33	10198.91	11.0
3	0.183	15.726	15.543	0.384	1.33	10671.41	11.5
0.5	0.183	15.726	15.543	0.384	1.6	6844.94	7.4
1	0.183	15.726	15.543	0.384	1.6	7317.43	7.9
1.5	0.183	15.726	15.543	0.384	1.6	7789.93	8.4
2	0.183	15.726	15.543	0.384	1.6	8262.43	8.9
2.5	0.183	15.726	15.543	0.384	1.6	8734.93	9.4
3	0.183	15.726	15.543	0.384	1.6	9207.43	9.9
0.5	0.183	15.726	15.543	0.384	2	5364.27	5.8
1	0.183	15.726	15.543	0.384	2	5836.77	6.3
1.5	0.183	15.726	15.543	0.384	2	6309.27	6.8
2	0.183	15.726	15.543	0.384	2	6781.77	7.3
2.5	0.183	15.726	15.543	0.384	2	7254.27	7.8
3	0.183	15.726	15.543	0.384	2	7726.77	8.3

Table-16, The variation of BCR with normalized shell height (h/D) for different shell diameter, for Coulomb wall (FOR $\phi = 34^o$ and $\delta = 25^o$)

h/D	K_a	K_p	K_p-K_a	δ	d/D	Q_u	BCR
							Q_u/q_u
0.5	0.254	10.193	9.939	0.4363	1	7937.97	38.6
1	0.254	10.193	9.939	0.4363	1	8150.75	39.7
1.5	0.254	10.193	9.939	0.4363	1	8363.53	40.7
2	0.254	10.193	9.939	0.4363	1	8576.31	41.8
2.5	0.254	10.193	9.939	0.4363	1	8789.10	42.8
3	0.254	10.193	9.939	0.4363	1	9001.88	43.8
0.5	0.254	10.193	9.939	0.4363	1.07	7412.42	36.1
1	0.254	10.193	9.939	0.4363	1.07	7625.21	37.1
1.5	0.254	10.193	9.939	0.4363	1.07	7837.99	38.2
2	0.254	10.193	9.939	0.4363	1.07	8050.77	39.2
2.5	0.254	10.193	9.939	0.4363	1.07	8263.55	40.2
3	0.254	10.193	9.939	0.4363	1.07	8476.34	41.3
0.5	0.254	10.193	9.939	0.4363	1.33	5935.15	28.9
1	0.254	10.193	9.939	0.4363	1.33	6147.93	29.9
1.5	0.254	10.193	9.939	0.4363	1.33	6360.71	31.0
2	0.254	10.193	9.939	0.4363	1.33	6573.49	32.0
2.5	0.254	10.193	9.939	0.4363	1.33	6786.28	33.0
3	0.254	10.193	9.939	0.4363	1.33	6999.06	34.1
0.5	0.254	10.193	9.939	0.4363	1.6	4895.91	23.8
1	0.254	10.193	9.939	0.4363	1.6	5108.69	24.9
1.5	0.254	10.193	9.939	0.4363	1.6	5321.47	25.9
2	0.254	10.193	9.939	0.4363	1.6	5534.26	26.9
2.5	0.254	10.193	9.939	0.4363	1.6	5747.04	28.0
3	0.254	10.193	9.939	0.4363	1.6	5959.82	29.0
0.5	0.254	10.193	9.939	0.4363	2	3852.12	18.8
1	0.254	10.193	9.939	0.4363	2	4064.91	19.8
1.5	0.254	10.193	9.939	0.4363	2	4277.69	20.8
2	0.254	10.193	9.939	0.4363	2	4490.47	21.9
2.5	0.254	10.193	9.939	0.4363	2	4703.25	22.9
3	0.254	10.193	9.939	0.4363	2	4916.04	23.9

Table-17, The variation of BCR with normalized shell height (h/D) for different shell diameter, for Coulomb wall (FOR $\phi = 38^o$ and $\delta = 25^o$)

h/D	K_a	K_p	K_p-K_a	δ	d/D	Q_u	BCR
							Q_u/q_u
0.5	0.217	13.901	13.684	0.4363	1	9319.65	22.0
1	0.217	13.901	13.684	0.4363	1	9662.56	22.8
1.5	0.217	13.901	13.684	0.4363	1	10005.47	23.6
2	0.217	13.901	13.684	0.4363	1	10348.38	24.4
2.5	0.217	13.901	13.684	0.4363	1	10691.29	25.2
3	0.217	13.901	13.684	0.4363	1	11034.20	26.0
0.5	0.217	13.901	13.684	0.4363	1.07	8699.90	20.5
1	0.217	13.901	13.684	0.4363	1.07	9042.81	21.3
1.5	0.217	13.901	13.684	0.4363	1.07	9385.72	22.1
2	0.217	13.901	13.684	0.4363	1.07	9728.63	22.9
2.5	0.217	13.901	13.684	0.4363	1.07	10071.54	23.7
3	0.217	13.901	13.684	0.4363	1.07	10414.45	24.5
0.5	0.217	13.901	13.684	0.4363	1.33	6953.67	16.4
1	0.217	13.901	13.684	0.4363	1.33	7296.58	17.2
1.5	0.217	13.901	13.684	0.4363	1.33	7639.49	18.0
2	0.217	13.901	13.684	0.4363	1.33	7982.40	18.8
2.5	0.217	13.901	13.684	0.4363	1.33	8325.31	19.6
3	0.217	13.901	13.684	0.4363	1.33	8668.22	20.4
0.5	0.217	13.901	13.684	0.4363	1.6	5719.51	13.5
1	0.217	13.901	13.684	0.4363	1.6	6062.43	14.3
1.5	0.217	13.901	13.684	0.4363	1.6	6405.34	15.1
2	0.217	13.901	13.684	0.4363	1.6	6748.25	15.9
2.5	0.217	13.901	13.684	0.4363	1.6	7091.16	16.7
3	0.217	13.901	13.684	0.4363	1.6	7434.07	17.5
0.5	0.217	13.901	13.684	0.4363	2	4471.50	10.5
1	0.217	13.901	13.684	0.4363	2	4814.41	11.3
1.5	0.217	13.901	13.684	0.4363	2	5157.32	12.1
2	0.217	13.901	13.684	0.4363	2	5500.23	13.0
2.5	0.217	13.901	13.684	0.4363	2	5843.14	13.8
3	0.217	13.901	13.684	0.4363	2	6186.05	14.6

Table-18, The variation of BCR with normalized shell height (h/D) for different shell diameter, for Coulomb wall (FOR $\phi = 42^o$ and $\delta = 25^o$)

h/D	K_a	K_p	K_p-K_a	δ	d/D	Q_u	BCR
							Q_u/q_u
0.5	0.183	19.758	19.575	0.4363	1	11103.78	12.0
1	0.183	19.758	19.575	0.4363	1	11685.45	12.6
1.5	0.183	19.758	19.575	0.4363	1	12267.12	13.2
2	0.183	19.758	19.575	0.4363	1	12848.79	13.8
2.5	0.183	19.758	19.575	0.4363	1	13430.46	14.5
3	0.183	19.758	19.575	0.4363	1	14012.13	15.1
0.5	0.183	19.758	19.575	0.4363	1.07	10360.32	11.2
1	0.183	19.758	19.575	0.4363	1.07	10941.99	11.8
1.5	0.183	19.758	19.575	0.4363	1.07	11523.66	12.4
2	0.183	19.758	19.575	0.4363	1.07	12105.33	13.0
2.5	0.183	19.758	19.575	0.4363	1.07	12687.00	13.7
3	0.183	19.758	19.575	0.4363	1.07	13268.67	14.3
0.5	0.183	19.758	19.575	0.4363	1.33	8257.82	8.9
1	0.183	19.758	19.575	0.4363	1.33	8839.49	9.5
1.5	0.183	19.758	19.575	0.4363	1.33	9421.16	10.1
2	0.183	19.758	19.575	0.4363	1.33	10002.83	10.8
2.5	0.183	19.758	19.575	0.4363	1.33	10584.50	11.4
3	0.183	19.758	19.575	0.4363	1.33	11166.17	12.0
0.5	0.183	19.758	19.575	0.4363	1.6	6761.30	7.3
1	0.183	19.758	19.575	0.4363	1.6	7342.97	7.9
1.5	0.183	19.758	19.575	0.4363	1.6	7924.64	8.5
2	0.183	19.758	19.575	0.4363	1.6	8506.32	9.2
2.5	0.183	19.758	19.575	0.4363	1.6	9087.99	9.8
3	0.183	19.758	19.575	0.4363	1.6	9669.66	10.4
0.5	0.183	19.758	19.575	0.4363	2	5232.44	5.6
1	0.183	19.758	19.575	0.4363	2	5814.11	6.3
1.5	0.183	19.758	19.575	0.4363	2	6395.78	6.9
2	0.183	19.758	19.575	0.4363	2	6977.45	7.5
2.5	0.183	19.758	19.575	0.4363	2	7559.12	8.1
3	0.183	19.758	19.575	0.4363	2	8140.80	8.8

Table-19, The variation of BCR with normalized shell height (h/D) & shell Diameter for different shell diameter & heights.
For Rankine wall ($\phi = 34^o$ and $\delta = 0^o$)

ANGLE OF	RADIUS OF LOG-SPIRAL								
LOG-SPIRAL	r_o	r_1	45-ϕ/2	d/D	h/D	K_p	K_a	Qu	BCR
θ									Q_u/q_u
56	0.603	1.166	90	1.000	1.166	3.537	0.283	7228.02	35.19
57	0.603	1.180	89	1.041	1.180	3.537	0.283	6950.38	33.83
58	0.603	1.194	88	1.083	1.193	3.537	0.283	6688.17	32.56
59	0.603	1.208	87	1.126	1.206	3.537	0.283	6440.33	31.35
60	0.603	1.222	86	1.171	1.219	3.537	0.283	6205.85	30.21
61	0.603	1.237	85	1.216	1.232	3.537	0.283	5983.82	29.13
62	0.603	1.251	84	1.262	1.245	3.537	0.283	5773.42	28.11
63	0.603	1.266	83	1.309	1.257	3.537	0.283	5573.87	27.13
64	0.603	1.281	82	1.357	1.269	3.537	0.283	5384.47	26.21
65	0.603	1.296	81	1.406	1.280	3.537	0.283	5204.56	25.34
66	0.603	1.312	80	1.456	1.292	3.537	0.283	5033.55	24.50
67	0.603	1.327	79	1.506	1.303	3.537	0.283	4870.88	23.71
68	0.603	1.343	78	1.558	1.314	3.537	0.283	4716.03	22.96
69	0.603	1.359	77	1.611	1.324	3.537	0.283	4568.54	22.24
70	0.603	1.375	76	1.665	1.334	3.537	0.283	4427.95	21.56
71	0.603	1.391	75	1.720	1.344	3.537	0.283	4293.86	20.90
72	0.603	1.408	74	1.776	1.353	3.537	0.283	4165.89	20.28
73	0.603	1.424	73	1.833	1.362	3.537	0.283	4043.68	19.68
74	0.603	1.441	72	1.891	1.371	3.537	0.283	3926.91	19.12
75	0.603	1.458	71	1.950	1.379	3.537	0.283	3815.26	18.57
76	0.603	1.476	70	2.009	1.387	3.537	0.283	3708.45	18.05
77	0.603	1.493	69	2.070	1.394	3.537	0.283	3606.21	17.56
78	0.603	1.511	68	2.132	1.401	3.537	0.283	3508.29	17.08
79	0.603	1.529	67	2.195	1.407	3.537	0.283	3414.46	16.62
80	0.603	1.547	66	2.258	1.413	3.537	0.283	3324.49	16.18
81	0.603	1.565	65	2.323	1.418	3.537	0.283	3238.19	15.76
82	0.603	1.584	64	2.388	1.423	3.537	0.283	3155.35	15.36
83	0.603	1.602	63	2.455	1.428	3.537	0.283	3075.81	14.97
84	0.603	1.621	62	2.522	1.432	3.537	0.283	2999.38	14.60
85	0.603	1.640	61	2.591	1.435	3.537	0.283	2925.91	14.24
86	0.603	1.660	60	2.660	1.438	3.537	0.283	2855.25	13.90
87	0.603	1.680	59	2.730	1.440	3.537	0.283	2787.25	13.57
88	0.603	1.699	58	2.801	1.441	3.537	0.283	2721.79	13.25
89	0.603	1.720	57	2.873	1.442	3.537	0.283	2658.74	12.94
90	0.603	1.740	56	2.946	1.442	3.537	0.283	2597.98	12.65
91	0.603	1.761	55	3.020	1.442	3.537	0.283	2539.39	12.36
92	0.603	1.781	54	3.094	1.441	3.537	0.283	2482.87	12.09
93	0.603	1.803	53	3.170	1.440	3.537	0.283	2428.33	11.82
94	0.603	1.824	52	3.246	1.437	3.537	0.283	2375.66	11.56
95	0.603	1.845	51	3.323	1.434	3.537	0.283	2324.78	11.32
96	0.603	1.867	50	3.401	1.430	3.537	0.283	2275.60	11.08
97	0.603	1.889	49	3.479	1.426	3.537	0.283	2228.05	10.85
98	0.603	1.912	48	3.558	1.421	3.537	0.283	2182.04	10.62
99	0.603	1.934	47	3.639	1.415	3.537	0.283	2137.50	10.41
100	0.603	1.957	46	3.719	1.408	3.537	0.283	2094.37	10.20
101	0.603	1.981	45	3.801	1.400	3.537	0.283	2052.58	9.99
102	0.603	2.004	44	3.883	1.392	3.537	0.283	2012.07	9.79
103	0.603	2.028	43	3.966	1.383	3.537	0.283	1972.77	9.60
104	0.603	2.052	42	4.049	1.373	3.537	0.283	1934.64	9.42
105	0.603	2.076	41	4.134	1.362	3.537	0.283	1897.62	9.24
106	0.603	2.101	40	4.218	1.350	3.537	0.283	1861.66	9.06
107	0.603	2.125	39	4.304	1.338	3.537	0.283	1826.71	8.89
108	0.603	2.151	38	4.389	1.324	3.537	0.283	1792.72	8.73
109	0.603	2.176	37	4.476	1.310	3.537	0.283	1759.66	8.57
110	0.603	2.202	36	4.563	1.294	3.537	0.283	1727.47	8.41
111	0.603	2.228	35	4.650	1.278	3.537	0.283	1696.12	8.26
112	0.603	2.254	34	4.738	1.261	3.537	0.283	1665.57	8.11

Table-20, The variation of BCR with normalized shell height (h/D) & shell Diameter for different shell diameter & heights.
For Rankine wall ($\phi = 38^o$ and $\delta = 0^o$)

ANGLE OF	RADIUS OF LOG-SPIRAL								
LOG-SPIRAL	r_o	r_1	45-ϕ/2	d/D	h/D	K_p	K_a	Qu	BCR
θ									Q_u/q_u
52	0.635	1.289	90	1.000	1.289	4.204	0.238	8661.20	20.40
53	0.635	1.307	89	1.046	1.307	4.204	0.238	8298.03	19.55
54	0.635	1.325	88	1.092	1.324	4.204	0.238	7956.76	18.74
55	0.635	1.343	87	1.141	1.341	4.204	0.238	7635.73	17.99
56	0.635	1.362	86	1.190	1.358	4.204	0.238	7333.45	17.28
57	0.635	1.380	85	1.241	1.375	4.204	0.238	7048.53	16.60
58	0.635	1.399	84	1.293	1.392	4.204	0.238	6779.73	15.97
59	0.635	1.419	83	1.346	1.408	4.204	0.238	6525.91	15.37
60	0.635	1.438	82	1.400	1.424	4.204	0.238	6286.03	14.81
61	0.635	1.458	81	1.456	1.440	4.204	0.238	6059.12	14.27
62	0.635	1.478	80	1.513	1.455	4.204	0.238	5844.31	13.77
63	0.635	1.498	79	1.572	1.471	4.204	0.238	5640.78	13.29
64	0.635	1.519	78	1.631	1.485	4.204	0.238	5447.81	12.83
65	0.635	1.539	77	1.693	1.500	4.204	0.238	5264.69	12.40
66	0.635	1.561	76	1.755	1.514	4.204	0.238	5090.80	11.99
67	0.635	1.582	75	1.819	1.528	4.204	0.238	4925.55	11.60
68	0.635	1.604	74	1.884	1.542	4.204	0.238	4768.40	11.23
69	0.635	1.626	73	1.951	1.555	4.204	0.238	4618.86	10.88
70	0.635	1.648	72	2.019	1.567	4.204	0.238	4476.45	10.55
71	0.635	1.671	71	2.088	1.580	4.204	0.238	4340.75	10.23
72	0.635	1.694	70	2.159	1.592	4.204	0.238	4211.35	9.92
73	0.635	1.717	69	2.231	1.603	4.204	0.238	4087.88	9.63
74	0.635	1.740	68	2.304	1.614	4.204	0.238	3970.00	9.35
75	0.635	1.764	67	2.379	1.624	4.204	0.238	3857.38	9.09
76	0.635	1.789	66	2.455	1.634	4.204	0.238	3749.73	8.83
77	0.635	1.813	65	2.533	1.643	4.204	0.238	3646.75	8.59
78	0.635	1.838	64	2.611	1.652	4.204	0.238	3548.18	8.36
79	0.635	1.863	63	2.692	1.660	4.204	0.238	3453.79	8.14
80	0.635	1.889	62	2.774	1.668	4.204	0.238	3363.33	7.92
81	0.635	1.915	61	2.857	1.675	4.204	0.238	3276.60	7.72
82	0.635	1.941	60	2.941	1.681	4.204	0.238	3193.38	7.52
83	0.635	1.968	59	3.027	1.687	4.204	0.238	3113.49	7.33
84	0.635	1.995	58	3.114	1.692	4.204	0.238	3036.75	7.15
85	0.635	2.022	57	3.203	1.696	4.204	0.238	2962.98	6.98
86	0.635	2.050	56	3.293	1.699	4.204	0.238	2892.04	6.81
87	0.635	2.078	55	3.384	1.702	4.204	0.238	2823.77	6.65
88	0.635	2.107	54	3.476	1.704	4.204	0.238	2758.03	6.50
89	0.635	2.136	53	3.570	1.705	4.204	0.238	2694.69	6.35
90	0.635	2.165	52	3.666	1.706	4.204	0.238	2633.62	6.20
91	0.635	2.195	51	3.762	1.705	4.204	0.238	2574.70	6.07
92	0.635	2.225	50	3.860	1.704	4.204	0.238	2517.83	5.93
93	0.635	2.255	49	3.959	1.702	4.204	0.238	2462.89	5.80
94	0.635	2.286	48	4.060	1.699	4.204	0.238	2409.78	5.68
95	0.635	2.318	47	4.161	1.695	4.204	0.238	2358.42	5.56
96	0.635	2.349	46	4.264	1.690	4.204	0.238	2308.70	5.44
97	0.635	2.382	45	4.368	1.684	4.204	0.238	2260.54	5.33
98	0.635	2.414	44	4.473	1.677	4.204	0.238	2213.86	5.22
99	0.635	2.447	43	4.580	1.669	4.204	0.238	2168.59	5.11
100	0.635	2.481	42	4.688	1.660	4.204	0.238	2124.65	5.01
101	0.635	2.515	41	4.796	1.650	4.204	0.238	2081.97	4.90
102	0.635	2.550	40	4.906	1.639	4.204	0.238	2040.48	4.81
103	0.635	2.585	39	5.017	1.627	4.204	0.238	2000.12	4.71
104	0.635	2.620	38	5.129	1.613	4.204	0.238	1960.83	4.62
105	0.635	2.656	37	5.243	1.599	4.204	0.238	1922.55	4.53
106	0.635	2.693	36	5.357	1.583	4.204	0.238	1885.23	4.44
107	0.635	2.730	35	5.472	1.566	4.204	0.238	1848.81	4.36
108	0.635	2.767	34	5.588	1.547	4.204	0.238	1813.24	4.27

Table-21, The variation of BCR with normalized shell height (h/D) & shell Diameter for different shell diameter & heights.
For Rankine wall ($\phi = 42^o$ and $\delta = 0^o$)

ANGLE OF	RADIUS OF LOG-SPIRAL								
LOG-SPIRAL	r_o	r_1	$45-\phi/2$	d/D	h/D	K_p	K_a	Qu	BCR
θ									Q_u/q_u
48	0.673	1.431	90	1.000	1.431	5.0447	0.198	10510.58	11.32
49	0.673	1.453	89	1.051	1.453	5.0447	0.198	10030.03	10.80
50	0.673	1.476	88	1.103	1.475	5.0447	0.198	9581.11	10.32
51	0.673	1.500	87	1.157	1.498	5.0447	0.198	9161.23	9.86
52	0.673	1.523	86	1.213	1.520	5.0447	0.198	8768.06	9.44
53	0.673	1.547	85	1.270	1.542	5.0447	0.198	8399.50	9.04
54	0.673	1.572	84	1.329	1.563	5.0447	0.198	8053.64	8.67
55	0.673	1.597	83	1.389	1.585	5.0447	0.198	7728.74	8.32
56	0.673	1.622	82	1.452	1.606	5.0447	0.198	7423.25	7.99
57	0.673	1.648	81	1.516	1.628	5.0447	0.198	7135.71	7.68
58	0.673	1.674	80	1.581	1.649	5.0447	0.198	6864.84	7.39
59	0.673	1.700	79	1.649	1.669	5.0447	0.198	6609.42	7.12
60	0.673	1.727	78	1.718	1.690	5.0447	0.198	6368.38	6.86
61	0.673	1.755	77	1.789	1.710	5.0447	0.198	6140.70	6.61
62	0.673	1.783	76	1.862	1.730	5.0447	0.198	5925.47	6.38
63	0.673	1.811	75	1.937	1.749	5.0447	0.198	5721.85	6.16
64	0.673	1.839	74	2.014	1.768	5.0447	0.198	5529.05	5.95
65	0.673	1.869	73	2.093	1.787	5.0447	0.198	5346.36	5.76
66	0.673	1.898	72	2.173	1.805	5.0447	0.198	5173.13	5.57
67	0.673	1.928	71	2.256	1.823	5.0447	0.198	5008.73	5.39
68	0.673	1.959	70	2.340	1.841	5.0447	0.198	4852.60	5.22
69	0.673	1.990	69	2.426	1.858	5.0447	0.198	4704.22	5.07
70	0.673	2.021	68	2.514	1.874	5.0447	0.198	4563.11	4.91
71	0.673	2.053	67	2.605	1.890	5.0447	0.198	4428.81	4.77
72	0.673	2.086	66	2.697	1.906	5.0447	0.198	4300.90	4.63
73	0.673	2.119	65	2.791	1.920	5.0447	0.198	4178.99	4.50
74	0.673	2.152	64	2.887	1.935	5.0447	0.198	4062.72	4.37
75	0.673	2.187	63	2.985	1.948	5.0447	0.198	3951.76	4.25
76	0.673	2.221	62	3.086	1.961	5.0447	0.198	3845.77	4.14
77	0.673	2.256	61	3.188	1.973	5.0447	0.198	3744.48	4.03
78	0.673	2.292	60	3.292	1.985	5.0447	0.198	3647.60	3.93
79	0.673	2.328	59	3.398	1.996	5.0447	0.198	3554.86	3.83
80	0.673	2.365	58	3.507	2.006	5.0447	0.198	3466.04	3.73
81	0.673	2.403	57	3.617	2.015	5.0447	0.198	3380.90	3.64
82	0.673	2.441	56	3.730	2.024	5.0447	0.198	3299.22	3.55
83	0.673	2.480	55	3.844	2.031	5.0447	0.198	3220.81	3.47
84	0.673	2.519	54	3.961	2.038	5.0447	0.198	3145.47	3.39
85	0.673	2.559	53	4.080	2.043	5.0447	0.198	3073.03	3.31
86	0.673	2.599	52	4.200	2.048	5.0447	0.198	3003.31	3.23
87	0.673	2.640	51	4.323	2.052	5.0447	0.198	2936.17	3.16
88	0.673	2.682	50	4.448	2.055	5.0447	0.198	2871.44	3.09
89	0.673	2.725	49	4.575	2.056	5.0447	0.198	2808.99	3.02
90	0.673	2.768	48	4.704	2.057	5.0447	0.198	2748.67	2.96
91	0.673	2.812	47	4.835	2.056	5.0447	0.198	2690.37	2.90
92	0.673	2.856	46	4.968	2.055	5.0447	0.198	2633.96	2.84
93	0.673	2.901	45	5.103	2.052	5.0447	0.198	2579.33	2.78
94	0.673	2.947	44	5.240	2.047	5.0447	0.198	2526.37	2.72
95	0.673	2.994	43	5.379	2.042	5.0447	0.198	2474.97	2.66
96	0.673	3.042	42	5.521	2.035	5.0447	0.198	2425.04	2.61
97	0.673	3.090	41	5.664	2.027	5.0447	0.198	2376.47	2.56
98	0.673	3.139	40	5.809	2.017	5.0447	0.198	2329.19	2.51
99	0.673	3.188	39	5.956	2.006	5.0447	0.198	2283.10	2.46
100	0.673	3.239	38	6.104	1.994	5.0447	0.198	2238.12	2.41
101	0.673	3.290	37	6.255	1.980	5.0447	0.198	2194.18	2.36
102	0.673	3.342	36	6.408	1.965	5.0447	0.198	2151.20	2.32
103	0.673	3.395	35	6.562	1.947	5.0447	0.198	2109.11	2.27
104	0.673	3.449	34	6.719	1.929	5.0447	0.198	2067.83	2.23

Table-22, The variation of BCR with normalized shell height (h/D) & shell Diameter for different shell diameter & heights.
For Coulomb wall ($\phi = 34^o$ and $\delta = 22^o$)

Angle of	Radius of log-spiral								
log-spiral	r_o	r_1	45-ϕ/2	d/D	h/D	K_p	K_a	Q_u	BCR
θ									Q_u/q_u
56	0.603	1.166	90	1.000	1.166	8.641	0.254	8191.07	39.87
57	0.603	1.180	89	1.041	1.180	8.641	0.254	7880.05	38.36
58	0.603	1.194	88	1.083	1.193	8.641	0.254	7586.09	36.93
59	0.603	1.208	87	1.126	1.206	8.641	0.254	7307.96	35.58
60	0.603	1.222	86	1.171	1.219	8.641	0.254	7044.58	34.29
61	0.603	1.237	85	1.216	1.232	8.641	0.254	6794.91	33.08
62	0.603	1.251	84	1.262	1.245	8.641	0.254	6558.03	31.92
63	0.603	1.266	83	1.309	1.257	8.641	0.254	6333.08	30.83
64	0.603	1.281	82	1.357	1.269	8.641	0.254	6119.26	29.79
65	0.603	1.296	81	1.406	1.280	8.641	0.254	5915.86	28.80
66	0.603	1.312	80	1.456	1.292	8.641	0.254	5722.20	27.86
67	0.603	1.327	79	1.506	1.303	8.641	0.254	5537.65	26.96
68	0.603	1.343	78	1.558	1.314	8.641	0.254	5361.64	26.10
69	0.603	1.359	77	1.611	1.324	8.641	0.254	5193.64	25.28
70	0.603	1.375	76	1.665	1.334	8.641	0.254	5033.15	24.50
71	0.603	1.391	75	1.720	1.344	8.641	0.254	4879.72	23.75
72	0.603	1.408	74	1.776	1.353	8.641	0.254	4732.91	23.04
73	0.603	1.424	73	1.833	1.362	8.641	0.254	4592.34	22.36
74	0.603	1.441	72	1.891	1.371	8.641	0.254	4457.62	21.70
75	0.603	1.458	71	1.950	1.379	8.641	0.254	4328.42	21.07
76	0.603	1.476	70	2.009	1.387	8.641	0.254	4204.41	20.47
77	0.603	1.493	69	2.070	1.394	8.641	0.254	4085.29	19.89
78	0.603	1.511	68	2.132	1.401	8.641	0.254	3970.78	19.33
79	0.603	1.529	67	2.195	1.407	8.641	0.254	3860.62	18.79
80	0.603	1.547	66	2.258	1.413	8.641	0.254	3754.55	18.28
81	0.603	1.565	65	2.323	1.418	8.641	0.254	3652.36	17.78
82	0.603	1.584	64	2.388	1.423	8.641	0.254	3553.82	17.30
83	0.603	1.602	63	2.455	1.428	8.641	0.254	3458.72	16.84
84	0.603	1.621	62	2.522	1.432	8.641	0.254	3366.88	16.39
85	0.603	1.640	61	2.591	1.435	8.641	0.254	3278.12	15.96
86	0.603	1.660	60	2.660	1.438	8.641	0.254	3192.26	15.54
87	0.603	1.680	59	2.730	1.440	8.641	0.254	3109.15	15.14
88	0.603	1.699	58	2.801	1.441	8.641	0.254	3028.63	14.74
89	0.603	1.720	57	2.873	1.442	8.641	0.254	2950.57	14.36
90	0.603	1.740	56	2.946	1.442	8.641	0.254	2874.83	13.99
91	0.603	1.761	55	3.020	1.442	8.641	0.254	2801.28	13.64
92	0.603	1.781	54	3.094	1.441	8.641	0.254	2729.80	13.29
93	0.603	1.803	53	3.170	1.440	8.641	0.254	2660.29	12.95
94	0.603	1.824	52	3.246	1.437	8.641	0.254	2592.63	12.62
95	0.603	1.845	51	3.323	1.434	8.641	0.254	2526.72	12.30
96	0.603	1.867	50	3.401	1.430	8.641	0.254	2462.46	11.99
97	0.603	1.889	49	3.479	1.426	8.641	0.254	2399.78	11.68
98	0.603	1.912	48	3.558	1.421	8.641	0.254	2338.56	11.38
99	0.603	1.934	47	3.639	1.415	8.641	0.254	2278.75	11.09
100	0.603	1.957	46	3.719	1.408	8.641	0.254	2220.26	10.81
101	0.603	1.981	45	3.801	1.400	8.641	0.254	2163.00	10.53
102	0.603	2.004	44	3.883	1.392	8.641	0.254	2106.93	10.26
103	0.603	2.028	43	3.966	1.383	8.641	0.254	2051.96	9.99
104	0.603	2.052	42	4.049	1.373	8.641	0.254	1998.04	9.73
105	0.603	2.076	41	4.134	1.362	8.641	0.254	1945.10	9.47
106	0.603	2.101	40	4.218	1.350	8.641	0.254	1893.09	9.22
107	0.603	2.125	39	4.304	1.338	8.641	0.254	1841.96	8.97
108	0.603	2.151	38	4.389	1.324	8.641	0.254	1791.64	8.72
109	0.603	2.176	37	4.476	1.310	8.641	0.254	1742.10	8.48
110	0.603	2.202	36	4.563	1.294	8.641	0.254	1693.27	8.24
111	0.603	2.228	35	4.650	1.278	8.641	0.254	1645.13	8.01
112	0.603	2.254	34	4.738	1.261	8.641	0.254	1597.63	7.78

Table-23, The variation of BCR with normalized shell height (h/D) & shell Diameter for different shell diameter & heights.
For Coulomb wall ($\phi = 38^o$ and $\delta = 22^o$)

Angle of	Radius of log-spiral								
log-spiral	r_o	r_1	45-ϕ/2	d/D	h/D	K_p	K_a	Q_u	BCR
θ									Q_u/q_u
52	0.635	1.289	90	1.000	1.289	11.466	0.217	9785.50	23.05
53	0.635	1.307	89	1.046	1.307	11.466	0.217	9385.47	22.11
54	0.635	1.325	88	1.092	1.324	11.466	0.217	9009.18	21.22
55	0.635	1.343	87	1.141	1.341	11.466	0.217	8654.81	20.39
56	0.635	1.362	86	1.190	1.358	11.466	0.217	8320.71	19.60
57	0.635	1.380	85	1.241	1.375	11.466	0.217	8005.35	18.86
58	0.635	1.399	84	1.293	1.392	11.466	0.217	7707.38	18.16
59	0.635	1.419	83	1.346	1.408	11.466	0.217	7425.53	17.49
60	0.635	1.438	82	1.400	1.424	11.466	0.217	7158.64	16.86
61	0.635	1.458	81	1.456	1.440	11.466	0.217	6905.66	16.27
62	0.635	1.478	80	1.513	1.455	11.466	0.217	6665.62	15.70
63	0.635	1.498	79	1.572	1.471	11.466	0.217	6437.62	15.17
64	0.635	1.519	78	1.631	1.485	11.466	0.217	6220.84	14.65
65	0.635	1.539	77	1.693	1.500	11.466	0.217	6014.53	14.17
66	0.635	1.561	76	1.755	1.514	11.466	0.217	5817.98	13.71
67	0.635	1.582	75	1.819	1.528	11.466	0.217	5630.55	13.26
68	0.635	1.604	74	1.884	1.542	11.466	0.217	5451.63	12.84
69	0.635	1.626	73	1.951	1.555	11.466	0.217	5280.66	12.44
70	0.635	1.648	72	2.019	1.567	11.466	0.217	5117.14	12.05
71	0.635	1.671	71	2.088	1.580	11.466	0.217	4960.58	11.69
72	0.635	1.694	70	2.159	1.592	11.466	0.217	4810.53	11.33
73	0.635	1.717	69	2.231	1.603	11.466	0.217	4666.59	10.99
74	0.635	1.740	68	2.304	1.614	11.466	0.217	4528.36	10.67
75	0.635	1.764	67	2.379	1.624	11.466	0.217	4395.47	10.35
76	0.635	1.789	66	2.455	1.634	11.466	0.217	4267.60	10.05
77	0.635	1.813	65	2.533	1.643	11.466	0.217	4144.43	9.76
78	0.635	1.838	64	2.611	1.652	11.466	0.217	4025.66	9.48
79	0.635	1.863	63	2.692	1.660	11.466	0.217	3911.01	9.21
80	0.635	1.889	62	2.774	1.668	11.466	0.217	3800.22	8.95
81	0.635	1.915	61	2.857	1.675	11.466	0.217	3693.06	8.70
82	0.635	1.941	60	2.941	1.681	11.466	0.217	3589.28	8.46
83	0.635	1.968	59	3.027	1.687	11.466	0.217	3488.68	8.22
84	0.635	1.995	58	3.114	1.692	11.466	0.217	3391.04	7.99
85	0.635	2.022	57	3.203	1.696	11.466	0.217	3296.19	7.76
86	0.635	2.050	56	3.293	1.699	11.466	0.217	3203.93	7.55
87	0.635	2.078	55	3.384	1.702	11.466	0.217	3114.10	7.34
88	0.635	2.107	54	3.476	1.704	11.466	0.217	3026.54	7.13
89	0.635	2.136	53	3.570	1.705	11.466	0.217	2941.10	6.93
90	0.635	2.165	52	3.666	1.706	11.466	0.217	2857.62	6.73
91	0.635	2.195	51	3.762	1.705	11.466	0.217	2775.98	6.54
92	0.635	2.225	50	3.860	1.704	11.466	0.217	2696.04	6.35
93	0.635	2.255	49	3.959	1.702	11.466	0.217	2617.68	6.17
94	0.635	2.286	48	4.060	1.699	11.466	0.217	2540.79	5.99
95	0.635	2.318	47	4.161	1.695	11.466	0.217	2465.26	5.81
96	0.635	2.349	46	4.264	1.690	11.466	0.217	2390.98	5.63
97	0.635	2.382	45	4.368	1.684	11.466	0.217	2317.84	5.46
98	0.635	2.414	44	4.473	1.677	11.466	0.217	2245.77	5.29
99	0.635	2.447	43	4.580	1.669	11.466	0.217	2174.66	5.12
100	0.635	2.481	42	4.688	1.660	11.466	0.217	2104.43	4.96
101	0.635	2.515	41	4.796	1.650	11.466	0.217	2035.00	4.79
102	0.635	2.550	40	4.906	1.639	11.466	0.217	1966.28	4.63
103	0.635	2.585	39	5.017	1.627	11.466	0.217	1898.21	4.47
104	0.635	2.620	38	5.129	1.613	11.466	0.217	1830.72	4.31
105	0.635	2.656	37	5.243	1.599	11.466	0.217	1763.73	4.15
106	0.635	2.693	36	5.357	1.583	11.466	0.217	1697.19	4.00
107	0.635	2.730	35	5.472	1.566	11.466	0.217	1631.02	3.84
108	0.635	2.767	34	5.588	1.547	11.466	0.217	1565.18	3.69

Table-24, The variation of BCR with normalized shell height (h/D) & shell Diameter for different shell diameter & heights.
For Coulomb wall ($\phi = 42^o$ and $\delta = 22^o$)

Angle of	Radius of log-spiral								
log-spiral	r_o	r_1	45-ϕ/2	d/D	h/D	K_p	K_a	Q_u	BCR
θ									Q_u/q_u
48	0.673	1.431	90	1.000	1.431	15.726	0.183	11994.45	12.91
49	0.673	1.453	89	1.051	1.453	15.726	0.183	11473.54	12.35
50	0.673	1.476	88	1.103	1.475	15.726	0.183	10986.36	11.83
51	0.673	1.500	87	1.157	1.498	15.726	0.183	10530.10	11.34
52	0.673	1.523	86	1.213	1.520	15.726	0.183	10102.22	10.88
53	0.673	1.547	85	1.270	1.542	15.726	0.183	9700.43	10.44
54	0.673	1.572	84	1.329	1.563	15.726	0.183	9322.64	10.04
55	0.673	1.597	83	1.389	1.585	15.726	0.183	8966.97	9.65
56	0.673	1.622	82	1.452	1.606	15.726	0.183	8631.68	9.29
57	0.673	1.648	81	1.516	1.628	15.726	0.183	8315.22	8.95
58	0.673	1.674	80	1.581	1.649	15.726	0.183	8016.15	8.63
59	0.673	1.700	79	1.649	1.669	15.726	0.183	7733.15	8.33
60	0.673	1.727	78	1.718	1.690	15.726	0.183	7465.04	8.04
61	0.673	1.755	77	1.789	1.710	15.726	0.183	7210.70	7.76
62	0.673	1.783	76	1.862	1.730	15.726	0.183	6969.11	7.50
63	0.673	1.811	75	1.937	1.749	15.726	0.183	6739.36	7.26
64	0.673	1.839	74	2.014	1.768	15.726	0.183	6520.58	7.02
65	0.673	1.869	73	2.093	1.787	15.726	0.183	6311.97	6.80
66	0.673	1.898	72	2.173	1.805	15.726	0.183	6112.79	6.58
67	0.673	1.928	71	2.256	1.823	15.726	0.183	5922.38	6.38
68	0.673	1.959	70	2.340	1.841	15.726	0.183	5740.08	6.18
69	0.673	1.990	69	2.426	1.858	15.726	0.183	5565.33	5.99
70	0.673	2.021	68	2.514	1.874	15.726	0.183	5397.58	5.81
71	0.673	2.053	67	2.605	1.890	15.726	0.183	5236.30	5.64
72	0.673	2.086	66	2.697	1.906	15.726	0.183	5081.04	5.47
73	0.673	2.119	65	2.791	1.920	15.726	0.183	4931.36	5.31
74	0.673	2.152	64	2.887	1.935	15.726	0.183	4786.82	5.15
75	0.673	2.187	63	2.985	1.948	15.726	0.183	4647.06	5.00
76	0.673	2.221	62	3.086	1.961	15.726	0.183	4511.70	4.86
77	0.673	2.256	61	3.188	1.973	15.726	0.183	4380.41	4.72
78	0.673	2.292	60	3.292	1.985	15.726	0.183	4252.87	4.58
79	0.673	2.328	59	3.398	1.996	15.726	0.183	4128.77	4.45
80	0.673	2.365	58	3.507	2.006	15.726	0.183	4007.83	4.32
81	0.673	2.403	57	3.617	2.015	15.726	0.183	3889.78	4.19
82	0.673	2.441	56	3.730	2.024	15.726	0.183	3774.38	4.06
83	0.673	2.480	55	3.844	2.031	15.726	0.183	3661.37	3.94
84	0.673	2.519	54	3.961	2.038	15.726	0.183	3550.55	3.82
85	0.673	2.559	53	4.080	2.043	15.726	0.183	3441.68	3.71
86	0.673	2.599	52	4.200	2.048	15.726	0.183	3334.58	3.59
87	0.673	2.640	51	4.323	2.052	15.726	0.183	3229.04	3.48
88	0.673	2.682	50	4.448	2.055	15.726	0.183	3124.88	3.36
89	0.673	2.725	49	4.575	2.056	15.726	0.183	3021.93	3.25
90	0.673	2.768	48	4.704	2.057	15.726	0.183	2920.03	3.14
91	0.673	2.812	47	4.835	2.056	15.726	0.183	2819.01	3.04
92	0.673	2.856	46	4.968	2.055	15.726	0.183	2718.71	2.93
93	0.673	2.901	45	5.103	2.052	15.726	0.183	2619.01	2.82
94	0.673	2.947	44	5.240	2.047	15.726	0.183	2519.76	2.71
95	0.673	2.994	43	5.379	2.042	15.726	0.183	2420.82	2.61
96	0.673	3.042	42	5.521	2.035	15.726	0.183	2322.08	2.50
97	0.673	3.090	41	5.664	2.027	15.726	0.183	2223.40	2.39
98	0.673	3.139	40	5.809	2.017	15.726	0.183	2124.67	2.29
99	0.673	3.188	39	5.956	2.006	15.726	0.183	2025.79	2.18
100	0.673	3.239	38	6.104	1.994	15.726	0.183	1926.63	2.07
101	0.673	3.290	37	6.255	1.980	15.726	0.183	1827.10	1.97
102	0.673	3.342	36	6.408	1.965	15.726	0.183	1727.11	1.86
103	0.673	3.395	35	6.562	1.947	15.726	0.183	1626.54	1.75
104	0.673	3.449	34	6.719	1.929	15.726	0.183	1525.31	1.64

Table-25, The variation of BCR with normalized shell height (h/D) & shell Diameter for different shell diameter & heights.
For Coulomb wall ($\phi = 34^o$ and $\delta = 25^o$)

Angle of	Radius of log-spiral								
log-spiral	r_o	r_1	45-ϕ/2	d/D	h/D	K_p	K_a	Q_u	BCR
θ									Q_u/q_u
56	0.603	1.166	90	1.000	1.166	10.193	0.254	8221.40	40.02
57	0.603	1.180	89	1.041	1.180	10.193	0.254	7909.63	38.50
58	0.603	1.194	88	1.083	1.193	10.193	0.254	7614.87	37.07
59	0.603	1.208	87	1.126	1.206	10.193	0.254	7335.90	35.71
60	0.603	1.222	86	1.171	1.219	10.193	0.254	7071.61	34.43
61	0.603	1.237	85	1.216	1.232	10.193	0.254	6821.00	33.21
62	0.603	1.251	84	1.262	1.245	10.193	0.254	6583.12	32.05
63	0.603	1.266	83	1.309	1.257	10.193	0.254	6357.11	30.95
64	0.603	1.281	82	1.357	1.269	10.193	0.254	6142.19	29.90
65	0.603	1.296	81	1.406	1.280	10.193	0.254	5937.63	28.90
66	0.603	1.312	80	1.456	1.292	10.193	0.254	5742.76	27.96
67	0.603	1.327	79	1.506	1.303	10.193	0.254	5556.94	27.05
68	0.603	1.343	78	1.558	1.314	10.193	0.254	5379.61	26.19
69	0.603	1.359	77	1.611	1.324	10.193	0.254	5210.23	25.36
70	0.603	1.375	76	1.665	1.334	10.193	0.254	5048.31	24.58
71	0.603	1.391	75	1.720	1.344	10.193	0.254	4893.38	23.82
72	0.603	1.408	74	1.776	1.353	10.193	0.254	4745.03	23.10
73	0.603	1.424	73	1.833	1.362	10.193	0.254	4602.84	22.41
74	0.603	1.441	72	1.891	1.371	10.193	0.254	4466.45	21.74
75	0.603	1.458	71	1.950	1.379	10.193	0.254	4335.52	21.11
76	0.603	1.476	70	2.009	1.387	10.193	0.254	4209.71	20.49
77	0.603	1.493	69	2.070	1.394	10.193	0.254	4088.74	19.90
78	0.603	1.511	68	2.132	1.401	10.193	0.254	3972.31	19.34
79	0.603	1.529	67	2.195	1.407	10.193	0.254	3860.17	18.79
80	0.603	1.547	66	2.258	1.413	10.193	0.254	3752.06	18.27
81	0.603	1.565	65	2.323	1.418	10.193	0.254	3647.76	17.76
82	0.603	1.584	64	2.388	1.423	10.193	0.254	3547.04	17.27
83	0.603	1.602	63	2.455	1.428	10.193	0.254	3449.70	16.79
84	0.603	1.621	62	2.522	1.432	10.193	0.254	3355.56	16.34
85	0.603	1.640	61	2.591	1.435	10.193	0.254	3264.42	15.89
86	0.603	1.660	60	2.660	1.438	10.193	0.254	3176.13	15.46
87	0.603	1.680	59	2.730	1.440	10.193	0.254	3090.51	15.04
88	0.603	1.699	58	2.801	1.441	10.193	0.254	3007.42	14.64
89	0.603	1.720	57	2.873	1.442	10.193	0.254	2926.71	14.25
90	0.603	1.740	56	2.946	1.442	10.193	0.254	2848.26	13.87
91	0.603	1.761	55	3.020	1.442	10.193	0.254	2771.92	13.49
92	0.603	1.781	54	3.094	1.441	10.193	0.254	2697.60	13.13
93	0.603	1.803	53	3.170	1.440	10.193	0.254	2625.16	12.78
94	0.603	1.824	52	3.246	1.437	10.193	0.254	2554.50	12.44
95	0.603	1.845	51	3.323	1.434	10.193	0.254	2485.53	12.10
96	0.603	1.867	50	3.401	1.430	10.193	0.254	2418.14	11.77
97	0.603	1.889	49	3.479	1.426	10.193	0.254	2352.24	11.45
98	0.603	1.912	48	3.558	1.421	10.193	0.254	2287.75	11.14
99	0.603	1.934	47	3.639	1.415	10.193	0.254	2224.58	10.83
100	0.603	1.957	46	3.719	1.408	10.193	0.254	2162.67	10.53
101	0.603	1.981	45	3.801	1.400	10.193	0.254	2101.92	10.23
102	0.603	2.004	44	3.883	1.392	10.193	0.254	2042.27	9.94
103	0.603	2.028	43	3.966	1.383	10.193	0.254	1983.66	9.66
104	0.603	2.052	42	4.049	1.373	10.193	0.254	1926.03	9.38
105	0.603	2.076	41	4.134	1.362	10.193	0.254	1869.30	9.10
106	0.603	2.101	40	4.218	1.350	10.193	0.254	1813.43	8.83
107	0.603	2.125	39	4.304	1.338	10.193	0.254	1758.36	8.56
108	0.603	2.151	38	4.389	1.324	10.193	0.254	1704.03	8.30
109	0.603	2.176	37	4.476	1.310	10.193	0.254	1650.41	8.03
110	0.603	2.202	36	4.563	1.294	10.193	0.254	1597.43	7.78
111	0.603	2.228	35	4.650	1.278	10.193	0.254	1545.07	7.52
112	0.603	2.254	34	4.738	1.261	10.193	0.254	1493.26	7.27
113	0.603	2.281	33	4.826	1.242	10.193	0.254	1441.98	7.02

Table-26, The variation of BCR with normalized shell height (h/D) & shell Diameter for different shell diameter & heights.
For Coulomb wall ($\phi = 38^o$ and $\delta = 25^o$)

Angle of	Radius of log-spiral								
Log-spiral	r_o	r_1	45-ϕ/2	d/D	h/D	K_p	K_a	Q_u	BCR
θ									Q_u/q_u
52	0.635	1.289	90	1.000	1.289	13.901	0.217	9861.03	23.23
53	0.635	1.307	89	1.046	1.307	13.901	0.217	9459.94	22.28
54	0.635	1.325	88	1.092	1.324	13.901	0.217	9082.49	21.40
55	0.635	1.343	87	1.141	1.341	13.901	0.217	8726.86	20.56
56	0.635	1.362	86	1.190	1.358	13.901	0.217	8391.39	19.77
57	0.635	1.380	85	1.241	1.375	13.901	0.217	8074.57	19.02
58	0.635	1.399	84	1.293	1.392	13.901	0.217	7775.02	18.32
59	0.635	1.419	83	1.346	1.408	13.901	0.217	7491.48	17.65
60	0.635	1.438	82	1.400	1.424	13.901	0.217	7222.80	17.01
61	0.635	1.458	81	1.456	1.440	13.901	0.217	6967.91	16.41
62	0.635	1.478	80	1.513	1.455	13.901	0.217	6725.84	15.84
63	0.635	1.498	79	1.572	1.471	13.901	0.217	6495.70	15.30
64	0.635	1.519	78	1.631	1.485	13.901	0.217	6276.66	14.79
65	0.635	1.539	77	1.693	1.500	13.901	0.217	6067.96	14.29
66	0.635	1.561	76	1.755	1.514	13.901	0.217	5868.89	13.83
67	0.635	1.582	75	1.819	1.528	13.901	0.217	5678.82	13.38
68	0.635	1.604	74	1.884	1.542	13.901	0.217	5497.12	12.95
69	0.635	1.626	73	1.951	1.555	13.901	0.217	5323.26	12.54
70	0.635	1.648	72	2.019	1.567	13.901	0.217	5156.70	12.15
71	0.635	1.671	71	2.088	1.580	13.901	0.217	4996.97	11.77
72	0.635	1.694	70	2.159	1.592	13.901	0.217	4843.61	11.41
73	0.635	1.717	69	2.231	1.603	13.901	0.217	4696.22	11.06
74	0.635	1.740	68	2.304	1.614	13.901	0.217	4554.39	10.73
75	0.635	1.764	67	2.379	1.624	13.901	0.217	4417.77	10.41
76	0.635	1.789	66	2.455	1.634	13.901	0.217	4286.02	10.10
77	0.635	1.813	65	2.533	1.643	13.901	0.217	4158.81	9.80
78	0.635	1.838	64	2.611	1.652	13.901	0.217	4035.86	9.51
79	0.635	1.863	63	2.692	1.660	13.901	0.217	3916.87	9.23
80	0.635	1.889	62	2.774	1.668	13.901	0.217	3801.59	8.96
81	0.635	1.915	61	2.857	1.675	13.901	0.217	3689.78	8.69
82	0.635	1.941	60	2.941	1.681	13.901	0.217	3581.19	8.44
83	0.635	1.968	59	3.027	1.687	13.901	0.217	3475.62	8.19
84	0.635	1.995	58	3.114	1.692	13.901	0.217	3372.85	7.95
85	0.635	2.022	57	3.203	1.696	13.901	0.217	3272.70	7.71
86	0.635	2.050	56	3.293	1.699	13.901	0.217	3174.98	7.48
87	0.635	2.078	55	3.384	1.702	13.901	0.217	3079.52	7.25
88	0.635	2.107	54	3.476	1.704	13.901	0.217	2986.15	7.03
89	0.635	2.136	53	3.570	1.705	13.901	0.217	2894.72	6.82
90	0.635	2.165	52	3.666	1.706	13.901	0.217	2805.09	6.61
91	0.635	2.195	51	3.762	1.705	13.901	0.217	2717.12	6.40
92	0.635	2.225	50	3.860	1.704	13.901	0.217	2630.68	6.20
93	0.635	2.255	49	3.959	1.702	13.901	0.217	2545.63	6.00
94	0.635	2.286	48	4.060	1.699	13.901	0.217	2461.87	5.80
95	0.635	2.318	47	4.161	1.695	13.901	0.217	2379.29	5.60
96	0.635	2.349	46	4.264	1.690	13.901	0.217	2297.77	5.41
97	0.635	2.382	45	4.368	1.684	13.901	0.217	2217.22	5.22
98	0.635	2.414	44	4.473	1.677	13.901	0.217	2137.53	5.04
99	0.635	2.447	43	4.580	1.669	13.901	0.217	2058.62	4.85
100	0.635	2.481	42	4.688	1.660	13.901	0.217	1980.40	4.67
101	0.635	2.515	41	4.796	1.650	13.901	0.217	1902.79	4.48
102	0.635	2.550	40	4.906	1.639	13.901	0.217	1825.70	4.30
103	0.635	2.585	39	5.017	1.627	13.901	0.217	1749.07	4.12
104	0.635	2.620	38	5.129	1.613	13.901	0.217	1672.81	3.94
105	0.635	2.656	37	5.243	1.599	13.901	0.217	1596.87	3.76
106	0.635	2.693	36	5.357	1.583	13.901	0.217	1521.16	3.58
107	0.635	2.730	35	5.472	1.566	13.901	0.217	1445.64	3.41
108	0.635	2.767	34	5.588	1.547	13.901	0.217	1370.25	3.23
109	0.635	2.805	33	5.705	1.528	13.901	0.217	1294.91	3.05

Table-27, The variation of BCR with normalized shell height (h/D) & shell Diameter for different shell diameter & heights.

For Coulomb wall ($\phi = 42^o$ and $\delta = 25^o$)

Angle of	Radius of log-spiral								
Log-spiral	r_o	r_1	45-ϕ/2	d/D	h/D	K_p	K_a	Q_u	BCR
θ									Q_u/q_u
48	0.673	1.431	90	1.000	1.431	19.758	0.183	12186.29	13.12
49	0.673	1.453	89	1.051	1.453	19.758	0.183	11664.17	12.56
50	0.673	1.476	88	1.103	1.475	19.758	0.183	11175.56	12.03
51	0.673	1.500	87	1.157	1.498	19.758	0.183	10717.66	11.54
52	0.673	1.523	86	1.213	1.520	19.758	0.183	10287.91	11.08
53	0.673	1.547	85	1.270	1.542	19.758	0.183	9884.02	10.64
54	0.673	1.572	84	1.329	1.563	19.758	0.183	9503.89	10.23
55	0.673	1.597	83	1.389	1.585	19.758	0.183	9145.63	9.85
56	0.673	1.622	82	1.452	1.606	19.758	0.183	8807.51	9.48
57	0.673	1.648	81	1.516	1.628	19.758	0.183	8487.96	9.14
58	0.673	1.674	80	1.581	1.649	19.758	0.183	8185.53	8.81
59	0.673	1.700	79	1.649	1.669	19.758	0.183	7898.92	8.50
60	0.673	1.727	78	1.718	1.690	19.758	0.183	7626.90	8.21
61	0.673	1.755	77	1.789	1.710	19.758	0.183	7368.38	7.93
62	0.673	1.783	76	1.862	1.730	19.758	0.183	7122.33	7.67
63	0.673	1.811	75	1.937	1.749	19.758	0.183	6887.81	7.42
64	0.673	1.839	74	2.014	1.768	19.758	0.183	6663.96	7.18
65	0.673	1.869	73	2.093	1.787	19.758	0.183	6449.97	6.94
66	0.673	1.898	72	2.173	1.805	19.758	0.183	6245.10	6.72
67	0.673	1.928	71	2.256	1.823	19.758	0.183	6048.66	6.51
68	0.673	1.959	70	2.340	1.841	19.758	0.183	5860.02	6.31
69	0.673	1.990	69	2.426	1.858	19.758	0.183	5678.58	6.11
70	0.673	2.021	68	2.514	1.874	19.758	0.183	5503.79	5.93
71	0.673	2.053	67	2.605	1.890	19.758	0.183	5335.14	5.74
72	0.673	2.086	66	2.697	1.906	19.758	0.183	5172.14	5.57
73	0.673	2.119	65	2.791	1.920	19.758	0.183	5014.34	5.40
74	0.673	2.152	64	2.887	1.935	19.758	0.183	4861.33	5.23
75	0.673	2.187	63	2.985	1.948	19.758	0.183	4712.70	5.07
76	0.673	2.221	62	3.086	1.961	19.758	0.183	4568.10	4.92
77	0.673	2.256	61	3.188	1.973	19.758	0.183	4427.17	4.77
78	0.673	2.292	60	3.292	1.985	19.758	0.183	4289.58	4.62
79	0.673	2.328	59	3.398	1.996	19.758	0.183	4155.02	4.47
80	0.673	2.365	58	3.507	2.006	19.758	0.183	4023.22	4.33
81	0.673	2.403	57	3.617	2.015	19.758	0.183	3893.88	4.19
82	0.673	2.441	56	3.730	2.024	19.758	0.183	3766.75	4.06
83	0.673	2.480	55	3.844	2.031	19.758	0.183	3641.59	3.92
84	0.673	2.519	54	3.961	2.038	19.758	0.183	3518.16	3.79
85	0.673	2.559	53	4.080	2.043	19.758	0.183	3396.24	3.66
86	0.673	2.599	52	4.200	2.048	19.758	0.183	3275.62	3.53
87	0.673	2.640	51	4.323	2.052	19.758	0.183	3156.10	3.40
88	0.673	2.682	50	4.448	2.055	19.758	0.183	3037.49	3.27
89	0.673	2.725	49	4.575	2.056	19.758	0.183	2919.61	3.14
90	0.673	2.768	48	4.704	2.057	19.758	0.183	2802.28	3.02
91	0.673	2.812	47	4.835	2.056	19.758	0.183	2685.34	2.89
92	0.673	2.856	46	4.968	2.055	19.758	0.183	2568.64	2.77
93	0.673	2.901	45	5.103	2.052	19.758	0.183	2452.01	2.64
94	0.673	2.947	44	5.240	2.047	19.758	0.183	2335.32	2.51
95	0.673	2.994	43	5.379	2.042	19.758	0.183	2218.43	2.39
96	0.673	3.042	42	5.521	2.035	19.758	0.183	2101.20	2.26
97	0.673	3.090	41	5.664	2.027	19.758	0.183	1983.50	2.14
98	0.673	3.139	40	5.809	2.017	19.758	0.183	1865.21	2.01
99	0.673	3.188	39	5.956	2.006	19.758	0.183	1746.22	1.88
100	0.673	3.239	38	6.104	1.994	19.758	0.183	1626.40	1.75
101	0.673	3.290	37	6.255	1.980	19.758	0.183	1505.66	1.62
102	0.673	3.342	36	6.408	1.965	19.758	0.183	1383.88	1.49
103	0.673	3.395	35	6.562	1.947	19.758	0.183	1260.95	1.36
104	0.673	3.449	34	6.719	1.929	19.758	0.183	1136.80	1.22
105	0.673	3.504	33	6.877	1.908	19.758	0.183	1011.31	1.09